

Zentrale Einrichtung Elektronenmikroskopie

(Leiter Prof. Dr. Paul Walther)

Universität Ulm

Nano-architecture and mineralization of the amorphous CaCO₃ deposits during the molt cycle of the terrestrial isopod *Porcellio scaber* (Crustacea)

Dissertation

Zur Erlangung des Doktorgrades (Dr. rer. Nat.)

an der Fakultät für Naturwissenschaften

der Universität Ulm

vorgelegt von

Helge-Otto Fabritius

aus Agnetheln

2008

Amtierender Dekan der Fakultät für Naturwissenschaften:

Prof. Dr. Klaus-Dieter Spindler

Erstgutachter:

Prof. Dr. Klaus-Dieter Spindler, Abteilung Allgemeine Zoologie und Endokrinologie, Universität Ulm

Zweitgutachter:

PD Dr. Andreas Ziegler, Zentrale Einrichtung Elektronenmikroskopie, Universität Ulm

Datum der Promotion: 10.07.2008

Die Arbeiten im Rahmen der vorgelegten Dissertation wurden in der Zentralen Einrichtung Elektronenmikroskopie der Universität Ulm durchgeführt und von Herrn PD Dr. Andreas Ziegler betreut.

Ulm, den 12.03. 2008

Contents

1. Introduction	1
2. Results	9
2.1 Natural formation and degradation of the CaCO ₃ deposits during the molt cycle.....	9
2.2 Ultrastructural organization of the organic matrix in fully developed CaCO ₃ deposits	11
2.3 Structural characterization of the mineral phase in fully developed CaCO ₃ deposits	15
2.4 Ultrastructural investigation of the aggregation zone in early stages of deposit formation....	16
2.5 Molecular characterization of the matrix proteins in the sternal CaCO ₃ deposits	18
3. Discussion	21
3.1 Formation of the deposits.....	21
3.2 Degradation of the deposits.....	22
3.3 Ultrastructure of organic matrix and ACC within the deposits.....	23
3.4 The role of the aggregation zone during deposit formation	25
3.5 Evolution of sternal deposits in terrestrial isopods (Oniscidea).....	26
3.6 Characterization of the organic matrix	27
3.7 Summary of main conclusions	28
4. References	30
5. Publications.....	35
5.1 Analysis of CaCO ₃ deposit formation and degradation during the molt cycle of the terrestrial isopod <i>Porcellio scaber</i> (Crustacea, Isopoda).....	35
5.2 Architecture of the organic matrix in the sternal CaCO ₃ deposits of <i>Porcellio scaber</i> (Crustacea, Isopoda).....	47
5.3 Structural characterisation of X-ray amorphous calcium carbonate (ACC) in sternal deposits of the Crustacea <i>Porcellio scaber</i>	58
6. Appendix	64
6.1 Material and Methods.....	64
6.2 Analytical techniques used for studying the sternal CaCO ₃ deposits of <i>P. scaber</i>	68
7. Deutschsprachige Zusammenfassung.....	71
8. Curriculum vitae	74
9. List of publications.....	75
9.1 Scientific journals.....	75
9.2 Abstracts.....	75
10. Acknowledgements.....	77

1. Introduction

Solid inorganic minerals fulfil a variety of important functions in many biological systems. They are used as skeletal structures (bone, corals, diatoms), protection against predation (mollusc shells), tools (teeth) or gravity sensors (statholiths). The processes of their formation in living organisms are commonly termed as biomineralization. Currently, over 60 different biogenic minerals are known, with calcium carbonate, calcium phosphate and silicon dioxide being only the most prominent examples (for recent reviews see Lowenstam and Weiner, 1989; Epple, 2003; Baeuerlein, 2004). Calcium carbonate is one of the most widespread biominerals. Some plants use it as calcium store in their leaves. In vertebrates it occurs for example in statholiths, gravity receptors located in the inner ear and the egg-shells of birds. The highest diversity of functions for calcium carbonate as biomineral is found in invertebrates. Here it serves as skeletal element in the shells of marine protists (Foraminifera, Coccolithophora) and corals (Cnidaria), as material for the shells of molluscs and echinoderms or in the exoskeletons of crustaceans (Meldrum, 2003).

With about 42000 known species, the Crustacea represent an important group inside the Arthropoda (Schminke, 1996). A common character of Arthropoda is the possession of a cuticle which covers the entire organism and fulfils a variety of functions. In almost all arthropods the cuticle forms an exoskeleton, whose basic task is to provide stability to their body and to enable movement by attachment of muscles and the formation of various joints. A large number of crustaceans have hard and sturdy exoskeletons, which give them protection against predators and mechanical stress in their habitats. In most cases, these cuticles are hardened by the incorporation of calcium carbonate (Passano, 1960). During their life cycle, crustaceans have to molt regularly in order to grow. During molt, the old cuticle is shed and replaced by a new, larger one which is already present underneath. This new cuticle is soft and flexible to enable growth for the animals. During this period they are extremely vulnerable to predation and mechanical stress caused by their environment. Thus, regaining full protection by hardening their exoskeletons quickly is crucial for crustaceans. Because the mineral used to harden the old cuticle is lost with the residual exuvia, the animals have to somehow replace it, which is usually by uptake from the environment (Neufeld and Cameron, 1993). The vast majority of all known crustaceans are aquatic animals, living in either marine, brackish or limnic habitats. Due to the high concentrations of calcium and carbonate present in seawater, marine crustaceans can replace lost mineral quickly by uptake of ions from the surrounding medium via their gills. Even freshwater contains sufficient Ca^{2+} for this mode of mineral replacement. Only in a small number of Crustacea groups we find taxa that have switched to terrestrial life, namely in Decapoda and

Isopoda. The terrestrial species are limited to the mineral present in their food and drinking water, where it is scarce. Thus, they had to evolve mechanisms for the conservation of cuticular CaCO_3 during molt, which was accomplished in a number of different ways. This feature is not limited to terrestrial species, but occurs also in some aquatic crustaceans. Examples for this are crayfish, decapods that store calcium as so-called gastroliths in the integument of the stomach (Greenaway, 1985); the semi-aquatic crab *Holthuisana transversa* which stores calcium as small granules in the hemolymph (Sparkes and Greenaway, 1984; Greenaway and Farrelly, 1991) and the terrestrial amphipod *Orchestia cavimana*, which stores calcium in calcareous concretions of spherules in the posterior caeca of the midgut (Graf and Meyran, 1985). While there exist only a few species of terrestrial crabs and land hermit crabs, the Oniscidea or terrestrial isopods represent a very successful group with about 3600 described species (see Schmalfuss, 2003). Terrestrial isopods are the only crustaceans which have become completely independent from their originally aquatic life.

The Oniscidea are subdivided into five major taxa, the Ligiidae, Tylidae, Mesoniscidae, Synocheta and Crinocheta (for an elaborate phylogenetic analysis see Erhard, 1997) (Fig. 1). They have adapted to a wide range of terrestrial habitats, from rocky shores and sandy beaches, wetlands, mesic forests to even arid, desert-like biotopes.

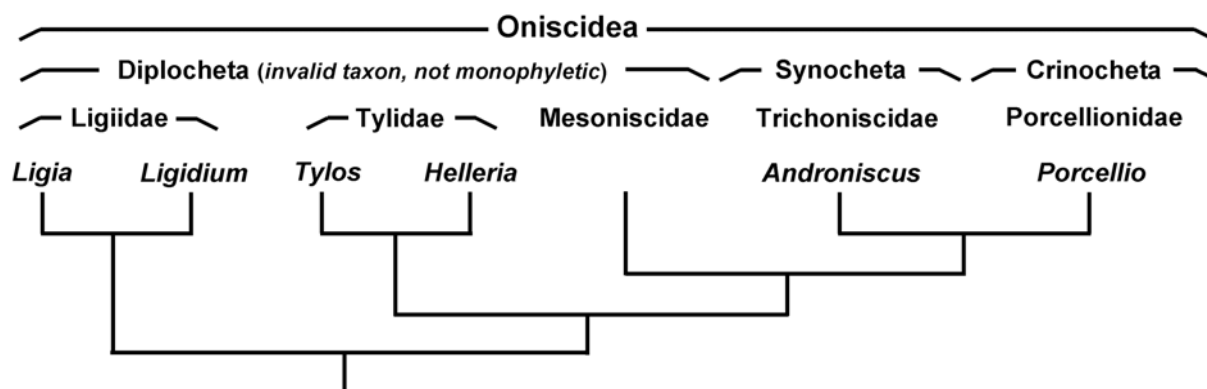


Figure 1. Phylogram of the Oniscidea or terrestrial isopods according to Erhard (1997). The taxon Oniscidea has the status of an order and contained originally three suborders, the Diplocheta with three families, the Synocheta with four families and the Crinocheta with 27 families. Recent results have shown that the Diplocheta are not monophyletic and in consequence this group is no longer valid.

The ability to conserve cuticular CaCO_3 during the molt represents an important adaptation to terrestrial life whose importance is often overlooked. Oniscidea have evolved a variety of ways to conserve CaCO_3 , differing both in storage sites and the amount of mineral recycled with each molt (Auzou, 1953; Numanoi, 1934; Steel, 1993; Štrus and Blejec, 2001; Ziegler et al., 2007). The most widespread way is the formation of large deposits located in the exuvial gap

between the old cuticle and the epithelium of the first four anterior sternites. Previous investigations of Ligiidae and Crinocheta have shown that three types of sternal deposits can be discerned with respect to their structure (Fig. 2). The Ligiidae live in biotopes with high humidity and have deposits with rather small storage capacity. Among those, the semi terrestrial species *Ligia italica* Fabricius, 1798 and *Ligia oceanica* (Linnaeus, 1767) live in the splash water zone of seashores. Their deposits consist of a layer of small, individual spherules (Fig. 2c). *Ligidium hypnorum* (Cuvier, 1792) lives in moist woodlands and has slightly larger CaCO_3 deposits consisting of two layers, a distal layer of fused spherules and a proximal layer of individual spherules (Fig. 2b). Most of the examined species of Tyliidae, Trichoniscidae and Crinocheta have large sternal deposits composed of three layers, distally a layer of fused spherules, a layer of individual spherules and an additional layer of homogeneous nature adjacent to the epithelium (Fig. 2a), which increases the storage capacity for calcium significantly.

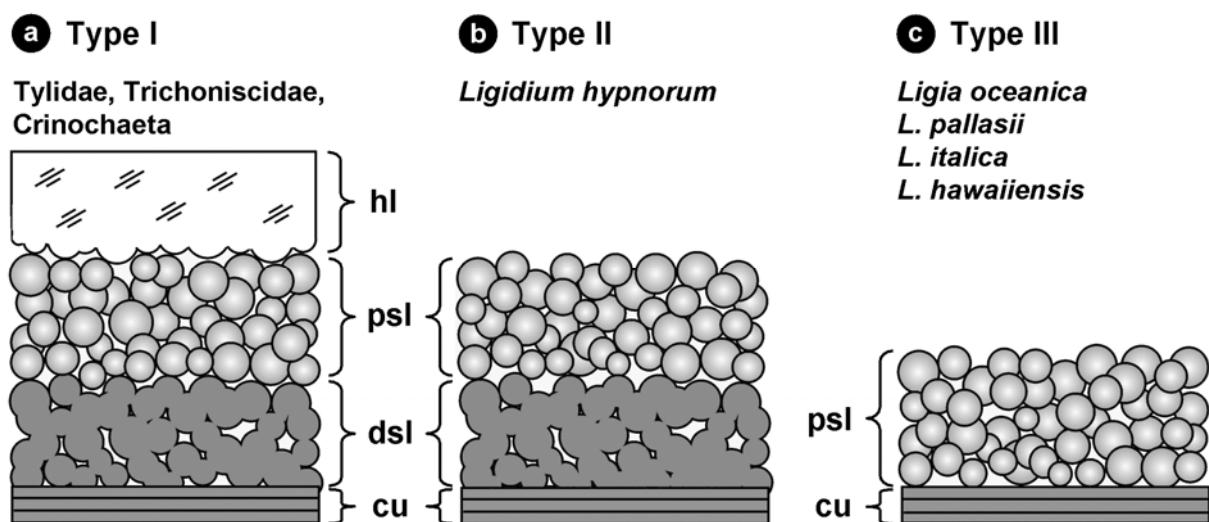


Figure 2. Schematic representation of the three different types of sternal CaCO_3 deposits that have been described in different species of Oniscidea (modified after Ziegler, 2003). (a) Type I deposits have three layers: a distal spherular layer (dsl) adjacent to the cuticle (cu) consisting of fused spherules, a proximal spherular layer (psl) consisting of individual spherules and a homogeneous layer (hl) adjacent to the epithelium. (b) Type II deposits consist of two layers, dsl with fused spherules and psl with individual spherules. (c) Type III deposits consist of one layer of individual spherules (psl) adjacent to the cuticle (cu).

These results suggested a correlation between the CaCO_3 storage capacity and the degree of terrestrialization in the investigated species (Ziegler and Miller, 1997). A recent complementary study on Tyliidae and Synocheta demonstrated an even greater variety in terms of deposit location and even mineral composition. The Tyliidae *Tylos europaeus* Arcangeli, 1938 forms deposits of calcium phosphate within the ventral integument of its pleomeres in addition to

three layered sternal CaCO_3 deposits, while *Helleria brevicornis* Ebner, 1868 that also belongs to the Tylidae has no sternal deposits at all, but stores CaCO_3 as spherules in the lateral fatty tissue. Members of the Trichoniscidae (Synocheta) store either calcium carbonate or calcium phosphate or both in deposits of various shapes in their hemolymph space in addition to their sternal deposits (Ziegler, 2003).

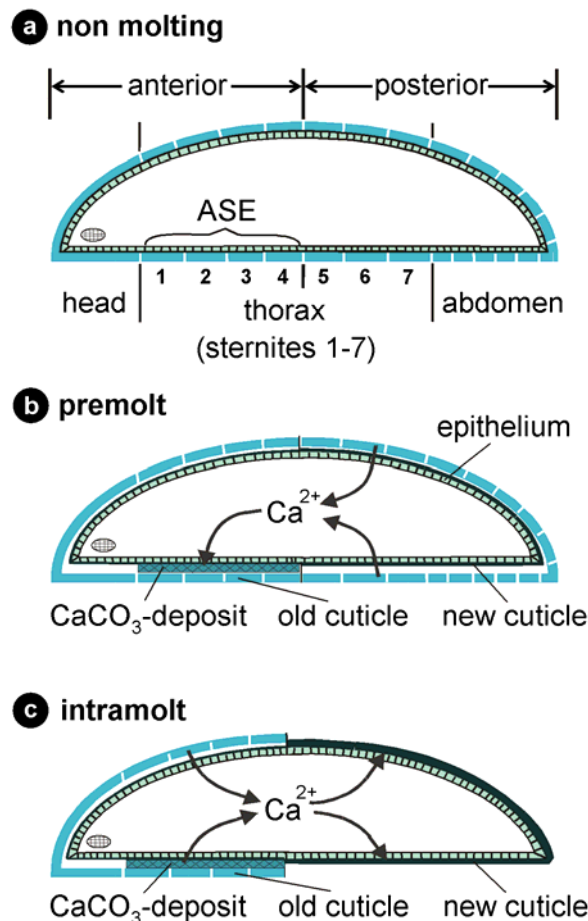


Figure 3. Schematic representation of the calcium pathways during the molt of terrestrial isopods as shown for *Porcellio scaber* by Ziegler and Merz (1999), modified. (a) During the non molting phase (intermolt) the whole cuticle is mineralized with incorporated calcium. (b) During premolt, calcium from the posterior cuticle is resorbed, transported across the epithelium and stored in deposits located in the ecdysial space of the first four anterior sternites. (c) After the posterior molt (intramolt), calcium from the deposits and the anterior cuticle is resorbed and used to mineralize the new posterior cuticle.

The deposition and resorption of cuticular CaCO_3 in the form of sternal deposits is closely linked to a feature common to all isopods, their biphasic molt cycle. Isopods molt first the posterior part of their body and shortly after the posterior cuticle is hardened the anterior part of their body (Messner, 1965). During the premolt phase, terrestrial isopods resorb calcium from the posterior cuticle into the hemolymph (Ziegler and Scholz, 1997) from where it is transported across the highly differentiated anterior sternal epithelium (Ziegler, 1996; Ziegler, 1997) of the

first four sternites into the exuvial gap where it remains stored until the posterior molt is finished (Fig. 3). During the short intramolt phase between posterior and anterior molt the deposits degrade, the calcium and probably also carbonate ions are resorbed and used together with mineral from the anterior cuticle to mineralise the new posterior cuticle (Steel, 1993). After each molt, most Oniscidea additionally ingest the shed cuticle, which still contains significant amounts of mineral. Calcium originating from the ingested cuticle is thought to be transported across the intestinal epithelium and used to mineralise the new anterior cuticle (Ziegler and Scholz, 1997).

Among the Crinochaeta, the most extensively investigated CaCO_3 deposits are those of *Porcellio scaber* Latreille 1804, the common woodlouse (Fig. 4).



Figure 4. The habitus of *Porcellio scaber* Latreille 1804, the common woodlouse or slater.

P. scaber molts about every six weeks (Drobne and Štrus, 1996; Zidar et al., 1998) and before molt, its deposits can be clearly recognized as white spots on the first four anterior sternites (Fig. 5a). The formation of the deposits starts about one or two weeks before the posterior molt simultaneously at four spots near a median groove within each sternite, two in the anterior and two in the posterior region (Wieser, 1964; Messner, 1965). During premolt, these spots expand in surface and in thickness until they fuse to their characteristic shape. In consequence to this growth mode, the development of the deposits is more advanced in their initiation areas where they are thicker than in the more lateral areas. The fully developed deposits of each sternite have a bilateral symmetry with the median groove separating the two halves. Additionally, every half is divided into an anterior and a posterior part by an oblique ridge running from median to the lateral side (Figs. 5b, c).

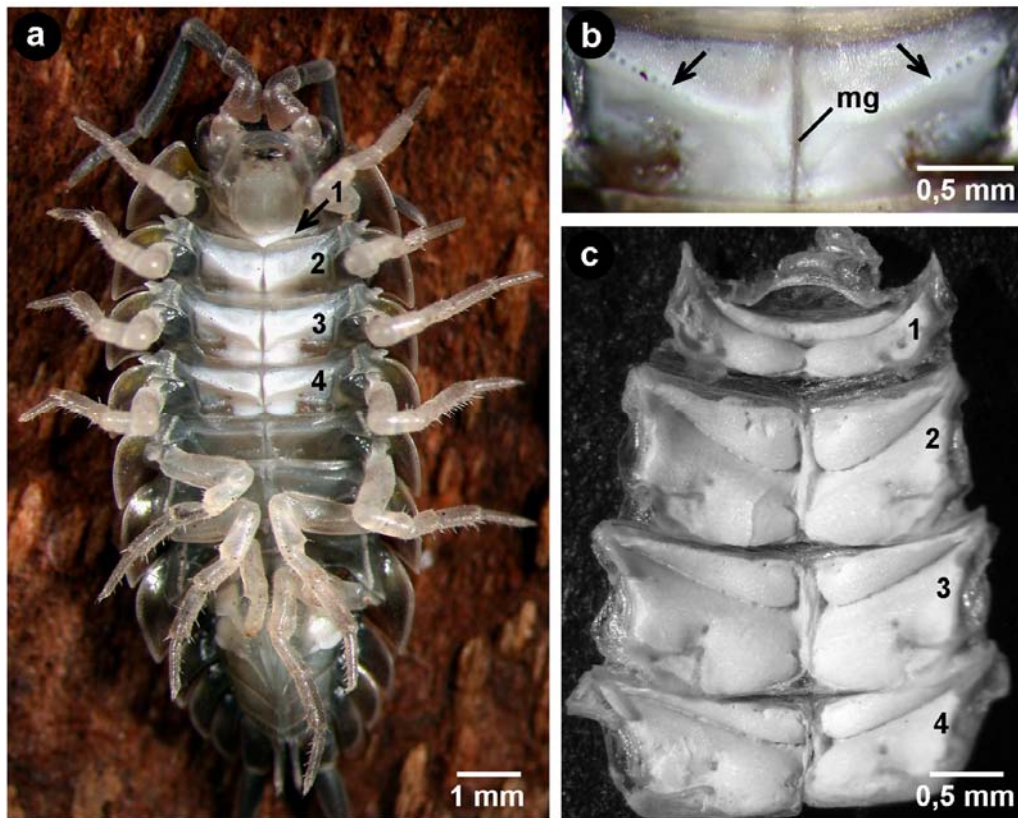


Figure 5. The sternal CaCO₃ deposits of *Porcellio scaber*. (a) Ventral view of *P. scaber* in late premolt stage showing the location of the CaCO₃ deposits on the first four anterior sternites (1-4). (b) At higher magnification the median groove (mg) which separates every deposit into two bilaterally symmetric halves can be observed. The arrows show the oblique ridges separating every half into a cranial and a caudal part. (c) Morphology of the proximal surface of dissected deposits (1-4) which are still attached to the cuticle.

Light microscopy of cleaved deposits revealed that they consist of a glassy layer adjacent to the cuticle secreting epithelium and an opaque layer adjacent to the old cuticle. Scanning electron microscopy (SEM) showed that the glassy layer is homogeneous, while the opaque layer consists of fused and free spherules typical for type II deposits (Fig. 2b). In *P. scaber*, the mostly fused spherules of the distal spherular layer (dsl) have diameters of about 500 nm while the individual spherules of the proximal spherular layer (psl) have diameters ranging from 500 nm in the distal regions up to 2 μ m in the proximal regions (Ziegler, 1994). Immediately after the posterior molt is completed, the deposits start to degrade and are completely resorbed in less than 24 hours.

Investigation of the deposit material in a transmission electron microscope (TEM) using electron diffraction resulted in the appearance of diffuse rings, indicating that the CaCO₃ is not in crystalline but in an amorphous state (Ziegler, 1994). Amorphous calcium carbonate (ACC) is known to be about ten times more soluble than crystalline CaCO₃ (Brečević and Nielson, 1989) and is therefore particularly suitable for transient calcium storage (Meldrum, 2003). The high solubility of ACC together with the large surface area of the spherular parts of the deposits

facilitate the quick mobilization of CaCO_3 during the short intramolt phase. Although ACC is unstable *in vitro*, an ever increasing number of reports show that it is stable in a variety of biological systems, where it fulfils a number of different roles (Baeuerlein, 2004; Epple, 2003; Weiner et al., 2003). It has been suggested to play a role as a transient precursor for crystalline CaCO_3 in sea urchin larval spicules (Beniash et al., 1997), in larval shells of the freshwater snail *Biomphalaria glabrata* (Hasse et al., 2000; Marxen et al., 2003) and of the marine bivalves *Mercenaria mercenaria* and *Crassostrea gigas* (Weiss et al., 2002). ACC was detected as final biomineralization product in plant cystoliths in the leaves of the rubber figs *Ficus retusa* and *Ficus microcarpa* (Taylor et al., 1993; Levi-Kalisman et al., 2002), in spicules of the ascidian *Pyura pachydermatina* (Aizenberg et al., 2002) and in the cuticles of the American lobster *Homarus americanus* (Levi-Kalisman et al., 2002), the isopods *Oniscus asellus* (Wood and Russell, 1987), *Porcellio scaber* and *Armadillidium vulgare* (Becker et al., 2004), where it is used for structural purposes. Finally, ACC also plays an important role in the transient storage of calcium, as shown for *P. scaber* (Ziegler, 1994) and the amphipod *Orchestia cavimana* (Raz et al., 2002). These studies have shown that there are significant structural differences between biogenic ACC phases, which are probably correlated with their different functions. In all these biological systems ACC remains stable over long periods of time, and therefore must be somehow stabilized in living organisms. A number of investigations have shown that biogenic CaCO_3 is always associated with an organic matrix consisting mostly of proteins which regulate crystallization (Mann, 1997; Coblentz et al., 1998). They influence the formation of specific crystal shapes and orientations and also which of the three main crystal phases of CaCO_3 is generated: vaterite, aragonite or calcite (Levi et al., 1998). These proteinaceous organic matrix components are also responsible for the stabilization of biogenic ACC (Aizenberg et al., 1996). TEM sections of decalcified *P. scaber* deposits have shown that they indeed contain such a matrix (Ziegler, 1994).

There is still little detailed knowledge about the processes of deposition, resorption and transient storage of cuticular CaCO_3 in the form of elaborately structured ACC deposits within the sternal ecdysial space of *P. scaber*. Some of the most prominent questions concern the process of spherule formation, especially how and where the initial spherules emerge, how the mineral and the organic matrix interact in this process, how spherules grow and what determines their final size. Another interesting issue is how the three structurally different layers of the deposits emerge and what causes the transition between them. It is still unclear how the spherules fuse in dsl, why this does not happen in psl and what causes the change from depositing mineral in the form of spherules to depositing homogeneous material towards the end of the premolt phase. Another issue arises from the position of the homogeneous layer lying

between the resorbing epithelium and the spherular layers. Due to their large surface area, spherules present the best possible deposit structure for quick dissolution after posterior molt, but the solid homogeneous layer seems to hamper this. The reason for this seemingly unfavourable deposition strategy has still to be elucidated. Furthermore, there is nothing known about how the organic matrix is organized within the deposits, its architecture remains to be investigated. There is no detailed information available about the components of the organic matrix. Finally, the evolutionary aspects of deposit morphology have to be discussed.

In the present work I have studied the complex processes taking place during formation and resorption of the sternal ACC deposits in *P. scaber* with the aim to resolve the issues summarized above. I investigated the structural changes during deposition and resorption as well as the ultrastructure of the organic matrix within the three different layers of the deposits and studied the process of spherule aggregation and dissolution using high resolution field emission scanning electron microscopy (HR-FESEM). Based on these results, the initiation of spherule growth was further investigated using TEM of deposits in early premolt stage. In collaboration with the groups of Prof. Matthias Eppele from the University of Duisburg-Essen and Prof. Ulrich Bismayer from the University of Hamburg we investigated the mineral phase of the deposits using high resolution X-ray diffraction (XRD), X-ray absorption spectroscopy (EXAFS) and reflection infrared microscopy (IR). In order to characterize the organic matrix I isolated the proteins of the sternal deposits and separated them using SDS polyacrylamide gel-electrophoresis (PAGE). An attempt was made to characterize selected components using Matrix-assisted Laser Desorption/Ionisation Time-of-flight (MALDI-TOF) mass spectrometry of proteolytic fragments.

The results show that the formation of the deposits is initiated within a specialized aggregation zone by the formation of nano-particles consisting of ACC and organic components. These particles aggregate forming spherical agglomerations, which further grow concentrically by continuous assembly of new particles at their surfaces. All three layers contain similar organic matrix structures, which form by self-assembly of proteins during deposit growth. Thus, the transition between the structurally different deposit layers can be explained by changes in the number of spherule nucleation sites, which also reflects the evolution of sternal CaCO_3 deposits in terrestrial isopods.

2. Results

2.1 Natural formation and degradation of the CaCO_3 deposits during the molt cycle (Fabritius and Ziegler, 2003)

Although formation and degradation of the sternal CaCO_3 deposits of *Porcellio scaber* during the molt cycle (Messner, 1965; Wieser, 1964) are well studied using light microscopy, the changes occurring on the ultrastructural level during these processes are still unknown. To study the formation of spherules and to investigate the sequence of events during formation and degradation of their three structurally distinct layers, deposits from animals in six different stages of the molt cycle were investigated using HR-FESEM.

In premolt, the animals form first the distal spherular layer (dsl) followed by the proximal spherular layer (psl) and the homogeneous layer (hl). The deposition of the dsl starts with the formation of a specialized aggregation zone which is located adjacent to the anterior sternal epithelium and has a soft, probably mucous consistency. This layer contains numerous, 20 nm thick filaments and granular structures with diameters between 10 and 30 nm (Fig. 6a). Spherular agglomerations of similar granules occur on the distal side of the aggregation zone, which increase in size with increasing distance from the aggregation zone and form spherules reaching diameters up to 200 nm. The surfaces of these early spherules consist of granules similar to those found in the aggregation zone (Fig. 6a). With the formation of spherules, the aggregation zone gradually separates from the cuticle. The size of the spherules increases from the regions adjacent to the aggregation zone to about 500 nm towards the more distal regions and remains constant in the older spherules. Later, the most distal spherules begin to fuse and show the typical appearance of the fully developed dsl (Fig. 6b). About two to three days before the posterior molt the first spherules which can be clearly associated to the psl appear. The aggregation zone is still present, but thin and discontinuous (Fig. 6c). As long as new spherules are formed during psl development distal spherules are larger than proximally and reach a final size of about 500 nm. In contrast to the earlier stages the spherules do not fuse any more (Fig. 6d). In the complete psl, the proximal spherules are larger than the distal ones, reaching diameters of up to 1.6 μm (Fig. 6e). With further deposition of CaCO_3 , the most proximal spherules get in contact to their neighbours and grow into polyhedron shaped structures (Figs. 6f, g). In the region proximal of this transition zone the hl is deposited. The material of the hl is compact and its proximal surface is formed of numerous, up to 15 μm wide spherical segments (Fig. 6h).

During the formation of the deposits, filamentous matrix elements are found frequently only in the aggregation zone and less abundant between the agglomerations of spherical granules

in its distal region. Occasionally, 20 nm thick filaments occur on the surface of spherules or interconnecting adjacent spherules.

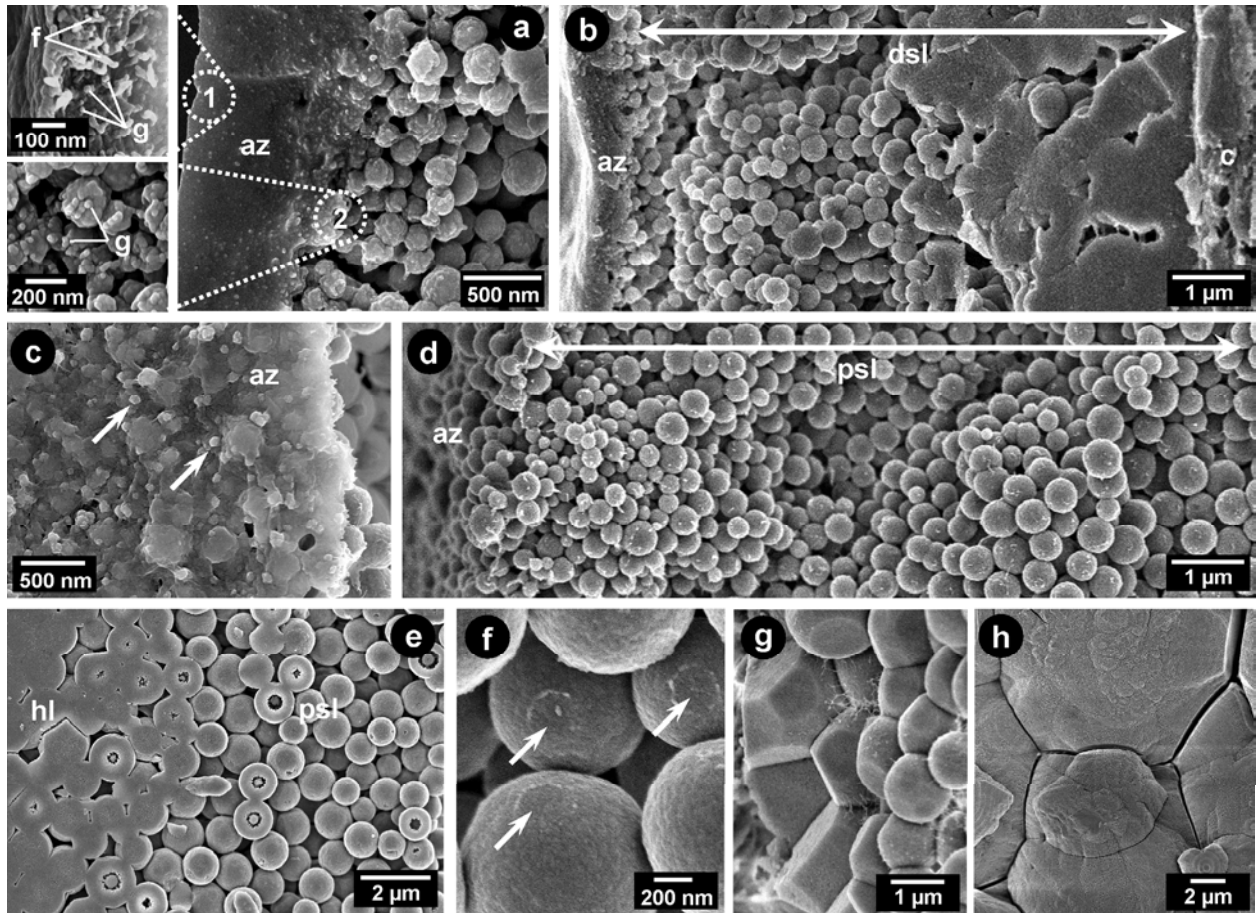


Figure 6. Formation of the sternal CaCO_3 deposits of *P. scaber*. (a) Cleaved aggregation zone in early premolt. Detail image 1 shows its structure with granules (g) and filaments (f) at higher magnification. Detail image 2 shows newly formed spherules with 10 to 30 nm thick granules on their surfaces. (b) Developing dsl in a later stage, size of spherules increases from proximal (left) to distal (right). Spherules near the cuticle (c) are fused. (c) During formation of the psl the aggregation zone is thin and discontinuous, but still contains granular structures in different sizes (arrows). (d) In developing psl, spherule size increases from proximal (left) to distal (right). (e) Transition between psl and hl, spherules increase in size from distal (right) to proximal (left) until they fuse. (f) Proximal spherules in fully developed psl with flattened surface areas (arrows). (g) Transition zone between psl and hl, the spherules fuse into polyhedron shaped structures. (h) Proximal surface of fully developed hl. aggregation zone (az); distal spherular layer (dsl); proximal spherular layer (psl); homogenous layer (hl).

The degradation of the deposits starts immediately after posterior molt and is finished in less than 24 hours. Investigation was carried out using animals dissected 1, 6, 12 and 20 hours after posterior molt. Surprisingly, the three layers are not dissolved exactly in the reverse order of deposition as expected. The first signs of degradation occur on the surface of hl, with the formerly smooth spherical segments becoming increasingly rough. On their margins, fissures and holes begin to appear which later widen and form deep crevasses that reach down into the psl

and expose the large surface area of the psl spherules (Fig. 7a). The spherules degrade in an unexpectedly complex manner. First, their surface roughness increases with the 10 to 30 nm wide granular structures becoming more prominent. Then, holes appear in the surface of the spherules, they occur frequently in the areas where the spherules are in contact with each other (Figs. 7b, c). The degradation of the now exposed core material leaves radial structures extending from the centre to the walls of the spherules (Figs. 7c, d). They are about 100 nm thick and are composed of granules with diameters between 20 and 50 nm (Fig. 7d). These radial structures and the outer walls of the spherules dissolve slower and are apparently more stable than the rest of the core material. In larger spherules, degradation often exposes an additional inner concentric spherular structure which also dissolves slower than the surrounding material. The spherules of the dsl degrade in a similar manner than those of the psl. Their core material is entirely degraded before the wall structures disintegrate into their granular substructures. In the regions with fused spherules, this leads to a sponge-like structure with holes interconnecting the lumina of the hollow spheres (Fig. 7e).

Shortly after the dissolution of the deposits commences, a thin, discontinuous degradation layer containing 20 to 50 nm thick matrix filaments appears on the proximal surface of the deposits. During the course of degradation its thickness increases from 100 nm in hl up to 800 nm in the distal regions of the dsl (Fig. 7e). After the deposits and the degradation layer have completely disappeared, the animals molt the anterior part of the body.

2.2 Ultrastructural organization of the organic matrix in fully developed CaCO_3 deposits (Fabritius, Walther and Ziegler, 2005)

Earlier investigations of the CaCO_3 deposits of *Porcellio scaber* using TEM have shown that both, the spherules and the homogeneous part contain an elaborate filamentous organic matrix (Ziegler, 1994). In order to increase our understanding of organic matrix organization, its ultrastructure was investigated with HR-FESEM. Decalcification experiments were performed to expose the structure of the organic matrix in all three layers of the deposits. Because parts of the organic matrix are dissolved together with the mineral compound during decalcification, a variety of decalcification protocols using ethylenediaminetetraacetic acid (EDTA) with and without glutaraldehyde (GA) for fixation of the proteins were employed. The effects of decalcification on the matrix structures were studied on the surface of whole deposits using EDTA solutions with 2.5% GA. With increasing degrees of decalcification, the surface roughness of spherules increases and more and more filamentous matrix components become exposed in the spherules and between them.

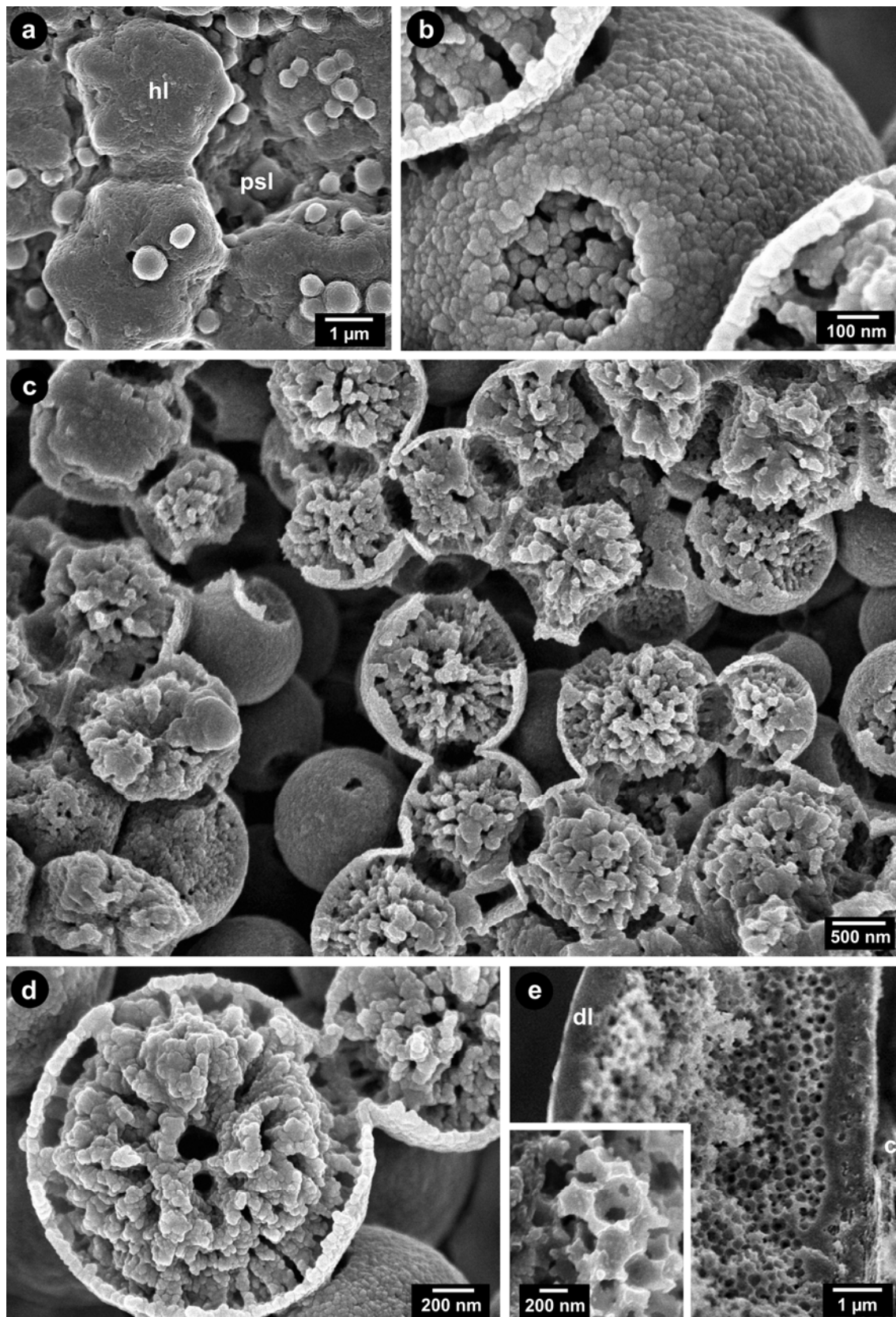


Figure 7. Degradation of the sternal CaCO_3 deposits of *P. scaber*. (a) Deep crevasses forming in hl expose the spherules of psl. (b) Dissolving psl spherules with holes appearing on the surface, preferably in the areas where neighbouring spherules are in contact. (c) Psl spherules in different stages of degradation exposing radial structures in the cores. (d) Detail of residual radial structures in degrading psl spherules. (e) Sponge-like residual structure of dsl in almost completely degraded deposits located between the cuticle (c) and the degradation layer (dl). distal spherular layer (dsl); proximal spherular layer (psl); homogenous layer (hl).

This process continues until their spherical structure is lost and large three-dimensional networks of probably reorganized filaments are left. Decalcification of deposits using EDTA without GA leaves large, diffuse clusters of 20 nm thick particles of fractal appearance which can also be observed at disintegrating walls of individual spherules. To study the organization of the matrix in the three different layers, deposits were sagittally cut and knife polished to obtain smooth surfaces. These surfaces were treated with decalcification solutions for up to 15 min and subsequently prepared for electron microscopy. The sagittal faces of samples mildly decalcified using Ches buffer (pH 10) for 5 min (without EDTA) show an inhomogeneous dissolution of the material in all three layers of the deposits (Figs. 8a-c). The fused spherules of dsl display characteristic polygonal patterns and dissolved areas around their centres (Fig. 8a). Spherules of psl also show dissolved areas around their centres which contain residual radial strands (Fig. 8b). In hl numerous stacked concentric lamellae appear (Fig. 8c). Micrographs of samples decalcified with EDTA show that the spherules of dsl consist of up to four 20 to 50 nm thick concentric layers containing particles with diameters between 10 and 40 nm. The concentric layers are interconnected by radial filament-like strands with diameters ranging from 5 to about 20 nm. Similar structures are also found connecting adjacent spherules (Fig. 8d). The spherules of psl display a similar matrix structure with the bigger spherules containing up to eight concentric layers connected by 5-20 nm thick radial strands. In many spherules the inner concentric layers seem to dissolve faster than those in the core and the peripheral areas, which often remain connected by the radial strands (Fig. 8e). The distances between the concentric layers do not differ significantly in spherules of dsl and psl. Images of spherules below the cutting plane reveal that the dissolving concentric matrix layers have a reticular structure consisting of filament-like strands with thicknesses of up to 20 nm similar to the radial strands connecting them (Figs. 8f-h). The hl consists of spherical segments originating from spherules in the transition zone between psl and hl (Figs. 8i, j), which show a similar pattern of stacked spherical layers interconnected by 5 to 20 nm thick radial strands (Fig. 8j). These results show that all three layers of the deposits contain similar matrix structures.

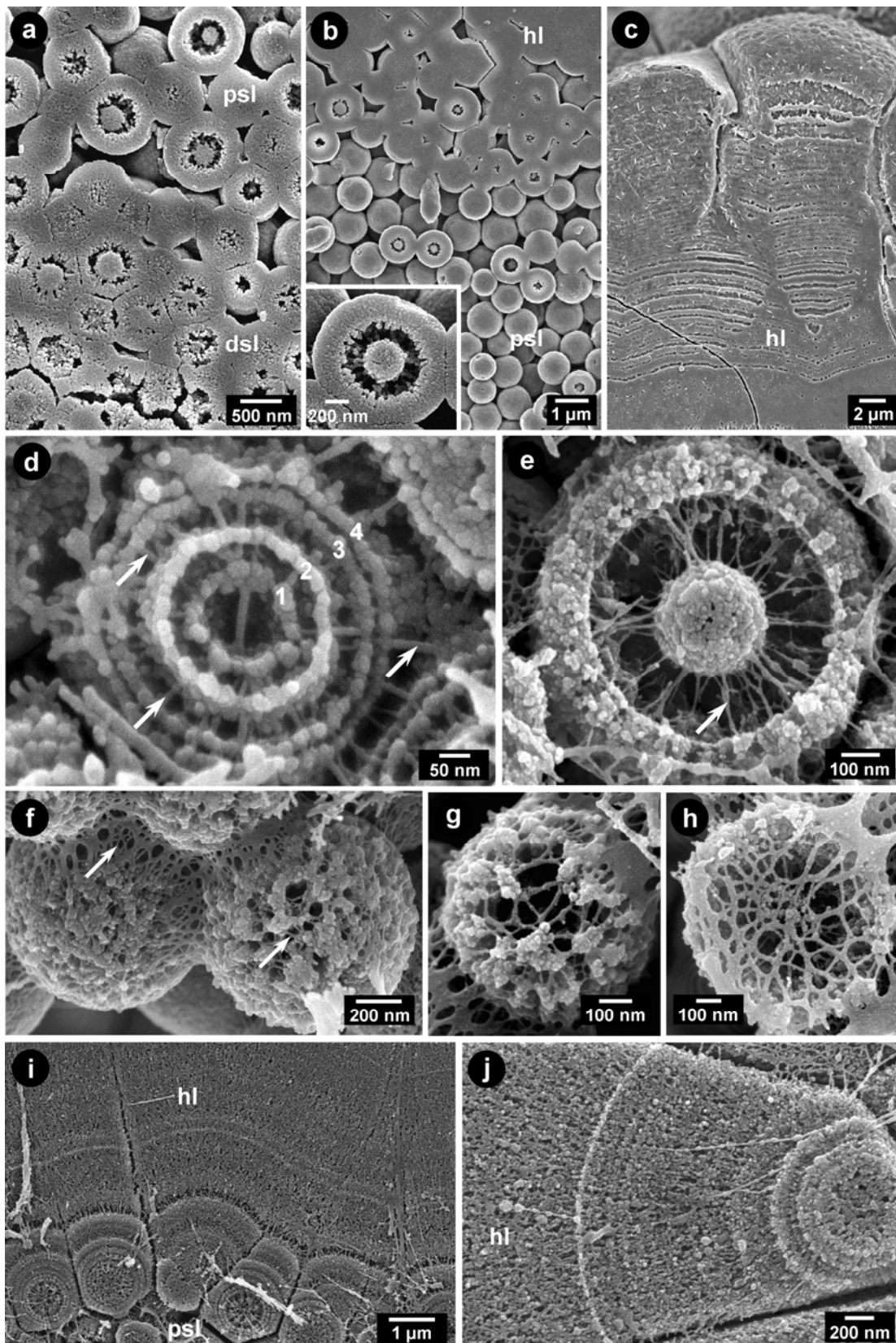


Figure 8. Dissolution behaviour of the sternal CaCO_3 deposits of *P. scaber* and structure of the organic matrix (a-c) Knife polished sagittal faces of deposits mildly decalcified using Ches buffer (pH 10; 5 min). (a) Transition between dsl and psl, fused dsl spherules show characteristic polygonal outlines. All spherules have dissolved areas around their centres. (b) Transition between psl and hl, the insert shows a psl spherule with residual radial strands around the dissolved area. (c) hl consists of numerous stacked concentric lamellae. (d-j) Deposits decalcified with EDTA in the presence of glutaraldehyde. (d) Concentric matrix layers (1-4), shown exemplarily for a dsl spherule. They

are interconnected by radial filament-like strands (arrows) which also connect adjacent spherules. (e) Example of a decalcified spherule with an inner spherical structure connected to the outer wall by radial strands. The outer wall contains 10-40 nm thick particles. (f) Concentric reticules within the outer wall of the spherules and between adjacent spherules (arrows) appear when the nano-particles at the spherule surface dissolve. (g) The concentric matrix layers consist of reticular structures formed by filament-like strands. (h) Inner side of spherule residue consisting of reticular concentric matrix. (i) Transition zone between psl and hl. (j) Matrix structure in hl.

2.3 Structural characterization of the mineral phase in fully developed CaCO_3 deposits (Becker et al., 2003).

Early investigations of the mineral phase in the sternal CaCO_3 deposits of *Porcellio scaber* using electron diffraction have shown that it consists of amorphous calcium carbonate (ACC) (Ziegler, 1994). The structural data published for different ACC phases make it evident that biogenic ACC occurs in a number of structurally different variations which is probably due to different mechanisms of formation and stabilization (Levi-Kalisman et al., 2002; Epple, 2003). Therefore, the structure of ACC within fully developed and air dried sternal CaCO_3 deposits of *P. scaber* in the late premolt stage were characterized using HR-FESEM, XRD, EXAFS (Extended X-ray absorption fine structure) and IR. For a short summary on the used analytical techniques see Appendix (Material and Methods, chapter 6.2). The analysis of cleaved surfaces of both the spherules and the homogeneous layer (hl) using HR-FESEM revealed that fully developed deposits consist of spherical particles with diameters from 10 to 30 nm. The XRD and EXAFS experiments were performed by Dipl.-Chem. Alexander Becker and Prof. Dr. Matthias Epple from the University of Duisburg-Essen at the Hamburger Synchrotronstrahlungslabor (HASYLAB) at Deutsches Elektronen-Synchrotron (DESY), Hamburg, at beamlines B2 and B4, respectively. The obtained X-ray powder diffractogram of ground deposit material was compared with the diffraction peak positions that would be expected for calcite and aragonite and shows no visible diffraction peaks. The obtained primary oscillations of the EXAFS spectra were Fourier transformed and fitted to a suitable model derived from crystalline CaCO_3 . The fitted result was then compared with aragonite, calcite, vaterite and monohydrocalcite. In the first coordination sphere (Ca-O), the calcium-oxygen distance of the *P. scaber* ACC phase resembles either vaterite or monohydrocalcite. The coordination number for Ca-O is closer to calcite, vaterite or monohydrocalcite than to aragonite. The higher shells are all weak, especially the characteristic fourth shell (Ca-Ca), which is important to distinguish between the crystalline CaCO_3 phases. The IR-spectroscopy was performed by Prof. Dr Ulrich Bismayer and co-workers from the University of Hamburg. IR-spectra of the spherular and the homogeneous regions of the *P. scaber* deposits show clearly distinguishable calcium carbonate signals resembling those of aragonite, calcite and vaterite.

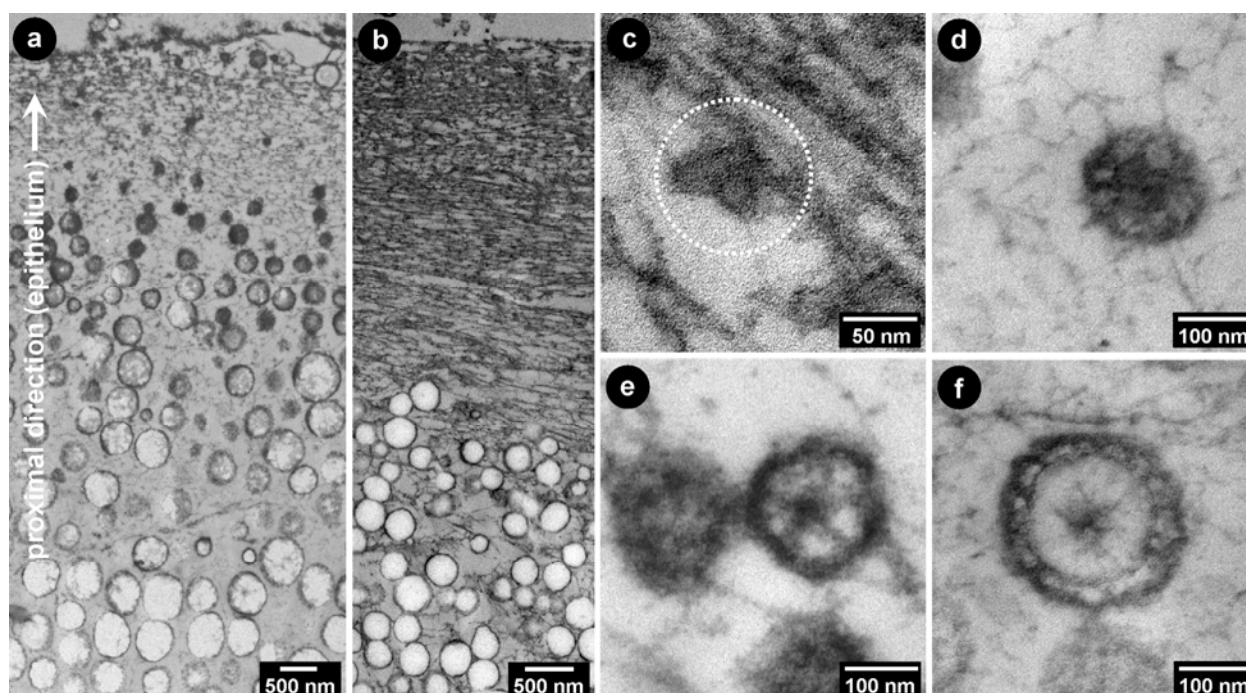


Figure 9. TEM micrographs of high pressure frozen and freeze substituted samples of the aggregation and growth zone of the deposits in the early premolt stage. (a) Filamentous network with interspersed granules and spherular structures whose sizes increase from proximal (adjacent to the epithelium) to distal (adjacent to the cuticle). (b) The density of the filamentous network decreases from the proximal to the distal areas of the aggregation zone. (c-f) Series of developing spherules. (c) Three 10 to 20 nm thick granules form a small aggregate connected to filaments (encircled area). (d) Larger, mulberry shaped aggregate of granules. (e) Aggregate of matrix granules with a vesicle like morphology. (f) Larger, spherule shaped aggregate from a more distal region of the aggregation zone with vesicle like structures in its periphery and radial filaments in the centre.

2.4 Ultrastructural investigation of the aggregation zone in early stages of deposit formation (for Material and Methods see Appendix, chapter 6.1.2, page 65)

HR-FESEM has shown that the spherules develop from agglomerations of small, 10- 30 nm thick granules in a specialized aggregation zone (see above). These agglomerations grow further in a concentric fashion through the formation of additional granules on their surface (Fabritius and Ziegler, 2003). Despite this mode of formation, the organic matrix incorporated in the spherules forms elaborate structures, consisting of concentric reticules and radial strands of filaments (Fabritius et al., 2005). To elucidate the formation of the spherules and how the matrix forms such complex structures, the aggregation zone of *Porcellio scaber* whose deposits had just started to grow were analysed using TEM. Two sets of samples using two different preparation methods were used. Dissected tissue containing the aggregation zone was high pressure frozen, freeze substituted and embedded in resin. Thin sections (60 nm) of these samples were viewed in a conventional Phillips 400 TEM (Fig. 9). 500 nm thick sections of chemically fixed decalcified deposits provided by PD Dr. Andreas Ziegler were viewed at an electron energy loss of $\Delta E = 30$ eV in a Zeiss CM 902 TEM (Fig. 10). The micrographs show that the aggregation zone is filled

with a dense network of long, ramified filaments (Figs. 9a, b; 10a). The density of this network gradually decreases from the proximal areas where the aggregation zone is bordered by the cells of the anterior sternal epithelium to the distal areas located near the old cuticle in the living animals. The main part of the filaments are oriented parallel to the adjacent epithelium. Small granules and larger spherical structures are interspersed in the filamentous network, and in most of the cases also connected with it (Figs. 10a, b). The spherical structures increase in size from the proximal side to the distal side of the aggregation zone (Figs. 9a, b). The granular structures have diameters of 10 to 20 nm. Occasionally, several of these granules are found forming small aggregates (Fig. 9c). The larger aggregates have the shape of a mulberry and consist of granules arranged in a concentric fashion around a smaller aggregate of granules (Fig. 9d). The mulberry shaped aggregates become successively larger and the matrix granules become more and more vesicle-like (Figs. 9e, 10c). In the more distal areas of the aggregation zone, the aggregates have the shape of small spherules covered with vesicle like structures and their centres contain radial filaments (Fig. 9f).

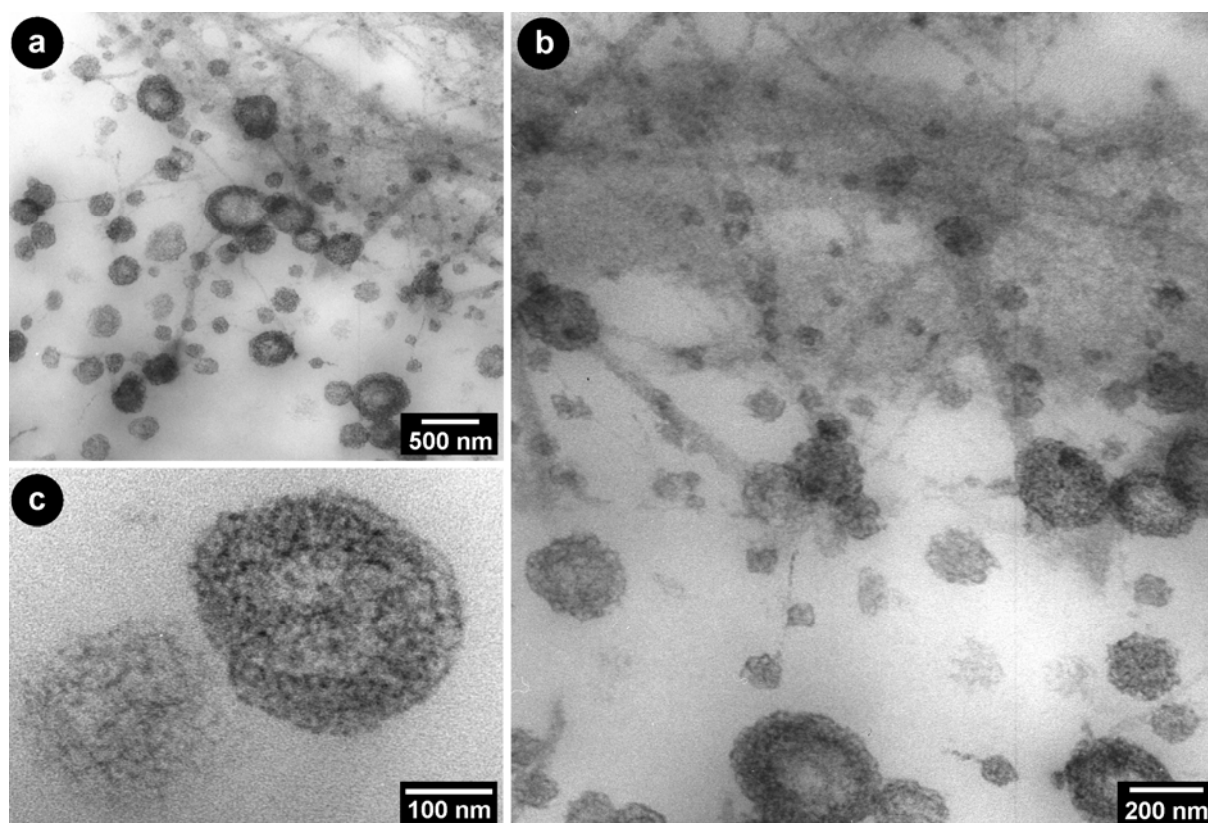


Figure 10. Energy filtered ($\Delta e = 30$ eV) TEM micrographs of 500 μm thick sections of chemically fixed aggregation zone. (a) Small granules and larger spherular matrix structures connected to long, often ramified filaments. (b) The spherular structures consist of aggregated small vesicle like structures giving them the shape of mulberries. (c) Mulberry shaped matrix aggregate viewed at a higher resolution.

2.5 Molecular characterization of the matrix proteins in the sternal CaCO_3 deposits (for Material and Methods see Appendix, chapters 6.1.3 – 6.1.5, pages 66-68)

In order to investigate the composition of the organic matrix present in the sternal CaCO_3 deposits of *P. scaber*, several attempts were made to characterize its components. For all experiments fully developed deposits from animals in late premolt stage were collected, pooled and demineralised using either aqueous EDTA solution (0.1M, pH 8.0) or Na-acetate buffer (pH 5.5-6.0) dialysed against double distilled water (ddw). In EDTA treated samples, the obtained solution containing the dissolved matrix was centrifuged and the supernatant was used to further investigate the water soluble components. The residual pellet was completely dissolved in Urea (8M), centrifuged and used to investigate the insoluble matrix components. SDS poly-acrylamid gel-electrophoresis (PAGE) of the water soluble fraction revealed at least seven different proteins, three strong bands at 76, 95 and 118 kD and four weak bands at 46, 50, 64 and 170 KD (Fig. 11a). The PAGE of the insoluble fraction revealed some very faint bands which were so weak that they were not considered significant enough for further investigation. The strong bands of water soluble proteins and, as a control experiment, a bovine serum albumin (BSA) band were excised, digested using trypsin and the obtained peptides were eluted. The proteolytic fragments were subjected to Matrix-assisted Laser Desorption/Ionisation Time-of-flight (MALDI-TOF) mass spectrometry, which was performed by Dr. Markus Wunderlin, Abteilung Pharmakologie und Toxikologie, in the Sektion Massenspektrometrie of the University of Ulm. While MALDI-TOF analysis of the BSA was successful, the analysis of the *P. scaber* matrix proteins failed.

In Na-acetate buffer treated samples, the isolated deposit material was transferred to dialysis tubing (MWCO 7000) containing double distilled water and decalcified against ddw followed by Na-acetate buffer (pH 5.5-6.0). Compared to the previous experiment, decalcification of the sample was much slower than in aqueous EDTA and ceased completely after some time leaving non-dissolved sample material. The obtained solution was centrifuged and the supernatant containing the water soluble matrix components was used for SDS-PAGE. The residual white insoluble pellet was solubilized with 8M urea and subsequently dialyzed against water followed by Na-acetate buffer pH 6.0. Further dissolution of the non-dissolved sample material could not be observed, and investigation of an aliquot with SEM and EDX revealed that its ultrastructure resembled the typical structure of partially decalcified deposits with still large amounts of CaCO_3 present. Therefore, the residual material was transferred to a Na-acetate solution containing 1% sodium dodecyl sulphate (SDS) which led to a quick dissolution. After centrifugation, this fraction was stored for further processing.

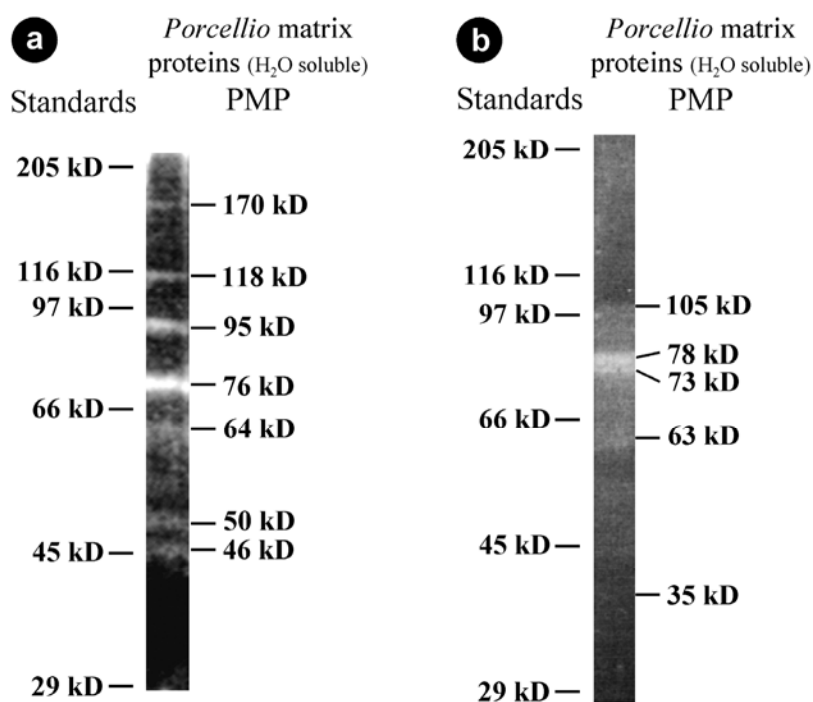


Figure 11. SDS poly-acrylamid gel-electrophoresis (PAGE) of the water soluble matrix fraction. **(a)** Obtained from deposits decalcified using aqueous EDTA solution (0.1M, pH 8.0). The gel reveals at least seven protein bands (PMP): three strong bands at 76, 95 and 118 kD and four weak bands at 46, 50, 64 and 170 kD. **(b)** Obtained from deposits decalcified in Na-acetate buffer (pH 5.5-6.0) dialysed against double distilled water. The gel reveals at least five protein bands (PMP): three strong bands at 63, 76 and 78 kD and two very weak bands at 35 and 105 kD (weak bands are not visible due to image quality limitations of the gel documentation system). Both gels were stained with Sypro Ruby. The standards used for determination of the molecular weight were carbonic anhydrase (29 kD), egg albumin (45 kD), bovine albumin (66 kD), phosphorylase B (97 kD), β -galactosidase (116 kD) and myosin (205 kD).

SDS-PAGE of the water soluble matrix fraction revealed at least five proteins with relatively strong bands at 78, 73 and 63 kD and very weak bands at 35 and 105 kD (Fig. 11b). The three strong protein bands, the BSA control and a blank sample were excised, digested using trypsin and processed for MALDI-TOF. The peptide mass fingerprints obtained from the mass spectra of the proteolytic fragments of the water soluble proteins (Figs. 12a-c) and BSA (Fig. 12d) were used to perform searches in various protein databases using the Mascot web interface (Perkins et al., 1999; www.matrixscience.com). While BSA was identified with a relatively high confidence factor, the mass fingerprints obtained for the matrix proteins yielded no satisfying results.

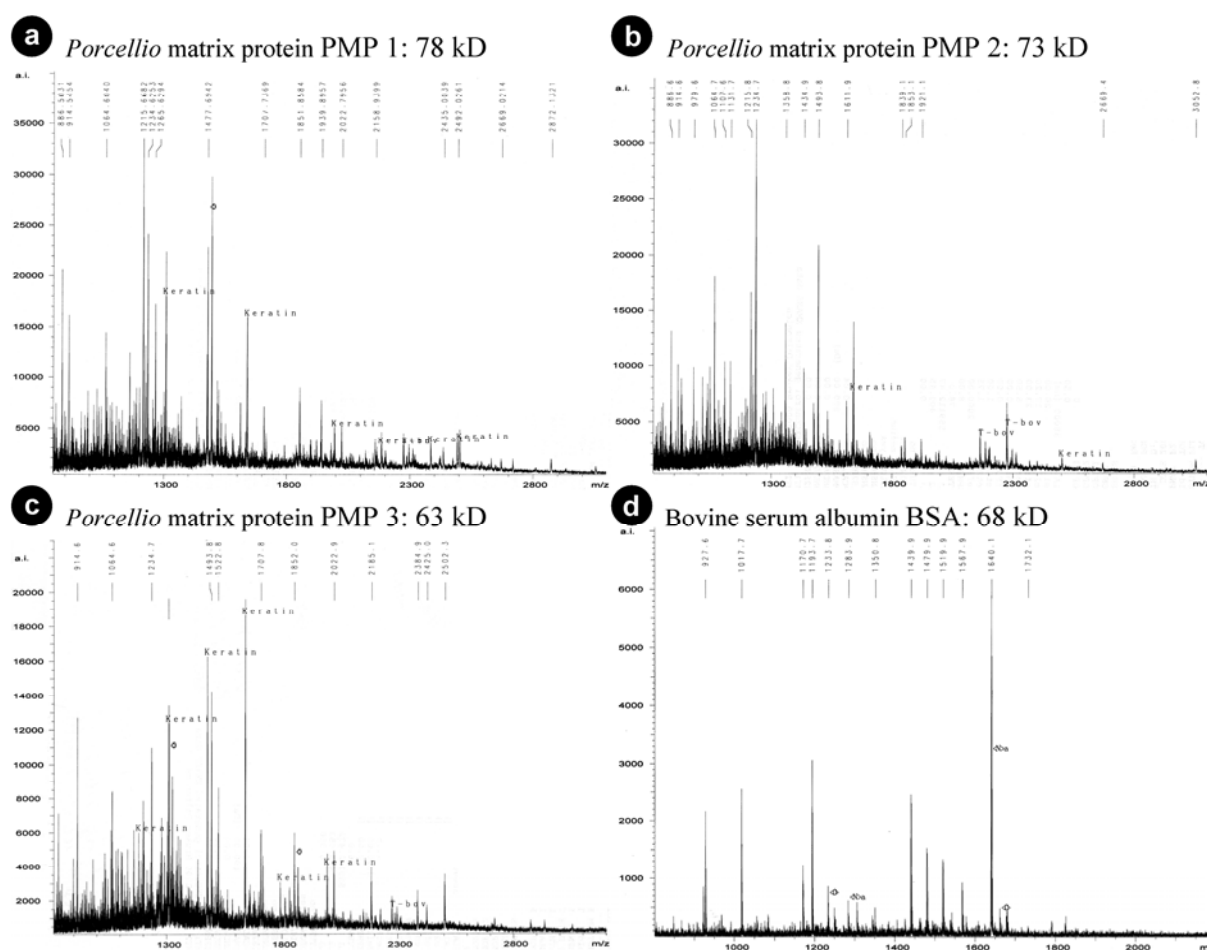


Figure 12. MALDI-TOF mass spectra of the proteolytic fragments of water soluble proteins isolated from the sternal CaCO_3 deposits of *P. scaber*. (a) PMP 1, molecular weight 78 kD. (b) PMP 2, molecular weight 73 kD. (c) PMP 3, molecular weight 63 kD. (d) Bovine serum albumin, used as control experiment.

3. Discussion

3.1 Formation of the deposits

The HR-FESEM analysis of developing deposits has led to a model that explains the growth pattern of spherules and the transition between the three structurally distinct layers of the deposits. Formation of spherules is initiated by the formation of small, 10-30 nm thick granular particles that form in a specialized aggregation zone (Figs. 6a, c). Agglomerations of similar granules occurring in the distal region of the aggregation zone suggest that spherules grow by aggregation of these small particles. The spherules grow further in a growth zone distally of the aggregation zone, as indicated by the successively increasing size of spherules in both dsl and psl (Figs. 6b, d). The absence of individual granules within the growth zone suggests that here the assembly of granules takes place directly on the spherule surfaces, leading to a concentric growth pattern. This and the fact that spherules of equal age and distance from the aggregation zone always have similar diameters further indicates that spherule nucleation takes place exclusively in the aggregation zone.

Polyhedral structures within the dsl observed in mildly decalcified sagittal faces suggest that spherules fuse to each other because concentric growth continues until most spaces between them are filled. It is of interest that within dsl the size of the spherules is more or less constant and rarely exceeds 500 nm, while the free spherules in psl grow larger depending on their distance to dsl with the largest spherules occurring proximally. Near hl individual spherules grow so large that they even fuse together in a similar manner as described above for spherules in dsl. This leads to the polyhedral structures found in the transition between psl and hl (Figs. 6f, g). As soon as all spaces between the spherules are filled the proximal surface of psl is closed and new material can only accumulate on the exposed surfaces of the most proximal spherules leading to the formation of hl (Fig. 6e). Thus, the transition between the deposition of psl spherules and homogeneous material can be explained by the continuous concentric growth of the most proximal psl spherules. Why spherules in psl do not fuse distally of hl and how the final size of individual spherules is determined cannot be completely clarified by the observations made during deposit formation. Several factors can be considered to determine the final size of spherules. One possibility is that at a certain distance from the aggregation zone the conditions within the medium surrounding the spherules become unfavourable for mineral deposition, possibly by a decrease in the concentrations of Ca^{2+} and HCO_3^- , but this does not explain the transition between fused and individual spherules. Another possibility would be that some components of the organic matrix of the spherules block the increase of size after a certain diameter is reached, which is supported by earlier reports of 50 nm thick wall structures of the

organic matrix at the surface of the spherules (Ziegler, 1994). The similarities in the nano-architecture of the organic matrix suggest that the structural differences between dsl, psl and hl result from changes in the deposition of mineral and matrix and not from different matrix components within the spherules. Initiation of the spherules as small granular structures and the decrease in spherule density between dsl and psl suggests that the transition between the layers is caused by a decrease in the number of nucleation sites from distal to proximal. Before the deposition of hl the nucleation of new spherules ceases. This results in continuous growth and fusion of the most proximal psl spherules, leading to the formation of hl. The broadening and narrowing of the stacked spherical calottes observed in knife polished and decalcified sagittal faces of hl indicate a competitive growth pattern of the stabilized ACC material. Profiles of circular concentric layers as observed in complete spherules are very rare on sagittal faces of hl which is also an indication that the formation of nucleation sites for new spherules has ceased almost completely in the stages of hl deposition. The decrease in size of the aggregation zone from 0,2 - 3,0 μm during dsl formation to a discontinuous layer of less than 200 nm during psl formation is possibly correlated to the proposed decrease in nucleation sites, since TEM micrographs show that initial granules and agglomerations of granules are in most cases connected to its filamentous network. Such filamentous matrix networks have been shown to act as nucleation sites for biominerals in extracellular mineralization processes in a large number of different organisms (Weiner and Dove, 2003). For Crustacea, proteinaceous nucleation sites for calcite formation were proposed for the postecdysial cuticle of the blue crab *Callinectes sapidus* (Shafer et al., 1995, Coblentz et al., 1998). However, it is important to note that spherule nucleation sites may be distinct from CaCO_3 nucleation. At the present stage of investigation we do not know the nature of spherule nucleation sites.

3.2 Degradation of the deposits

Degradation of the deposits is probably triggered by an increase in the activity of a V-type H^+ -ATPase within the apical plasma membrane of the anterior sternal epithelial cells, which pump protons to the deposits (Ziegler et al., 2004). The observations made during the SEM study of deposit degradation show that there are several mechanisms which speed CaCO_3 dissolution in addition to the fact that the mineral is amorphous and thus highly soluble (Brečević and Nielson, 1989). During the degradation of hl, deep holes and crevasses open into psl, enabling both the homogeneous material and the spherules to degrade simultaneously (Fig. 7a). A similar principle applies during degradation of individual spherules. The holes forming in the spherule surfaces lead to core material being degraded simultaneously to the surface walls and even within the core material the surface area increases, as indicated by the residual radial structures

appearing during dissolution (Figs. 7b, c). Since the spherules are composed of 10–30 nm large ACC granules stabilized by a proteinaceous matrix, this implies that variations occur in the stability of the ACC. This is supported by observations on decalcified deposits where the particles are often preserved in some of the concentric layers and at the surface of radial strands of the organic matrix. Moreover, the knife polished sagittal faces of deposits etched using Ches buffer also show that some areas in the spherules and hl dissolve faster than others (Figs. 8a, b). Therefore, one can assume that some particles must be stabilized to a higher degree than the dissolved material between radial strands and some of the concentric layers. This may be caused by differences in the matrix components incorporated in individual granules and those forming the concentric layers and radial strands. The degradation zone appearing on the proximal side of the deposits during degradation is very similar in appearance to the aggregation zone. Like the aggregation zone, it is located adjacent to the sternal epithelial cells, contains numerous filaments and seems to be of soft consistency. It may consist of accumulating matrix components that are degraded, probably by the action of hydrolytic enzymes. The increasing thickness of the layer observed during progressing deposit degradation suggests that it is resorbed at a slower pace than the mineral component.

3.3 Ultrastructure of organic matrix and ACC within the deposits

TEM studies of decalcified deposits have shown that the mineral in the homogeneous parts contains an organic matrix consisting of radial and concentric elements while the matrix of the spherules consists of filamentous meshes in the form of hollow spheres with a wall thickness of 50 nm (Ziegler, 1994). Since parts of the organic matrix can dissolve in addition to the mineral during decalcification, a detailed ultrastructural study of the organic matrix required the investigation of the effect of a wide variety of decalcification and fixation protocols. Best results were obtained with short incubation times (5–10 min) in aqueous EDTA (0.1M) solution containing 2.5% GA for fixation. The results showed that both the spherules of dsl and psl as well as the homogeneous layer contain virtually similar matrix components. All three layers contain matrix filaments with diameters ranging from 5 to 20 nm which constitute two different types of matrix structures: reticules that form concentric layers in spherules (Figs. 8d, e) or spherical calottes in hl (Fig. 8c), and radial strands, which connect the reticular structures (Fig. 8d). Statistical analysis of the distances between the concentric matrix layers shows that it is similar in the spherules of dsl and psl as well as in hl. In consequence, the difference in size between the spherules of dsl and psl results from differences in the number of concentric layers rather than differences in the distance between adjacent concentric layers. Apart from contributing to the development of the shape of the deposits, the organic matrix also stabilizes

the mineral component of the deposits, which consists of ACC in *Porcellio scaber* (Ziegler, 1994). It has been shown for other biological systems that an organic matrix consisting of specialized proteins stabilizes amorphous CaCO_3 (Aizenberg et al., 1996; Beniash et al., 1997; Boskey, 1998) and prevents crystal nucleation (Coblentz et al., 1998).

In recent years, increasing interest in biomineralization and the improvement of analytical methods have lead to the discovery of a large number of stable biogenic ACC phases in different organisms (Baeuerlein, 2004; Becker et al., 2004; Beniash et al., 1997; Epple, 2003; Levi-Kalisman et al., 2002; Raz et al., 2002; Weiner et al., 2003; Weiss et al., 2002). The formation of ACC seems to be particularly widespread in Crustacea (Addadi et al., 2003). The absence of any visible diffraction peaks in high resolution X-ray diffraction recordings of the sternal CaCO_3 deposits of *P. scaber* shows that the deposit material is fully X-ray amorphous (Becker et al. 2003), which is in accordance to earlier results obtained by electron diffraction (Ziegler, 1994). Although fully amorphous, X-ray absorption spectroscopy (EXAFS) of isolated deposit material of *P. scaber* shows that the material is not without structure. EXAFS provides information about the distance of the coordination spheres of crystalline material and is also used to characterize differences in the structure of ACC (Epple, 2003). Comparison with known crystalline CaCO_3 phases shows that the first coordination sphere within the deposits, which gives the distance between calcium and oxygen (Ca-O shell) and is characteristic for the short-range order resembles either vaterite or monohydrocalcite. The fourth shell which gives the distance between neighbouring calcium atoms (Ca-Ca) is very weak, indicating a high degree of disorder beyond the first shell. These results show that the ACC of the sternal deposits has a well-defined short-range order, but a particularly poor long-range order which is confirmed by comparison with EXAFS data of other biogenic ACC phases from literature (Taylor et al., 1993; Hasse et al., 2000; Levi-Kalisman et al., 2000; 2002; Marxen et al., 2003). Therefore, it can be assumed that the thermodynamic stability of the material is low, which leads to a high solubility. This is in accordance to the biological role of this ACC phase for temporary storage of calcium and carbonate during the molt cycle of *P. scaber*, in which the deposits have to be completely resorbed in less than 24 hours during the intramolt phase between posterior and anterior molt. The IR scattering signals of the spherular and the homogeneous regions of the deposits reveal the presence of nanocrystalline calcium carbonate with some degree of short range order. Together, these results propose a nanocrystalline material resembling either vaterite or monohydrocalcite with a particle size of the corresponding coherent lattice smaller than 10 nm, but larger than a few interatomic distances. Interestingly, high resolution field-emission scanning electron micrographs of all three layers of the deposits show that both the spherules and the homogeneous part consist of small spherical particles with diameters between 10 and 30 nm. These particles

are the smallest mineralized substructures found in *P. scaber* deposits. The coincidence of their size with the maximum particle size proposed by XRD, EXAFS and IR measurements suggests that they consist of just one or several ACC nanoparticles.

3.4 The role of the aggregation zone during deposit formation

The fact that the spherules and the homogeneous deposit material are formed by agglomeration of ACC nanoparticles raises the question how the elaborate concentric and radial matrix structures found within them form. Since both in SEM and in TEM unmineralized matrix components are rarely visible between the spherules, even not within the growth zone, matrix precursors must be already incorporated in the 10 to 30 nm large granules. This implies that both the radial and concentric matrix elements found inside the spherules organize themselves during growth of the spherules and the homogeneous layer. The matrix components inside the granules seem to reorganize themselves to vesicle like structures in the agglomerations, as indicated by the TEM micrographs (Figs. 9, 10). Later, these matrix components must somehow assemble with those of neighbouring granules and form the complex concentric and radial matrix structures found throughout the deposits. How the radial strands and concentric layers within mature spherules develop from the mulberry like structures, and to what extent components of the filamentous network of the aggregation zone become incorporated into the matrix of the spherules remains to be clarified.

Since the essential processes of ACC deposition take place in the aggregation zone and an adjacent growth zone extending over several μm one has to assume that the aggregation zone constantly provides mineral and matrix components to the deposits (Fig. 13). These components are most probably provided by the anterior sternal epithelial cells (Ziegler et al., 2005). Indeed, an earlier TEM study has demonstrated proteinaceous material at the apical side of the epithelium, which is probably secreted into the ecdysial space of the anterior sternites where the deposits form (Ziegler, 1997). In addition, it has been proposed that the Ca^{2+} concentration within the aggregation medium is under control of the anterior sternal epithelium. It has been shown that the expression of a plasma membrane Ca^{2+} -ATPase and a $\text{Na}^+/\text{Ca}^{2+}$ -exchanger increases during CaCO_3 -deposit formation (Ziegler et al., 2002). Moreover, x-ray electron-microprobe analysis of the elemental composition of freeze dried cryo-sections of shock-frozen epithelial cells revealed an increase in the number of areas with high calcium concentrations, indicating epithelial Ca^{2+} -transport (Ziegler, 2002). During deposit formation an increase of the cytoplasmic magnesium concentration has been detected within the anterior sternal epithelial cells. This suggests that epithelial Mg^{2+} transport takes place, since considerable concentrations of magnesium (150 mmol/kg dry mass) have been measured within spherules of the sternal

deposits (Ziegler, 2002). This is of particular interest, because it is known that Mg^{2+} ions can block the formation of calcite in the presence of biopolymers and therefore favour precipitation of amorphous CaCO_3 (Raz et al., 2000). The filamentous network observed within the aggregation zone using TEM (Figs. 9a, b, 10a, b) may contain components of the organic matrix of the deposits, but could also function as a medium that provides nucleation sites for new granules. Based on these observations, we can conclude that in the aggregation zone calcium and carbonate ions together with matrix components form small initial ACC granules with diameters between 10 and 30 nm. Probably these granules are of colloidal consistency to allow rearrangement of organic matrix components. They form irregular shaped agglomerations which become spherule shaped during further growth, either by aggregation or formation of further granules on their surface.

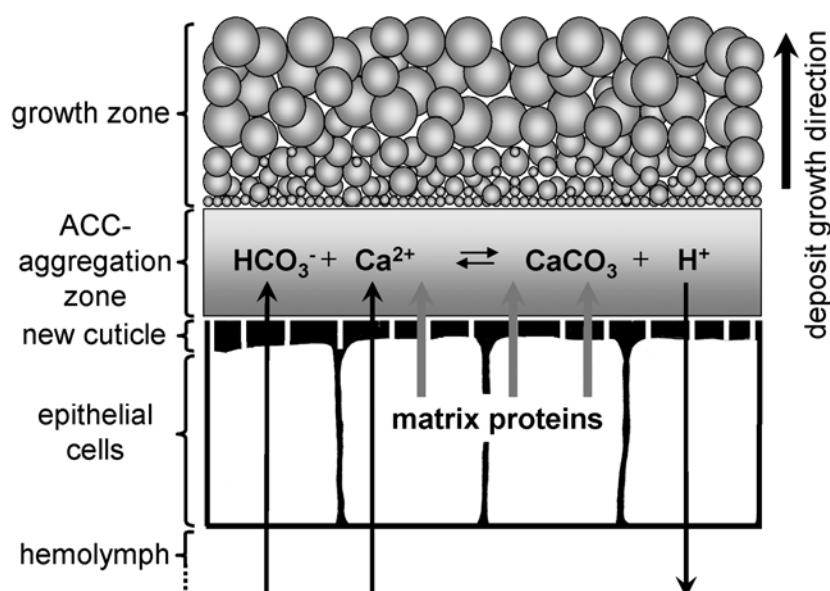


Figure 13. Schematic overview of the processes taking place during spherule formation in growing sternal CaCO_3 deposits. In a specialized aggregation zone, mineral and organic matrix components provided by the sternal epithelial cells nucleate forming ACC granules stabilized by incorporated matrix proteins. These granules aggregate forming larger spherular agglomerations which grow in a concentric fashion, probably through the nucleation of further particles on their surface. Image courtesy of PD Dr. A. Ziegler, modified.

3.5 Evolution of sternal deposits in terrestrial isopods (Oniscidea)

The investigation of the ultrastructure of the organic matrix in the sternal CaCO_3 deposits of *P. scaber* shows that the formation of the three structurally different layers can be explained by a reduction of spherule nucleation sites during their deposition. This change in number of nucleation sites also provides a possible explanation for the evolution of the complex three-layered type I deposits as found in *P. scaber* from primordial single-layered type III deposits during the adaptation to terrestrial life. Ziegler and Miller (1997) proposed that three-layered

deposits evolved from deposits with a single layer of free spherules as found in the semi terrestrial species *Ligia* over an intermediate stage with a distal layer of fused spherules and a proximal layer of free spherules as found in the wetland species *Ligidium hypnorum*. However, the sequence in which the three-layered deposits are formed in *P. scaber* (Fabritius and Ziegler, 2003) contradicts the evolutionary sequence. This conflict can be solved if we propose that during evolution of type II deposits the initial layer of free spherules is converted to one with fused spherules by an increase of the density of spherule nucleation sites. Possibly, this may have lead to the development of an intermediate type of deposit consisting of fused spherules only. Type II deposits may have evolved from such a hypothetical intermediate type if the initial overall increase in nucleation site density is followed by a decrease during deposit formation. Further modification of this sequence such that spherule nucleation ceases before the deposition of CaCO_3 is completed may have lead to the formation of homogeneous material and thus to the evolution of the three-layered type I deposits.

3.6 Molecular characterization of the organic matrix

The structural analysis of the sternal ACC-deposits of *P. scaber* and the investigation of early spherule formation have shown that proteinaceous matrix components play an important role in the development of the spherules by forming a scaffold of concentric reticules and radial strands. Furthermore, proteins are required to precipitate and stabilize the ACC of the deposits, as has been shown for polyanionic proteins which are responsible for CaCO_3 precipitation and the stabilization of ACC in other biological systems (Aizenberg et al., 1996; Boskey, 2003; Weiner and Dove, 2003). Indeed, gel electrophoresis of organic matrix extracted from deposits using aqueous EDTA solution (0.1M, pH 8.0) revealed that it contains at least seven water soluble proteins as well as some insoluble proteins. The attempt to characterize the isolated water soluble *P. scaber* matrix proteins using MALDI-TOF analysis yielded no satisfactory results, but the control experiment using BSA as standard was successful. Therefore, it can be assumed that the experimental setup was in principle appropriate to the task. Critical reflection identified the use of EDTA during sample decalcification as a possible reason for failure, since EDTA has been shown to bind irreversibly to proteins leading to the formation of aggregates. To avoid interaction of the proteins with salts, the second attempt was performed by dialysis of deposits against Na-acetate buffer (pH 5.5-6.0). This time MALDI-TOF analysis of the three obtained strong bands of water soluble proteins yielded mass fingerprints, however, no significant sequence similarities were obtained by search in protein databases. At this point, investigation was stopped due to the considerable time and effort necessary to obtain sufficient material for further experiments. In conclusion, the small quantity of proteins obtained from a considerable

amount of sternal deposits together with losses during the experimental procedure is likely to pose the major problem for characterization of the organic matrix, since there is not sufficient material available to optimize the experimental setup. Finally, there is still the possibility that the obtained peptide mass spectra actually represent proteins that simply do not match any data set in the consulted protein databases because similar proteins have not been described before. Nevertheless, the dissolution behaviour of the deposits in the dialysis experiment provides some hints about the nature of the organic matrix. After an initial phase of slow, but continuous dissolution a considerable amount of deposit material did not dissolve further, but retained the typical deposit ultrastructure. This indicates that components of the dissolving organic matrix in the supernatant protect CaCO_3 from dissolution. Repeated transfer of the sample to fresh decalcification medium showed only very little effect, suggesting an irreversible binding effect. Since the addition of SDS to the decalcification solution resulted in quick and complete dissolution of the deposit material, one can assume that some protein from the matrix prevents dissolution of the mineral, probably the same protein that inhibits crystallization during the formation of the ACC deposits by binding to crystal nucleation sites.

Further work on characterization of the organic matrix within the sternal ACC deposits of *P. scaber* requires the accumulation of substantially larger quantities of deposit material to allow for optimization of the protein isolation and purification protocol. The resulting larger quantities of individual proteins, both water soluble and insoluble, should enable more reliable MALDI-TOF experiments including partial sequencing at the ends of the proteolytic fragments which allows characterizing proteins that cannot be identified from the databases.

3.7 Summary of main conclusions

The ultrastructural investigations of deposit formation and degradation show that the formation of spherules is initiated within a specialized aggregation zone by the formation of granular nano-particles consisting of mineral and organic components provided by the anterior sternal epithelium. The mineral phase is ACC, which is stabilized by the proteinaceous organic matrix. Concentric growth of the spherules takes place in a growth zone extending several μm distal to the aggregation zone, possibly by continuous assembly of granules at the surface of the spherules. In all three layers of the sternal ACC-deposits the organic matrix forms concentric reticules connected by radial strands, most probably through a self-assembly process. The transition between the three structurally different layers can be explained by a reduction of the number of spherule nucleation sites during deposit formation. Such a change in the number of spherule nucleation sites during CaCO_3 deposition has probably also lead to the development of two and three layered deposits from primordial single layered deposits during the evolution of

terrestrial isopods. During degradation of spherules a maximum of surface area is exposed due to differential stabilisation of amorphous CaCO_3 by components of the organic matrix, which increases the speed of Ca^{2+} and HCO_3^- mobilization during the short intramolt phase.

4. References

- Addadi, L., Raz, S. and Weiner, S. (2003). Taking advantage of disorder: Amorphous calcium carbonate and its roles in biomineralization. *Advanced Materials* **15**, No. 12, 959-970.
- Aizenberg, J., Lambert, G., Addadi, L. and Weiner, S. (1996). Stabilization of amorphous calcium carbonate by specialized macromolecules in biological and synthetic precipitates. *Advanced Materials* **8**, 222-226.
- Aizenberg, J., Lambert, G., Weiner, S. and Addadi, L. (2002). Factors involved in the formation of amorphous and crystalline calcium carbonate: a study of an ascidian skeleton. *Journal of the American Chemical Society* **124**, 32-39.
- Auzou, M.-L. (1953). Recherches biologiques et physiologiques sur deux isopodes onisciens: *Porcellio scaber* Latr. et *Oniscus asellus* L.. *Annales des Sciences Naturelles* **15**, 71-98.
- Baeuerlein, E. (2004). Biomineralization, 2nd Rev. Wiley-VCH, Weinheim.
- Becker, A., Bismayer, U., Eppe, M., Fabritius, H., Hasse, B., Shi, J. and Ziegler, A. (2003). Structural characterisation of X-ray amorphous calcium carbonate (ACC) in sternal deposits of the Crustacea *Porcellio scaber*. *Dalton Transactions* **2003**, 551-555.
- Becker, A., Eppe, M., Ziegler, A. (2004). The mineral phase in the cuticles of two species of Crustacea consists of magnesium calcite, amorphous calcium carbonate, and amorphous calcium phosphate. *Dalton Transactions* **2005**, 1814-1820.
- Beniash, E., Aizenberg, J., Addadi, L. and Weiner, S. (1997). Amorphous calcium carbonate transforms into calcite during sea urchin larval spicule growth. *The Royal Society* **264**, 461-465.
- Boskey, A. L. (1998). Biomineralization: conflicts, challenges, and opportunities. *Journal of Cellular Biochemistry Supplements* **30/31**, 83-91.
- Boskey, A. L. (2003) Biomineralization: An Overview. *Connective Tissue Research* **44:1**, 5-9.
- Brečević, L. and Nielson, A. E. (1989). Solubility of amorphous calcium carbonate. *Journal of Crystal Growth* **98**, 504-510.
- Coblentz, F. E., Shafer, T. H. and Roer, R. D. (1998). Cuticular proteins from the blue crab alter in vitro calcium carbonate mineralization. *Comparative Biochemistry and Physiology Part B* **121**, 349-360.
- Drobne, D. and Štrus, J. (1996). Moults frequency of the isopod *Porcellio scaber*, as a measure of zinc-contaminated food. *Environmental Toxicology and Chemistry* **15**, 126-130.

- Eppler, M. (2003). Biomaterialien und Biomineralisation. B. G. Teubner Verlag, Wiesbaden.
- Erhard, F. (1997). Das pleonale Skelett-Muskel-System von *Titanethes albus* (Synocheta) und weiterer Taxa der Oniscidea (Isopoda), mit Schlussfolgerungen zur Phylogenie der Landasseln. *Stuttgarter Beiträge zur Naturkunde* **550**, 1-70.
- Fabritius, H., Walther, P. and Ziegler, A. (2005). Architecture of the organic matrix in the sternal CaCO_3 deposits of *Porcellio scaber* (Crustacea, Isopoda). *Journal of Structural Biology*, **150**, 190-199.
- Fabritius, H. and Ziegler, A. (2003). Analysis of CaCO_3 deposit formation and degradation during the molt cycle of the terrestrial isopod *Porcellio scaber* (Crustacea, Isopoda). *Journal of Structural Biology* **142**, 281-291.
- Graf, F. and Meyran, J.-C. (1985). Calcium reabsorption in the posterior caeca of the midgut in a terrestrial crustacean, *Orchestia cavimana*. *Cell and Tissue Research* **242**, 83-95.
- Greenaway, P. (1985). Calcium balance and moulting in the crustacea. *Biological Reviews* **60**, 425-454.
- Greenaway, P. and Farrelly, C. A. (1991). Trans-epidermal transport and storage of calcium in *Holthuisana transversa* (Brachyura: Sundathelphusidae) during premolt. *Acta Zoologica Fennica* **72**, 29-40.
- Gruner, H.-E. (1966). Isopoda, in Dahl, M. and Peus, F. (Eds.), Die Tierwelt Deutschlands und der angrenzenden Meeressteile, 53. Teil: Krebstiere oder Crustacea V: Isopoda, 2. Lieferung, pp. 151-380, VEB Gustav Fischer Verlag, Jena.
- Hasse, B., Ehrenberg, H., Marxen, J. C., Becker, W. and Eppler, M. (2000). Calcium carbonate modifications in the mineralized shell of the freshwater snail *Biomphalaria glabrata*. *Chemistry European Journal* **6**, 3679-3684.
- Laemmli, U.K. (1970). Cleavage of structural proteins during assembly of the head of bacteriophage T4. *Nature* **227**, 680-685.
- Levi, Y., Albeck, S., Brack, A., Weiner, S. and Addadi, L. (1998). Control over aragonite crystal nucleation and growth: An in vitro study of biomineralization. *Chemistry European Journal* **4**, 389-396.
- Levi-Kalishman, Y., Raz, S., Weiner, S., Addadi, L. and Sagi, I. (2000). X-ray absorption spectroscopy studies on the structure of a biogenic "amorphous" calcium carbonate phase. *Journal of Chemical Society, Dalton Transactions*, 3977-3982.

- Levi-Kalisman, Y., Raz, S., Weiner, S., Addadi, L. and Sagi, I. (2002). Structural differences between biogenic amorphous calcium carbonate phases using X-ray absorption spectroscopy. *Advanced Functional Materials* **12**, 43-48.
- Lowenstam, H. A. and Weiner, S. (1989). *On Biomineralization*. Oxford University Press, New York
- Mann, S. (1997). Biomineralization: the form(id)able part of bioinorganic chemistry. *Dalton Transactions* **2003**, 3953-3961.
- Marxen, J. C., Becker, W., Finke, D., Hasse, B. and Epple, M. (2003). Early mineralization in *Biomphalaria glabrata*: Microscopic and structural results. *Journal of Molluscan Studies* **69**, 113-121.
- Meldrum, F. C. (2003). Calcium carbonate in biomineralisation and biomimetic chemistry. *International Materials Reviews* **48**, 187-224.
- Messner, B. (1965). Ein morphologisch- histologischer Beitrag zur Häutung von *Porcellio scaber* Latr. und *Oniscus asellus* L. (Isopoda terrestria). *Crustaceana* **9**, 285-301.
- Neufeld, D. S. and Cameron, J. N. (1993). Transepithelial movement of calcium in crustaceans. *Journal of Experimental Biology* **184**, 1-16.
- Numanai, H. (1934). Calcium contents of the carapace and other organs of *Ligia exotica* during non-molting and molting phases. *Journal of the Faculty of Science, University of Tokyo, Sec. IV* **3**, 359-364.
- Passano, L. M. (1960). Molting and its control, in Waterman, T. H. (Ed.), *The physiology of Crustacea I*, pp. 473-536, Academic Press, New York.
- Perkins, D. N., Pappin, D. J. C., Creasy, D. M. and Cottrell, J. S. (1999). Probability-based protein identification by searching sequence databases using mass spectrometry data. *Electrophoresis* **20**, 3551-3567.
- Raz, S., Testeniere, O., Hecker, A., Weiner, S. and Luquet, G. (2002). Stable amorphous calcium carbonate is the main component of the calcium storage structures of the crustacean *Orchestia cavimana*. *Biological Bulletin* **203**, 269-274.
- Raz, S., Weiner, S. and Addadi, L. (2000). Formation of high-magnesium calcites via an amorphous precursor phase: possible biological implications. *Advanced Materials* **12**, 38-42.
- Schmalfuss, H. (2003). World catalog of terrestrial isopods (Isopoda: Oniscidea). *Stuttgarter Beiträge zur Naturkunde* **654**, Serie A, 341pp.

- Schminke, H. K. (1996). Crustacea, in Westheide, R. and Rieger, R. (Eds.), *Spezielle Zoologie Teil 1: Einzeller und Wirbellose Tiere*, pp. 501-581, Gustav Fischer Verlag, Stuttgart Jena New York.
- Shafer, T. H., Roer, R. D., Midgette-Luther, C. and Brookins, T. A. (1995). Postecdysial cuticle alteration in the blue crab, *Callinectes sapidus*: Synchronous changes in glycoproteins and mineral nucleation. *Journal of Experimental Zoology* **271**, 171-182.
- Sparkes, S. and Greenaway, P. (1984). The haemolymph as a storage site for cuticular ions during premoult in the freshwater/land crab *Holthuisana transversa*. *Journal of Experimental Biology* **113**, 43-54.
- Steel, C. G. H. (1993). Storage and translocation of integumentary calcium during the moult cycle of the terrestrial isopod *Oniscus asellus* (L.). *Canadian Journal of Zoology* **71**, 4-10.
- Štrus, J. and Blejec, A. (2001). Microscopic anatomy of the integument and digestive system during the molt cycle in *Ligia italica* (Oniscidea), in Kensley, B. and Brusca, R. C. (Eds.), *Isopod Systematics and Evolution*, pp. 343-352, Rotterdam.
- Taylor, M. G., Simkiss, K., Greaves, G. N., Okazaki, M. and Mann, S. (1993). An X-ray absorption spectroscopy study of the structure and transformation of amorphous calcium carbonate from plant cystoliths. *Proceedings of the Royal Society of London B* **252**, 75-80.
- Weiner, S. and Dove, P. M. (2003). An Overview of Biomineralization Processes and the Problem of the Vital Effect. *Reviews in Mineralogy and Geochemistry* **54** (1), 1-29.
- Weiner, S., Levi-Kalishman, Y., Raz, S. and Addadi, L. (2003). Biologically formed amorphous calcium carbonate. *Connective Tissue Research* **44** (Suppl. 1), 214-218.
- Weiss, I. M., Tuross, N., Addadi, L. and Weiner, S. (2002). Mollusc larval shell formation: Amorphous calcium carbonate is a precursor phase for aragonite. *Journal of Experimental Zoology* **293**, 478-491.
- Wieser, W. (1964). Über die Häutung von *Porcellio scaber* Latr.. *Verhandlungen der Deutschen Zoologischen Gesellschaft* **1964**, 178-195.
- Wood, S. and Russell, J. D. (1987). On the nature of the calcium carbonate in the exoskeleton of the woodlouse *Oniscus asellus* L.(Isopoda, Oniscoidea). *Crustaceana* **53**, 49-53.
- Zidar, P., Drobne, D. and Štrus, J. (1998). Determination of moult stages of *Porcellio scaber* (Isopoda) for routine use. *Crustaceana* **72**, 1-9.
- Ziegler, A. (1994). Ultrastructure and electron spectroscopic diffraction analysis of the sternal calcium deposits of *Porcellio scaber* Latr. (Isopoda, Crustacea). *Journal of Structural Biology* **112**, 110-116.

- Ziegler, A. (1996). Ultrastructural evidence for transepithelial calcium transport in the anterior sternal epithelium of the terrestrial isopod *Porcellio scaber* (Crustacea) during the formation and resorption of CaCO_3 deposits. *Cell and Tissue Research* **284**, 459-466.
- Ziegler, A. (1997). Ultrastructural changes of the anterior and posterior sternal integument of the terrestrial isopod *Porcellio scaber* Latr. (Crustacea) during the moult cycle. *Tissue & Cell* **29**, 63-76.
- Ziegler, A. (2002) X-ray microprobe analysis of epithelial calcium transport. *Cell Calcium* **31**, 307-321.
- Ziegler, A. (2003). Variations of calcium deposition in terrestrial isopods. In: Sfenthourakis, S., De Araujo, P.B., Hornung, E. et al. (Eds.), *The Biology of Terrestrial Isopods*, Crustaceana Monographs, vol. 2., Koninklijke Brill NV, Leiden, pp. 299–309.
- Ziegler, A., Fabritius, H. and Hagedorn, M. (2005). Microscopical and functional aspects of calcium transport and deposition in terrestrial isopods. *Micron* **36**, 137-153.
- Ziegler, A., Hagedorn, M., Ahearn, G.A. and Carefoot, T.H. (2007). Calcium translocations during the moulting cycle of the semiterrestrial isopod *Ligia hawaiiensis* (Oniscidea, Crustacea). *Journal of Comparative Physiology B* **177**, 99-108.
- Ziegler, A. and Merz, E. (1999). Membrane particle distribution in the sternal epithelia of the terrestrial isopod *Porcellio scaber* Latr. (Crustacea, Oniscidea) during CaCO_3 deposit formation and resorption, a freeze-etch analysis. *Journal of Structural Biology* **127**, 263-278.
- Ziegler, A. and Miller, B. (1997). Ultrastructure of CaCO_3 deposits of terrestrial isopods (Crustacea, Oniscidea). *Zoomorphology* **117**, 181-187.
- Ziegler, A. and Scholz, F. H. E. (1997). The ionic hemolymph composition of the terrestrial isopod *Porcellio scaber* Latr. during molt. *Journal of Comparative Physiology B* **167**, 536-542.
- Ziegler, A., Weihrauch, D., Hagedorn, M., Towle, D. W. and Bleher, R. (2004). Expression and polarity reversal of V-type H^+ -ATPase during the mineralization-demineralization cycle in *Porcellio scaber* sternal epithelial cells. *Journal of Experimental Biology* **207**, 1749-1756.
- Ziegler, A., Weihrauch, D., Towle, D.W. and Hagedorn, M. (2002). Expression of Ca^{2+} -ATPase and $\text{Na}^+/\text{Ca}^{2+}$ -Exchanger is up regulated during epithelial Ca^{2+} -transport in hypodermal cells of *P. scaber*. *Cell Calcium* **32**, 131-141.

5. Publications

5.1 Analysis of CaCO_3 deposit formation and degradation during the molt cycle of the terrestrial isopod *Porcellio scaber* (Crustacea, Isopoda).



Analysis of CaCO_3 deposit formation and degradation during the molt cycle of the terrestrial isopod *Porcellio scaber* (Crustacea, Isopoda)

Helge Fabritius and Andreas Ziegler*

Central Facility for Electron Microscopy, University of Ulm, 89069 Ulm, Germany

Received 8 November 2002, and in revised form 27 January 2003

Abstract

Terrestrial isopods store cuticular calcium in large sternal deposits composed of an amorphous CaCO_3 compound. A large part of the deposits consists of numerous small spherules that increase the exposed surface to facilitate resorption of CaCO_3 during cuticle mineralization. It is not known how these spherules are formed and how they are dissolved. This paper presents for the first time an analysis of ultrastructural changes occurring in the sternal CaCO_3 deposits of a terrestrial isopod during their formation and degradation. Our results indicate that formation of the spherules takes place in a specialized aggregation zone, in which 10- to 30-nm-thick granules form agglomerations that then increase in size to form spherules that reveal a concentric growth pattern. Degradation of the deposits occurs in a manner that exposes a maximum of surface area on all levels of their structural organization. © 2003 Elsevier Science (USA). All rights reserved.

Keywords: Amorphous; Biomineralization; Calcification; Decalcification; Ecdysis; Matrix; Molt

1. Introduction

Most crustaceans use CaCO_3 as the main mineral for hardening their cuticle so as to provide stability for their exoskeleton (Passano, 1960). Development and associated growth force crustaceans to replace their cuticle frequently. During ecdysis, most of the calcium is lost with the residual exuvia and must be replaced by absorption of the mineral from the environment (Neufeld and Cameron, 1993). Therefore, many crustaceans have evolved structures for Ca^{2+} storage, such as the gastroliths of semi-aquatic decapod species and those living in brackish or freshwater habitats (Greenaway, 1985). The greatest evolutionary pressure to store cuticular calcium is found in terrestrial crustaceans because they depend on calcium taken up with their diet. They have developed various storage sites such as the hemolymph in the decapod *Holthuisana transversa* (Sparkes and Greenaway, 1984) or caeca of the midgut in amphipods

(Graf and Meyran, 1985). Terrestrial isopods have evolved a variety of storage sites (Štrus and Blejec, 2001; Ziegler, 2002a), which include the sternal CaCO_3 deposits (Fig. 1a) in almost all terrestrial isopods. The latter are formed and degraded during the unique bi-phasic molt of isopods. Isopods molt first the posterior and then the anterior part of the body (Messner, 1965). During premolt, large amounts of CaCO_3 are resorbed from the posterior cuticle and stored between the cuticle and epithelium of the first four anterior sternites. During the short interval between the posterior and anterior molt (intramolt), the deposits degrade, and Ca^{2+} and probably also carbonate ions are used to mineralize the posterior cuticle (Steel, 1993; Ziegler and Scholz, 1997). The deposit of each sternite has a bilateral symmetry, with the halves separated by a median groove (Fig. 1b). An oblique ridge running from median to the lateral sides divides each half in an anterior (cranial) and a posterior (caudal) region. Formation of the deposits within each sternite starts almost simultaneously at four spots, two in the cranial and two in the caudal region (Messner, 1965; Wieser, 1964). These spots expand during premolt both in surface and in thickness, until

* Corresponding author. Fax: +49-731-502-3383.

E-mail address: andreas.ziegler@medizin.uni-ulm.de (A. Ziegler).

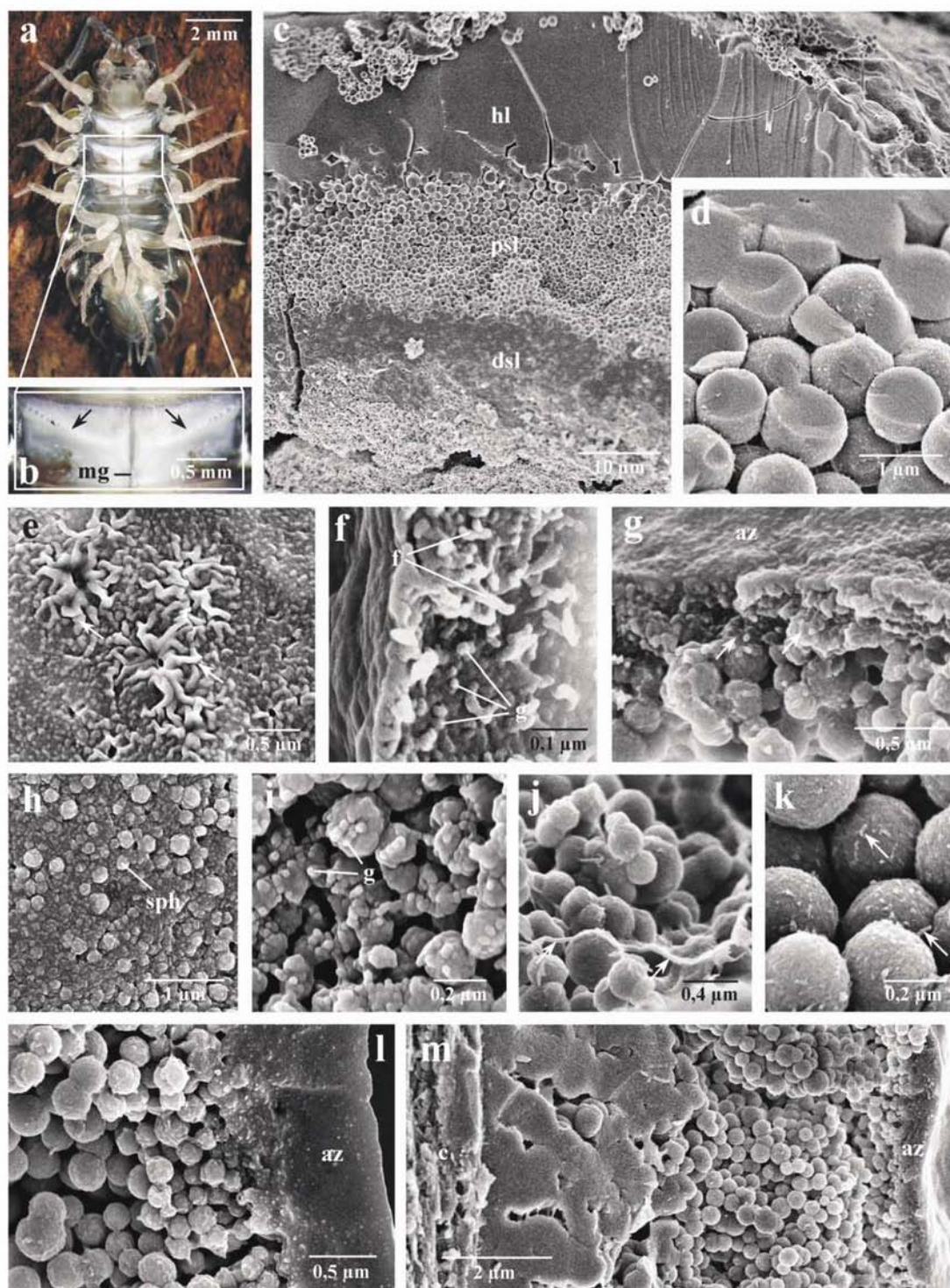


Fig. 1. The sternal CaCO_3 deposits of *Porcellio scaber* and the formation of the distal spherular layer. (a, b) Light micrographs showing the shape and appearance of the deposits in late premolt, oblique ridges (arrows), median groove (mg); for explanation see Introduction. (c) Profile of a fully developed deposit showing the characteristic appearance of the distal spherular layer (dsl), the proximal spherular layer (psl), and the homogeneous layer (hl). (d) Profile of the transition between psl and hl. The cleaved spherules are compact. (e, f) Structure of the aggregation zone in stage I. (e) Artificial wrinkles (arrows). (f) Cleaved surface exposing granules (g) between 10 and 30 nm in diameter and 20-nm-thick filaments (f). (g) Aggregation zone of stage II. Granules with diameters between 10 and 30 nm can be seen on agglomerations (arrows) within the aggregation zone (az). (h, i) Distal region of the aggregation zone in stage IV. (h) Spherical agglomerations of granules (sph) in increasing sizes. (i) Spherical agglomerations of granules (g). (j) Proximal region of developing dsl in stage IV, with horizontal filaments (arrows). (k) Free dsl spherules in stage IV. Filaments (arrows) with a diameter of 20 nm found on the surface. (l, m) Profile of developing dsl in stage IV, aggregation zone (az). (l) Size of spherules increases from proximal (right) to distal (left). (m) The spherules near the cuticle (c) are fused.

they fuse to their characteristic shape. As a result, the development at the initiation sites precedes that in more distal regions, where the deposits remain rather thin.

Previous studies revealed that the deposits consist of two distinct regions, a distal opaque region consisting of spherules and a proximal glassy layer of homogeneous nature (Ziegler, 1994). The spherular region is further divided into a distal spherular layer (dsl) with small, partially fused spherules and a proximal spherular layer (psl) consisting of free spherules (Figs. 1c and d), the diameters of which increase from distal to proximal (Ziegler and Miller, 1997). In all three layers CaCO_3 is associated with an organic matrix consisting of radial and concentric elements, suggesting that the organic components function as a template for spherule formation (Ziegler, 1994). The mineral phase of the deposits is amorphous upon high resolution X-ray visualization, with a primary particle size of a few nanometers (Becker et al., 2003). In what manner the organic matrix and the primary mineral particles aggregate during deposit formation is unknown. Amorphous CaCO_3 is considerably more soluble compared with crystalline phases (Brečević, 1989), and the small spherules of the psl and dsl provide a large surface of the CaCO_3 deposits, which should also facilitate their dissolution. Still, the solid homogeneous layer (hl) between the resorbing epithelium and the spherular layer would hamper a quick dissolution of the spherules.

To elucidate the sequence of events leading to spherule aggregation and dissolution, we analyzed structural changes within the CaCO_3 deposits during their formation and degradation using field-emission scanning electron microscopy. The results indicate that spherule formation is initiated in a specialized aggregation zone near the anterior sternal epithelium; furthermore, the dissolution of spherules occurs in an unexpectedly complex manner, in which those in the psl dissolve simultaneously with the resorption of hl.

2. Materials and methods

2.1. Animals

Porcellio scaber Latreille, 1804 were reared in the laboratory in plastic containers and fed with potatoes, carrots, and dry oak leaves. Molting stage was determined by the shape of the sternal CaCO_3 deposits according to Wieser (1964). For this, individual *P. scaber* were kept in small Petri dishes with water supply and pieces of dry oak leaves for food. Specimens used for studying formation and resorption of the CaCO_3 deposits were isolated after they completed a molt. The appearance of sternal CaCO_3 deposits was controlled on a daily basis until the sternal deposits developed to the desired premolt or intramolt stage. We used two isopods

in which the deposits had just started to appear (stages I and II according to Wieser, 1964), four isopods with halfway-completed deposits (stages IV and V), and three late-premolt isopods with more or less completely developed deposits (stage VI). In our isopods, stages I and II occur >7 days, stage IV 3–7 days, stage V 2–3 days, and stage VI 1 day before posterior molt. In nature, however, these time intervals depend on the season, climate, and food supply (Drobne and Štrus, 1996; Messner, 1965). For the analysis of degrading sternal deposits, two isopods were dissected 1 h, one isopod 6 h, two isopods 12 h, and two isopods ~20 h after posterior molt, when the deposits have almost disappeared.

2.2. Sample preparation

The isopods were decapitated and the first four sternites carefully dissected. To remove body fluids the sternites were rinsed in double-distilled water for 1 s and the washing water was quickly removed by dipping the specimens in 100% methanol for about another second. Then the specimens were air-dried overnight at 35°C. Previous studies using electron optical diffraction analysis (Ziegler, 1994) and high-resolution synchrotron X-ray diffraction analysis (Becker et al., 2003) have shown that this treatment does not lead to crystallization in the specimens. To expose structures between spherules, a few additional specimens from stage VI were fixed either in 90% ethanol with 2.5% glutaraldehyde for 4 h or in 0.04 M EDTA and 2.5% glutaraldehyde for 2 h. After dehydration in isopropanol, these specimens were critical point dried in a Baltec CPD 030 device. For electron microscopy, the dried sternites were separated from one another and mounted on sample holders using self-adhesive carbon pads. A part of the sternites were broken either sagittally or transversely so as to expose the inner cleaved surfaces. Mounted samples were rotary shadowed with platinum (2 nm) in a Balzers BAF 300 freeze-fracturing device and examined in a Hitachi S-5200 field-emission scanning electron microscope at acceleration voltages between 1.5 and 10 kV using a secondary electron detector. Photoshop 5.0 was used to adjust contrast and brightness of digital images. Because the deposits do not develop uniformly over the whole inner surface of the sternites, we concentrated our studies on the middle region. The figures presented in this paper show air-dried specimens unless specified explicitly in the legends.

2.3. Statistical analysis

The changes in size distribution of spherules were determined in 0.4- (stage IV) or 1.6- μm (stages V and VI)-wide intervals at various distances from the proximal edge of spherule-containing layers. The median, the 25th and 75th percentiles, and the highest and lowest

values were plotted using GraphPad 3.0 Prism software (San Diego, CA, USA; <http://www.graphpad.com>). Analysis of variance and Tukey's multiple comparisons tests were used to assign significant differences between the mean spherule diameters of the distance intervals.

3. Results

The formation of the distal spherular layer (dsl) in the stages I–IV (stages according to Wieser, 1964) requires ~70% of the total deposition time, whereas the rather thin psl and hl are quickly formed within stages V and VI of the premolt phase. The time of CaCO_3 deposition of ≥ 7 days (see Materials and methods) is somewhat longer than that reported previously by Drobne and Štrus (1996).

In stages I and II, deposition begins with the formation of a 200-nm to 1- μm -thick layer attached directly to the cuticle (Figs. 1e and f). This layer is of soft consistency as indicated by artificial wrinkles encountered in air-dried specimens (Fig. 1e) and will be designated here as "aggregation zone" (see Discussion). The layer contains numerous granular structures of diameters between 10 and 30 nm and 20-nm-thick filaments (Fig. 1f). Agglomerations of 10- to 30-nm-thick granules occur on the distal surface of the aggregation zone (Fig. 1g). Here, agglomerations of granules 50–200 nm in size can be observed (Figs. 1g–i). The surface of the spherules contains granules that resemble the individual granules within the aggregation zone (Fig. 1i). In stage IV, the aggregation zone reaches a thickness of $\leq 3\mu\text{m}$ and separates from the cuticle, leaving numerous spherules in between (Fig. 1m). In this stage, spherules along the cuticle have diameters of ~500 nm. The most distal spherules are often fused and show the typical appearance of the fully developed dsl (Fig. 1m). Near the aggregation zone the size of the spherules increases from proximal to distal areas (Figs. 1l, m, and 3a). Filamentous structures occur in two characteristic forms: long, ~50-nm-thick, more or less horizontally oriented filaments occurring occasionally between the more proximal regions of dsl (Fig. 1j); and small, 20-nm-thick filaments, visible at the surface of spherules (Fig. 1k). The completely formed dsl consists of spherules with a relatively constant diameter of 500 nm (not shown). The distal spherules appear to be embedded in a calcareous matrix, whereas more proximally areas with free spherules occur between areas of embedded or fused spherules (Fig. 1c).

Spherules, which can be clearly associated with the proximal spherular layer, do not appear until the shape of the deposits corresponds to stage V. The most proximal structure in the developing psl is a layer similar in appearance to the one found during development of the dsl, but not thicker than 200 nm; however, it is not

continuous but contains irregular openings (Figs. 2a and b). Granular structures of 10–30 nm in diameter can be found on the proximal side as well as within the layer, along with spherical agglomerations of granules or spherules with diameters between 50 and 250 nm (Figs. 2b–e). In a region ~7 μm distal to the aggregation zone, the size of spherules increases from proximal to distal (Figs. 2g and 3b). More distally, most spherules have a similar size of ~500 nm (Figs. 2g and 3b). In the complete psl, the proximal spherules are larger than the distal ones. Over a depth of 8 μm from the proximal border of psl, the size of the spherules decreases gradually from 1.6 μm to 500 nm (Figs. 2h and 3c). In spherules with diameters of ~1 μm and more, flattened surface areas can be seen at sites where they were in contact with other spherules (Fig. 2i). Spherules in all stages of development reveal granular structures of 10–30 nm on the surface (Fig. 2j). In the aggregation zone, matrix filaments with an exposed length between 100 and 200 nm and 10–20 nm thick can be found connecting individual spherules (Fig. 2d). Small, 10- to 50-nm-thick filaments with an exposed length of 50 nm can be found projecting from the surface of spherules. The same type of filaments was sometimes found to connect adjacent spherules (Figs. 2f and j). The completely formed psl varies between 10 and 20 μm in the middle regions of the deposits (Fig. 1c).

The homogeneous layer is the last to appear a few days before molt (between stages V and VI). It is formed by fusion of the most proximal spherules of the psl (Figs. 1c, d, 2h, and 4a). In the transition zone between psl and hl, the spherules merge and grow into structures of polyhedron-like appearance (Fig. 4a). In hl the borders between the structures become undistinguishable. The proximal surface of hl is formed of numerous spherical segments, $\leq 15\mu\text{m}$ wide, whose straight margins give it a characteristic polygonal pattern (Fig. 4b). The surface of these segments and that of cleaved surfaces have a fine texture exposing granular structures 10 nm in width (Fig. 4c). The complete hl is $\leq 50\mu\text{m}$ thick.

After the posterior molt is completed, the CaCO_3 deposits immediately start to degrade. The homogeneous layer is the first to show signs of degradation. The proximal, previously spherical segments flatten, and concentric rings appear on their surfaces (Fig. 4d). Between the spherical segments, fissures and holes begin to appear, the latter preferably at sites where at least three spherical segments merge (Fig. 4e). Spherical structures between 0.2 and 1.0 μm in diameter become visible, and the fissures and holes widen and finally form deep crevasses, surrounding column-like residues of hl (Fig. 4f). As soon as the crevasses in hl become deep enough, the spherules of the proximal spherular layer degrade simultaneously with hl. The first signs of degradation in psl is an increase in the roughness of the spherules'

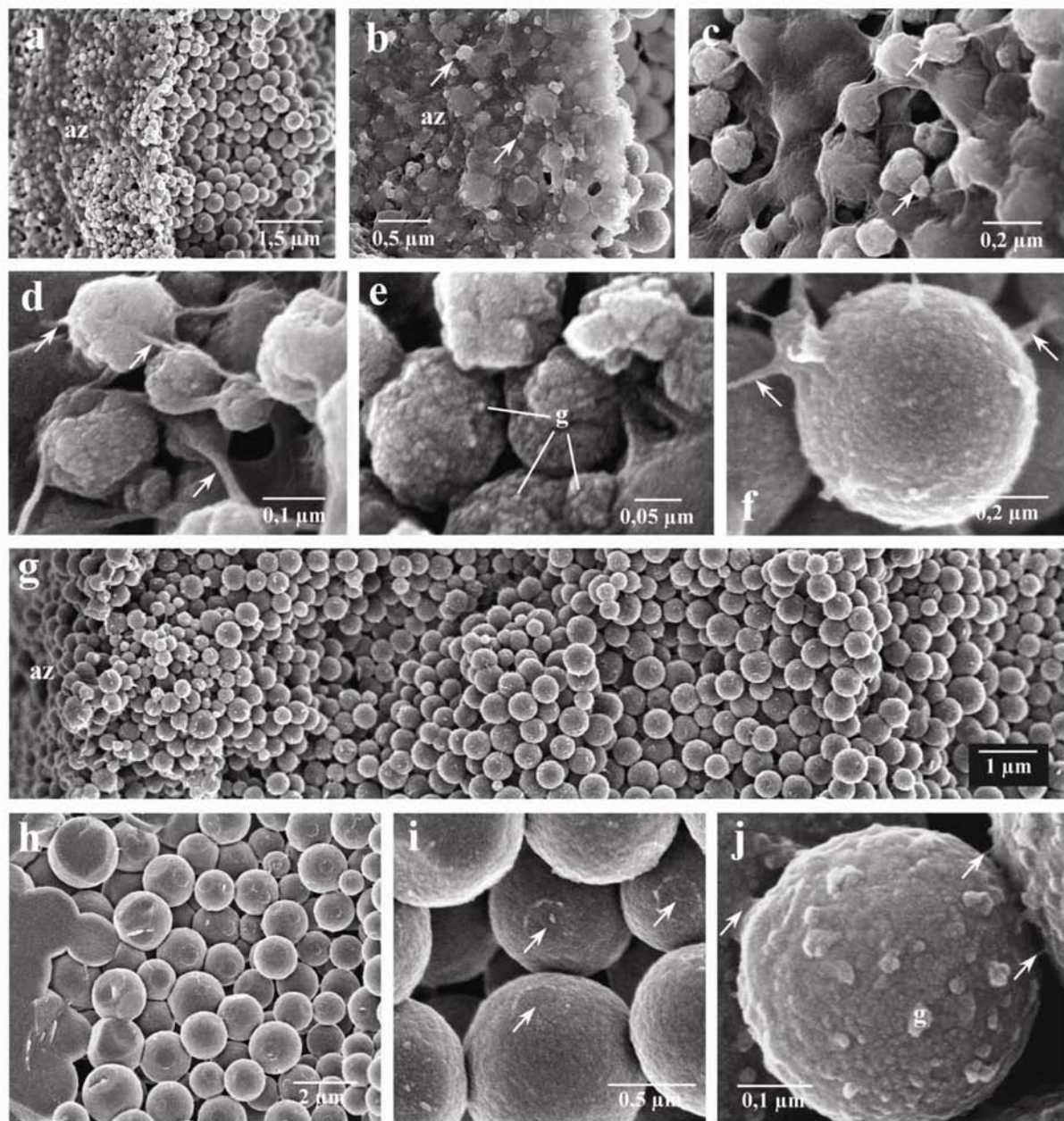


Fig. 2. Formation of the proximal spherular layer. (a–e) Structure of the aggregation zone (az) in stage V, (a) covers the already formed psl spherules as a thin and discontinuous layer. (b, c) Spherical agglomerations (arrows) within the aggregation zone (az). (d) Matrix filaments (arrows) connecting individual agglomerations. (e) Spherical agglomerations of 10- to 30-nm-thick granules (g). (f) Spherules within psl expose small filaments (arrows) on their surface (specimen treated with 90% ethanol with 2.5% glutaraldehyde and critical point dried). (g) Structure of the developing psl in stage V. Spherules increase in size from proximal (left) to distal (right). The spherules more distal to the aggregation zone (az) are of about the same size of 500 nm. (h–j) The proximal spherules in the fully developed psl. (h) Spherules increase in size from distal (right) to proximal (left). (i) Flattened surface areas (arrows) found in large spherules. (j) Detail of a small spherule found between the large spherules. The surface exposes numerous granules (g) and filaments (arrows), some of them <10 nm.

surfaces with the 10- to 30-nm granular structures becoming more prominent (Figs. 5a–c). Holes with diameters of ~200 nm form in the outer wall of the spherules, frequently in areas where spherules were in contact with one another (Fig. 5b). Then the core material is degraded, leaving radial structures extending from the center to the wall of the spherules. The radial structures

are ~100 nm thick and are composed of 20- to 50-nm-thick granules (Figs. 5d and e). Within spherules >1 μm in diameter, degradation exposes an additional inner concentric spherular structure ~400 nm in size (Figs. 5f and g). Radial structures ~120 nm long and 50 nm thick connect the inner spherules with the wall of the surrounding sphere (Fig. 5f).

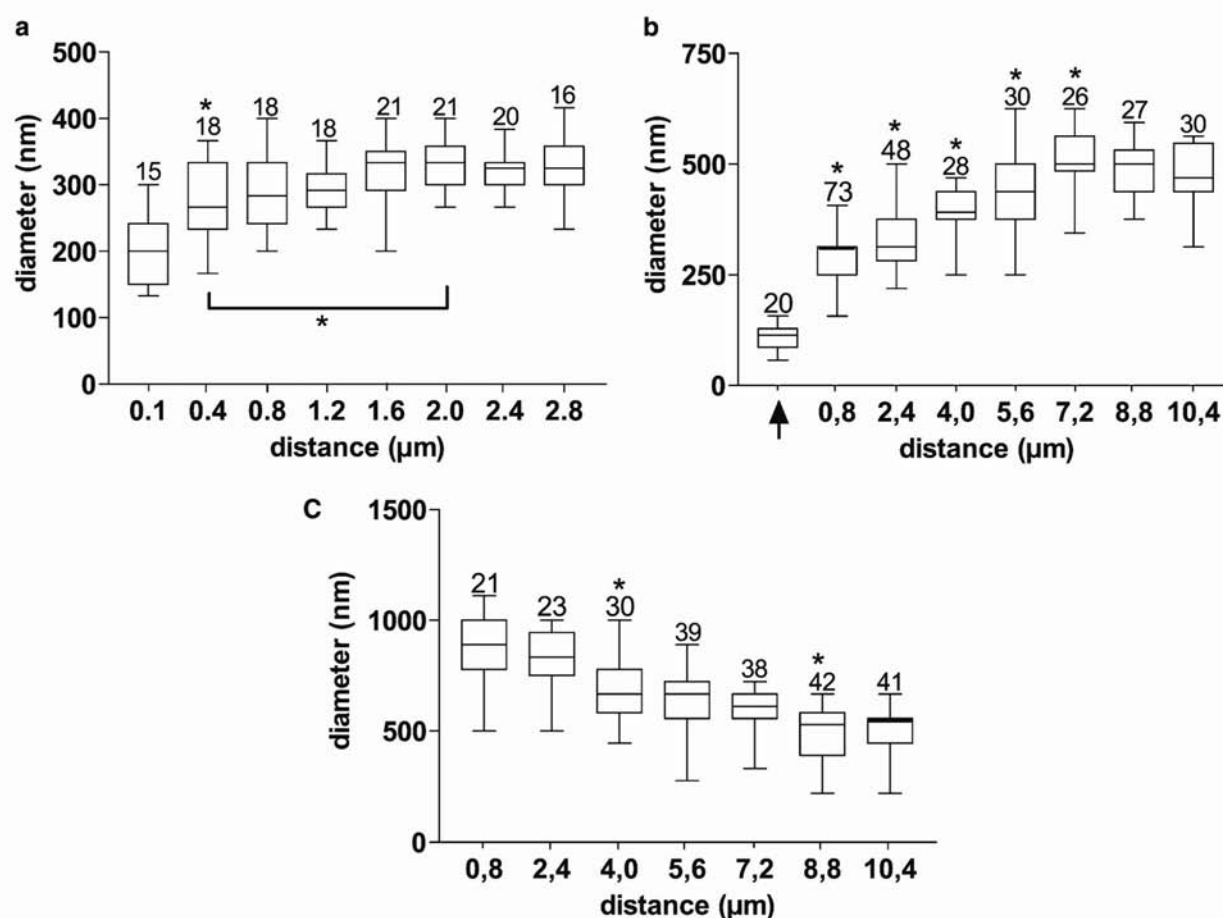


Fig. 3. Statistical analysis of spherule diameter versus distance for three different stages of deposit formation. (a) Analysis of an animal in stage IV during formation of dsl. Diameters measured from the distal edge of the aggregation zone in intervals of 0.2 μm for the first and 0.4 μm for the remaining measurements. (b) Analysis of an isopod in stage V during formation of psl. Diameters measured from the distal edge of the aggregation zone. Measurements for the first value (marked by arrow) were done on the proximal surface of the aggregation zone, all others in intervals of 1.6 μm. (c) Analysis of an isopod in stage VI, psl in fully developed deposits. Diameters of spherules measured distally of the psl–hl transition in intervals of 1.6 μm. The boxes extend from the 25th to the 75th percentile with a line in the median; bars above and below the boxes show the highest and lowest values. Numbers on top of the bars give the number of observations, and asterisks above the numbers indicate significant ($P < 0.01$) differences from the mean diameter of the preceding interval. The bracket indicates a significant ($P < 0.01$) increase of the mean diameter from the second to the sixth interval.

In the distal spherular layer, degradation starts after completion of the degradation of psl ~12 h after posterior molt. Degrading free spherules are similar in appearance to the ones in psl; however, they never exceed 500 nm in width. The core material is entirely degraded before the wall structures disintegrate into their granular substructures (Fig. 6a). Residual radial-shaped material as just described was not observed in spherules of the dsl. In the fused spherules the core material also degrades before their walls throughout the whole remaining dsl, leaving sponge-like structures with holes intercommunicating the lumina of hollow spherules (Figs. 6b, c, e, and f).

A discontinuous degradation layer, <1 μm thick, containing 20- to 50-nm-thick filamentous matrix structures, covers the degrading spherules of psl (Fig. 5a), and, later, of dsl (Figs. 6b and d). In the specimens

examined immediately after posterior molt, this degradation layer seems to be absent, but in later stages, where hl is still present, it covers large parts of its surface. The thickness of the degradation layer increases with advanced stages of degradation from 100 nm in hl to ≤800 nm in the distal regions of dsl. After the complete degradation of dsl and the degradation layer, the isopods molt the anterior part of the body.

4. Discussion

Our results show that formation of spherules in the distal (dsl) and proximal spherular layer (psl) takes place in a specialized aggregation zone near the anterior sternal epithelium. This is indicated by 10- to 30-nm-thick granules at the distal surface of the aggregation

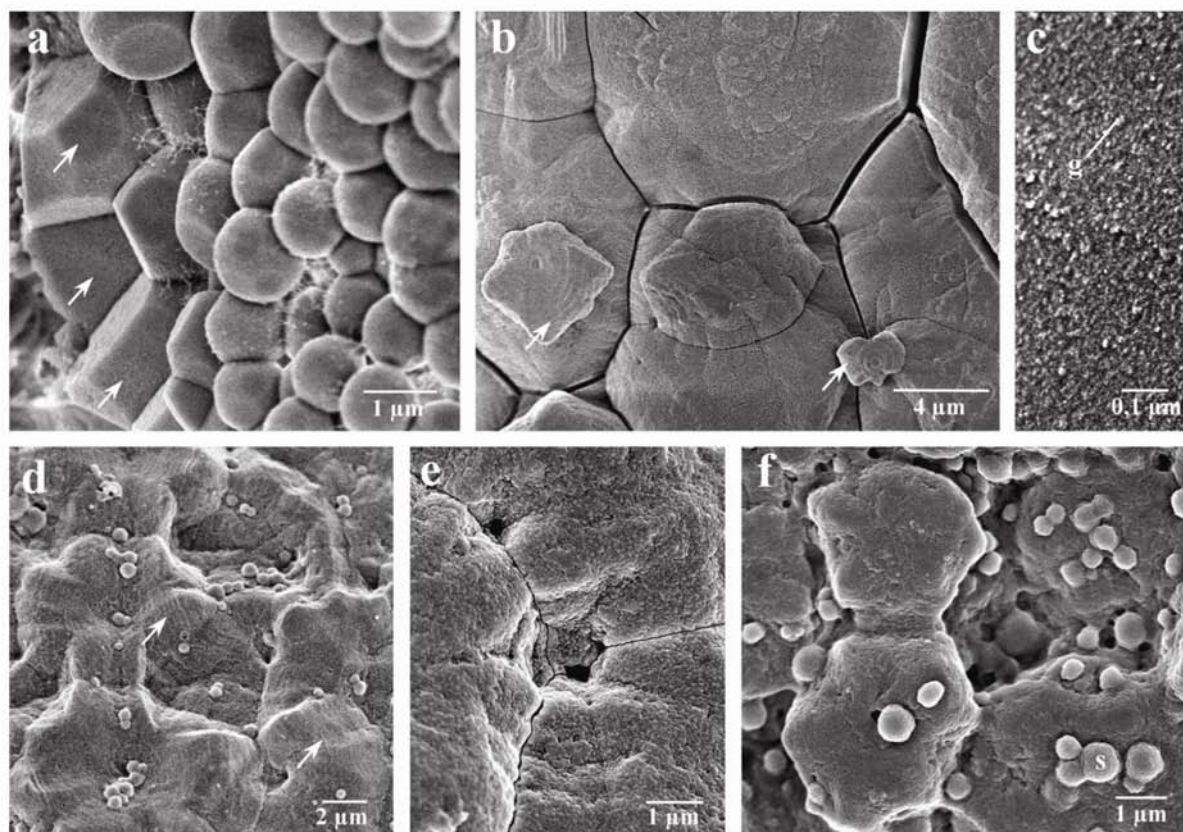


Fig. 4. Formation and degradation of the homogeneous layer. (a–c) Structure of hl, stage VI. (a) Transition zone between psl and hl; the spherules fuse into polyhedron structures (arrows). Note the filamentous structures in between (specimen treated with 0.04 M EDTA and 2.5% glutaraldehyde and critical point dried). (b) Polygonal pattern of spherical segments on the proximal surface of hl. Concentric structures can be seen on pieces lying upside down (arrows) (specimen treated with 90% ethanol and 2.5% glutaraldehyde and critical point dried). (c) Granular structures (g) on the surface of hl. (d, e) Degradating hl 1 h after posterior molt. (d) Concentric structures (arrows) on the proximal surface of hl. (e) Holes and fissures appear at the borders of the spherical segments on the surface of hl. (f) Degradating hl 6 h after posterior molt. Deep crevasses around residues of spherical segments expose more distal regions of hl and spherical structures (s).

zone, occurring along with agglomerations of increasing sizes and small spherular structures that apparently consist of particles similar to the individual granules. Furthermore, the size of the spherules increases from proximal to distal, also indicating initiation of spherule growth within the aggregation zone. The aggregation zone seems to be of a mucous or gel-like consistency, as suggested by the shrinking artifacts due to desiccation of the samples (Fig. 1e). Filamentous structures within the zone may be components of an elaborate organic matrix of the deposits, which forms hollow spheres near the surface, and radial components in large spherules and the homogeneous layer (hl) (Ziegler, 1994).

In light of our observations, we propose the following sequence of events during CaCO_3 deposit formation. After the initial assemblage of 10- to 30-nm-thick granules, aggregation of these granules leads to the formation of irregular agglomerations, which become spherule-shaped during further growth, probably by addition of more granules. In the initial layers, spherules grow within the aggregation zone. This is probably the

reason why the dsl is very dense near the old cuticle (Fig. 1m). Later, the aggregation zone separates from the cuticle, leaving free spherules in between. From this point onward, growth of spherules takes place in a region distal to the aggregation zone in both the dsl and psl. This is indicated by the successively increasing size of spherules within that growing zone (Figs. 1l, 2g, 3a, and b). Because we do not observe individual granules within the growing zone, it is likely that here the assembly of granular structures takes place directly on the surface of the spherules leading to a concentric growth pattern. In the dsl and distal regions of the psl, the spherules reach a limited size and do not grow further distal to the growing zone. How the final size of the spherules is determined during deposition remains to be clarified. It seems possible that at some distance from the aggregation zone the conditions within the medium surrounding the spherules become unfavorable for mineral deposition, possibly by a decrease in the concentrations of Ca^{2+} and HCO_3^- . Alternatively, some factor within the matrix of the spherules itself may block

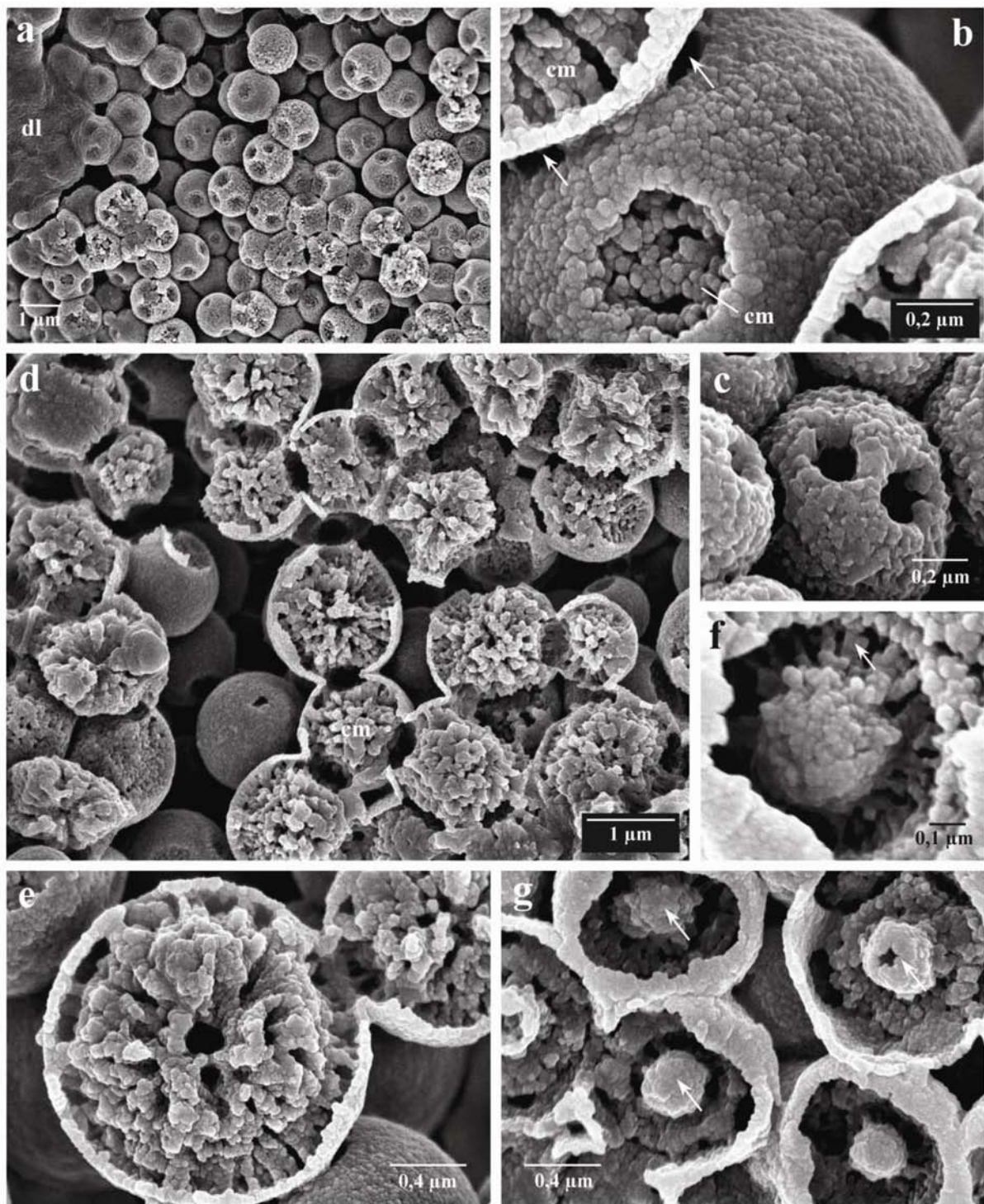


Fig. 5. Degradation of the proximal spherular layer, 6 h after posterior molt. (a) Beginning degradation of psl spherules, partially covered by the degradation layer (dl). (b) Detail of dissolving spherules. Holes appear on the surface, preferably in the areas where spherules are in contact with one another (arrows); cm, Core material. (c) Example of small spherule with holes. (d) Spherules in different stages of degradation exposing radial structures in the cores (cm). (e) Detail of residual radial structures in degrading psl spherules. (f, g) Degrading large spherules in the proximal areas of psl. (f) Radial structures (arrows) connect an inner spherular structure with the surrounding spherule. (g) Concentric spherular structures (arrows) exposed in the lumina of spherules $>1\ \mu\text{m}$ in diameter.

the increase of size after a certain diameter is reached. The latter is supported by earlier reports of 50-nm-thick wall structures of the organic matrix within the surface

of the spherules (Ziegler, 1994). It is of particular interest that, despite the assembly of spherules from small granules, the organic matrix can form elaborate spher-

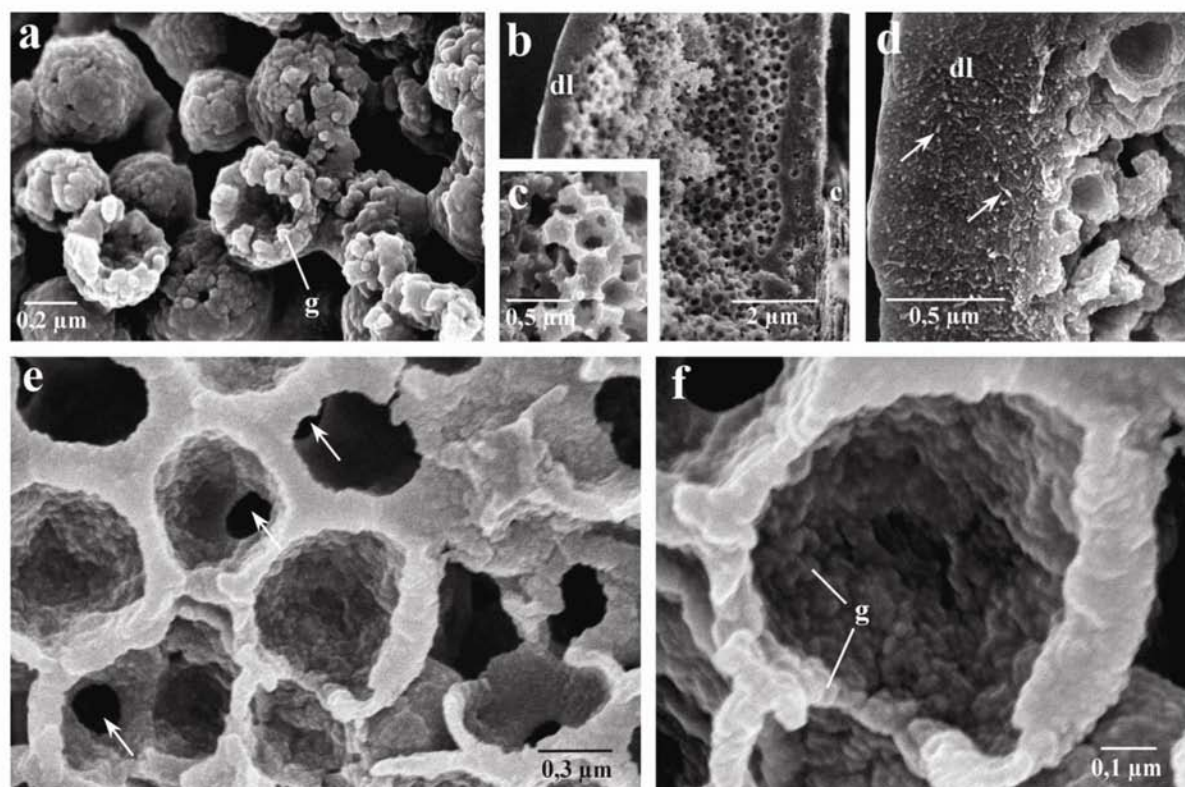


Fig. 6. Degradation of the distal spherular layer. (a) Degradation of free spherules in dsl 12h after posterior molt. Hollow spheres disintegrate into granular substructures (g). (b–f) Degradation of fused spherules in dsl 20h after posterior molt. (b) Degrading deposit, exposing a sponge-like residual structure between the cuticle (c) and the degradation layer (dl). (c) Detail of the sponge-like structure. (d) Detail of the degradation layer (dl), filaments between 20 and 50 nm in width (arrows). (e) Residual hollow spheres of degrading fused spherules with holes (arrows) interconnecting them. (f) Hollow spheres disintegrate into granular substructures (g).

ical and radial structures within the spherules of the sternal deposits (Ziegler, 1994). A likely explanation would be that during spherule growth, matrix components within aggregating granules are able to self-assemble with the matrix components of adjacent granules in an organized manner.

Differences in the thickness of the aggregation zone (e.g., 0.2–3.0 μm in dsl, 200 nm and discontinuous in psl) suggest that availability of some organic and/or inorganic component within the aggregation zone triggers the transition from the dsl to the psl by completely suppressing the ability of spherules to form fused structures. In the psl, the most proximal spherules continue to grow in contrast to the more distal ones. Even after individual spherules attach to each other, concentric growth continues until all spaces between the spherules are filled, leading to polyhedral patterns found in the transition between psl and hl (Fig. 4a). As soon as the proximal surface of psl is closed, mineral can only accumulate on the exposed surfaces of the most proximal spherules and hl starts to form.

The mineral in both the spherular and the homogeneous parts of the deposits is associated with an organic matrix consisting of radial and concentric elements as

revealed by transmission electron micrographs of decalcified deposits (Ziegler, 1994). Because unmineralized matrix components are rarely visible between the spherules, even not within the growth zone, matrix precursors must be incorporated in granules or their agglomerations. This implies that both the radial and concentric matrix elements found inside the spherules organize themselves during initiation and growth of the spherules and the homogeneous layer. The small filaments found projecting from spherules in dsl and psl and the filamentous structures within the aggregation zone support this hypothesis.

Our model implies that the aggregation zone constantly provides matrix components to the deposits. These components must be replenished, most probably by the anterior sternal epithelial cells. This inference is supported by transmission electron microscopy (Ziegler, 1997), demonstrating proteinaceous material at the apical side of the epithelium, which is probably secreted into the ecdysial space of the anterior sternites where the deposits are formed. In addition, the Ca^{2+} concentration within the aggregation medium seems to be under control of the anterior sternal epithelium. It has been shown that the expression of a plasma membrane Ca^{2+} -ATPase

and a $\text{Na}^+/\text{Ca}^{2+}$ -exchanger increases during CaCO_3 deposit formation (Ziegler et al., 2002). Moreover, X-ray electron-microprobe analysis of the elemental composition of dehydrated cryo-sections of shock-frozen epithelial cells revealed an increase in the number of areas with high calcium concentrations, indicating epithelial Ca^{2+} transport (Ziegler, 2002b). In addition, an increase of the cytoplasmic magnesium concentration has been detected within the anterior sternal epithelial cells during deposit formation. This suggests epithelial Mg^{2+} transport, because a considerable concentration of 150 mmol/kg dry mass magnesium has been measured within spherules of the sternal deposits (Ziegler, 2002b). Such findings are of particular interest, because it is known that Mg^{2+} ions can block the formation of calcite and therefore favor precipitation of amorphous CaCO_3 (Raz et al., 2000).

Electron-spectroscopic diffraction analysis (Ziegler, 1994) and, recently, high-resolution synchrotron X-ray diffractometry (Becker et al., 2003) show that the mineral phase of the sternal deposits is fully electron and X-ray amorphous. IR reflection and synchrotron X-ray absorption spectroscopy, however, indicate some structure similar to vaterite or monohydroxycalcite with a coherent lattice <10 nm but larger than a few interatomic distances (Becker et al., 2003). Vaterite and monohydroxycalcite are unstable under ambient conditions. The means by which further crystallization of the mineral particles is prevented and how they are precipitated are not yet clear. However, it has been shown in other systems that specialized proteins are able to stabilize amorphous CaCO_3 (Aizenberg et al., 1996; Benish et al., 1997) and to prevent crystal nucleation (Coblentz et al., 1998). The smallest mineral subunits we found within the aggregation zone, on the surfaces of spherules and hl as well as in the core material of degrading spherules, were granules with diameters of ~10 nm, suggesting that they consist of just one or several mineral particles stabilized by a limited number of protein molecules. Spherular structures 50 nm in diameter consisting of calcite have been found in the exo- and endocuticle of *Carcinus maenas* (Decapoda), strung together in the orientation of organic fibers (Roer and Dillaman, 1984). Amorphous CaCO_3 has recently been detected in the cuticle of the decapod crustacean *Homarus americanus* (Levi-Kalisman et al., 2002).

Amorphous CaCO_3 has a considerably greater solubility compared with microcrystalline phases (Brečević, 1989), so deposits composed of amorphous CaCO_3 are advantageous because degradation is facilitated. Because the sternal CaCO_3 deposits are attached to the old sternal cuticle, they must be completely resorbed before the anterior molt so as to prevent an excess loss of calcium during ecdysis. This requires a quick dissolution of CaCO_3 from the deposits because of the short time span between posterior and anterior molt. Our results show

that during resorption of the deposits, several mechanisms speed CaCO_3 dissolution. The CaCO_3 deposit layers degrade in a manner that is not exactly in the inverse sequence of their formation. Instead, the hl degrades in a way that exposes a maximum of surface area by the formation of deep holes and crevasses. These finally open into psl, exposing the large surface of the spherules. A similar principle applies during degradation of the individual spherules. Thus, holes and gaps between the granules forming the surface of the spherules lead to core material being degraded simultaneously to the surface wall. Even within the core material, surface area increases during degradation, as indicated by the residual radial structures appearing during dissolution (Figs. 5a–g). Degradation of the deposits is probably triggered by the accumulation of a V-type H^+ -ATPase within the apical plasma membrane of the anterior sternal epithelial cells, which pumps protons to the deposits (Ziegler et al., 2000). Degrading spherules with diameters >1 μm often expose a second small spherule in their center. Similar multilayered spherules were described by Simkiss (1976) as type B granules in a variety of invertebrates. These granules also contain organic components, occur in intra- and intercellular spaces, and grow by addition of subsequent layers.

It is interesting that during degradation a layer very similar in appearance to the aggregation zone is found covering the proximal surface of the deposits. Like the aggregation zone, this degradation layer seems to be soft and contains numerous filaments. The increasing thickness of the layer during progressing degradation suggests that it consists of accumulating matrix components of the deposit that degrade at a slower pace than the mineral component, probably by the action of hydrolytic enzymes.

In conclusion, our results suggest that formation of spherules is initiated within an aggregation zone by the formation of nanoparticles consisting of mineral and organic components. Concentric growth of the spherules takes place in a growth zone extending several microns distal to the aggregation zone, probably by continuous assembly of nanoparticles at the surface of the spherules. During degradation of spherules, a maximum of surface area is exposed possibly by differential stabilization of amorphous CaCO_3 by components of the organic matrix. The large surface increases the speed of Ca^{2+} and HCO_3^- mobilization during the quick degradation of the deposits.

Acknowledgments

We thank Edward Koenig (Department of Physiology and Biophysics, University at Buffalo, School of Medicine) for critically reading the manuscript. This work was supported by the *Deutsche Forschungsgesellschaft*.

meinschaft (Zi 368/4-1) within the research program “Principles of Biomineralisation” (SPP 1117).

References

- Aizenberg, J., Lambert, G., Addadi, L., Weiner, S., 1996. Stabilization of amorphous calcium carbonate by specialized macromolecules in biological and synthetic precipitates. *Adv. Mater.* 8, 222–226.
- Becker, A., Bismayer, U., Epple, M., Fabritius, H., Hasse, B., Shi, J., Ziegler, A., 2003. Structural characterisation of amorphous calcium carbonate (ACC) in sternal deposits of the crustacean *Porcellio scaber*. *Dalton Trans.* 2003, 551–555.
- Beniash, E., Aizenberg, J., Addadi, L., Weiner, S., 1997. Amorphous calcium carbonate transforms into calcite during sea urchin larval spicule growth. *R. Soc.* 264, 461–465.
- Brečević, L., 1989. Solubility of amorphous calcium carbonate. *J. Cryst. Growth* 98, 504–510.
- Coblentz, F.E., Shafer, T.H., Roer, R.D., 1998. Cuticular proteins from the blue crab alter in vitro calcium carbonate mineralization. *Comp. Biochem. Physiol. B* 121, 349–360.
- Drobne, D., Štrus, J., 1996. Moulting frequency of the isopod *Porcellio scaber*, as a measure of zinc-contaminated food. *Environ. Toxicol. Chem.* 15, 126–130.
- Graf, F., Meyran, J.-C., 1985. Calcium reabsorption in the posterior caeca of the midgut in a terrestrial crustacean, *Orchestia cavimana*. *Cell Tissue Res.* 242, 83–95.
- Greenaway, P., 1985. Calcium balance and moulting in the crustacea. *Biol. Rev.* 60, 425–454.
- Levi-Kalishman, Y., Raz, S., Weiner, S., Addadi, L., Sagi, I., 2002. Structural differences between biogenic amorphous calcium carbonate phases using X-ray absorption spectroscopy. *Adv. Funct. Mater.* 12, 43–48.
- Messner, B., 1965. Ein morphologisch-histologischer Beitrag zur Häutung von *Porcellio scaber* Latr. und *Oniscus asellus* L. (*Isopoda terrestria*). *Crustaceana* 9, 285–301.
- Neufeld, D.S., Cameron, J.N., 1993. Transepithelial movement of calcium in crustaceans. *J. Exp. Biol.* 184, 1–16.
- Passano, L.M., 1960. Molting and its control. In: Waterman, T.H. (Ed.), *The Physiology of Crustacea*, vol. 1. Academic Press, New York, pp. 473–536.
- Raz, S., Weiner, S., Addadi, L., 2000. Formation of high-magnesium calcites via an amorphous precursor phase: possible biological implications. *Adv. Mater.* 12, 38–42.
- Roer, R., Dillaman, R., 1984. The structure and calcification of the crustacean cuticle. *Am. Zool.* 24, 893–909.
- Simkiss, K., 1976. Intracellular and extracellular routes in biomineralization. In: Duncan, C.J. (Ed.), *Calcium in Biological Systems*, Symposium of the Society for Experimental Biology, vol. 15. Cambridge University Press, Cambridge, pp. 423–444.
- Sparkes, S., Greenaway, P., 1984. The haemolymph as a storage site for cuticular ions during premoult in the freshwater/land crab *Holthuisana transversa*. *J. Exp. Biol.* 113, 43–54.
- Steel, C.G.H., 1993. Storage and translocation of integumentary calcium during the moult cycle of the terrestrial isopod *Oniscus asellus* (L.). *Can. J. Zool.* 71, 4–10.
- Štrus, J., Blejec, A., 2001. Isopod systematics and evolution. *Crustacean Issues*, The Netherlands, Rotterdam, 13, Balkema: pp. 343–352.
- Wieser, W., 1964. Über die Häutung von *Porcellio scaber* Latr. *Verh. Dtsch. Zool. Ges.* 1964, 178–195.
- Ziegler, A., 1994. Ultrastructure and electron spectroscopic diffraction analysis of the sternal calcium deposits of *Porcellio scaber* Latr. (Isopoda, Crustacea). *J. Struct. Biol.* 112, 110–116.
- Ziegler, A., 1997. Ultrastructural changes of the anterior and posterior sternal integument of the terrestrial isopod *Porcellio scaber* Latr. (Crustacea) during the moult cycle. *Tissue Cell* 29, 63–76.
- Ziegler, A., 2002a. Variations of calcium deposition in terrestrial isopods. *Crustaceana*, in press.
- Ziegler, A., 2002b. X-ray microprobe analysis of epithelial calcium transport. *Cell Calcium* 31, 307–321.
- Ziegler, A., Miller, B., 1997. Ultrastructure of CaCO_3 deposits of terrestrial isopods (Crustacea, Oniscidea). *Zoomorphology* 117, 181–187.
- Ziegler, A., Scholz, F.H.E., 1997. The ionic hemolymph composition of the terrestrial isopod *Porcellio scaber* Latr. during molt. *J. Comp. Physiol. B* 167, 536–542.
- Ziegler, A., Weihrauch, D., Bleher, R., 2000. A V-type H^+ -ATPase in the calcium transporting anterior sternal epithelial cells of *Porcellio scaber*. *Eur. J. Cell Biol. Suppl.* 50, 80.
- Ziegler, A., Weihrauch, D., Towle, D.W., Hagedorn, M., 2002. Expression of Ca^{2+} -ATPase and $\text{Na}^+/\text{Ca}^{2+}$ -exchanger is upregulated during epithelial Ca^{2+} -transport in hypodermal cells of *P. scaber*. *Cell Calcium* 32, 131–141.

5.2 Architecture of the organic matrix in the sternal CaCO_3 deposits of *Porcellio scaber* (Crustacea, Isopoda).



Architecture of the organic matrix in the sternal CaCO_3 deposits of *Porcellio scaber* (Crustacea, Isopoda)

Helge Fabritius, Paul Walther, Andreas Ziegler *

Central Facility for Electron Microscopy, University of Ulm, 89069 Ulm, Germany

Received 2 August 2004, and in revised form 5 January 2005

Available online 5 March 2005

Abstract

Before the molt terrestrial isopods resorb calcium from the posterior cuticle and store it in large deposits within the first four anterior sternites. In *Porcellio scaber* the deposits consist of three structurally distinct layers consisting of amorphous CaCO_3 (ACC) and an organic matrix that consists of concentric and radial elements. It is thought that the organic matrix plays a role in the structural organization of deposits and in the stabilization of ACC, which is unstable in vitro. In this paper, we present a thorough analysis of the ultrastructure of the organic matrix in the CaCO_3 deposits using high-resolution field-emission scanning electron microscopy. The spherules and the homogeneous layer contain an elaborate organic matrix with similar structural organization consisting of concentric reticules and radial strands. The decalcification experiments reveal an inhomogeneous solubility of ACC within the spherules probably caused by variations in the stabilizing properties of matrix components. The transition between the three layers can be explained by changes in the number of spherule nucleation sites.

© 2005 Elsevier Inc. All rights reserved.

Keywords: ACC; Biomineralization; Calcification; Ecdysis; Matrix; Mineralization; Molt; Molt

1. Introduction

Calcium carbonate is the most widespread mineral in invertebrate calcified tissues. The mechanical properties of these tissues like their strength and hardness, their shape and solubility depend on the properties of the mineral component and the chemical and structural organization of their organic matrix. During the biomineralization process the organic matrix can regulate crystallization to favour specific crystal shapes and one of the main crystal phases: vaterite, aragonite, and calcite (Coblentz et al., 1998; Mann, 1997). A constantly increasing number of investigations demonstrated the presence of amorphous calcium carbonate (ACC) in calcified tissues. ACC is found as a precursor of the

crystalline phases (Beniash et al., 1997) and is thought to play an important role in the initiation of biomineralization processes. In addition, ACC is used as a transient store for calcium in some biological systems (Aizenberg et al., 1996, 2002; Raz et al., 2002; Taylor et al., 1993; Ziegler, 1994). Since ACC is about 10 times more soluble than the crystalline phases (Brecevic and Nielson, 1989), it is unstable in vitro. In living organisms, however, it seems to be stabilized by components of the organic matrix.

Crustaceans are interesting model organisms for the study of biomineralization processes. Most of them have a rigid exoskeleton, which serves as a protective shell and is mineralized by calcium carbonate. To grow, crustaceans frequently shed their exoskeleton (molt) and minerals that are lost during molt must be replaced by uptake from their environment. While it is easy for marine, and to a lesser degree for limnic species to replace calcium by taking it up from the water via their

* Corresponding author. Fax: +49 731 502 3383.

E-mail address: andreas.ziegler@medizin.uni-ulm.de (A. Ziegler).

gills, terrestrial crustaceans depend on calcium taken up with their diet, which contains little calcium. Therefore, many terrestrial species have evolved storage sites for cuticular calcium. Some decapods store calcium in the so-called gastroliths at specialized regions in the integument of the stomach, others store calcium in granules within the hemocoel and subepidermal connective tissue (Greenaway, 1985; Greenaway and Farrelly, 1991; Sparkes and Greenaway, 1984). The terrestrial amphipod *Orchestia cavimana* stores cuticular calcium in calcareous concretions in the posterior caeca of the midgut (Graf and Meyran, 1985). Terrestrial isopods store calcium in a variety of storage sites (Ziegler, 2003). The most common among these are the sternal CaCO_3 deposits located within the ecdysial gap between the epithelium and the old cuticle of the first four anterior sternites (Ziegler and Miller, 1997; Ziegler, 2003) (Fig. 1A). The formation and degradation of these deposits is closely linked with the unique biphasic molt of isopods, which molt first the posterior half of the body and, about 1 or 2 days later, the anterior half. The calcium and probably also carbonate of the deposits originate from the old posterior cuticle from which the ions are resorbed before the molt. After posterior molt, the mineral of the sternal deposits and part of the mineral in the anterior cuticle is mobilized and used to mineralize the new posterior cuticle (Steel, 1993; Ziegler and Scholz, 1997). Electron spectroscopic diffraction analysis and high-resolution synchrotron X-ray diffraction of the deposits of *Porcellio scaber* revealed that the deposits are fully electron and X-ray amorphous (Becker et al., 2003; Ziegler, 1994). However, as shown by X-ray absorption spectroscopy the material has similarities to vaterite or mono-hydroxy calcite with a particle size between a few interatomic distances and about 10 nm (Becker et al.,

2003). Light microscopical and ultrastructural analysis have shown that the fully developed sternal CaCO_3 deposits of *P. scaber* consist of a opaque region next to the old cuticle composed of numerous microspherules and a glassy layer of homogeneous appearance (hl) adjacent to the sternal epithelium (Figs. 1B and C) (Ziegler, 1994). The spherular region is further subdivided into a distal spherular layer (dsl) consisting of spherules with diameters of 500 nm that are mostly fused (Fig. 1D) and a proximal spherular layer (psl) of free spherules (Figs. 1B and C) with diameters ranging from 500 nm in the distal to about 2 μm in the proximal regions (Ziegler and Miller, 1997). The deposits contain an organic matrix organized in radial and concentric structures which seem to serve as a template for the structural organization of the various layers and which must stabilize the amorphous state of the deposits (Ziegler, 1994). The matrix consists of at least seven different proteins, and of additional probably chitinous filaments occurring in the very distal regions only (Fabritius, unpublished). A recent study on structural changes during natural formation and degradation of the deposits employing high-resolution field-emission scanning electron microscopy (HR-FESEM) revealed variations in ACC stability in specific regions within the homogeneous layer and even within individual spherules. In particular, regions within the core of the spherules dissolve faster than regions in their periphery leading to a very high surface area, which facilitates quick mobilization of calcium and carbonate. Most probably differences in matrix components are responsible for these variations in ACC stability (Fabritius and Ziegler, 2003). While the structure of the mineral phase of the sternal CaCO_3 deposits was well investigated, little is known about the structure and organization of the matrix components. Because of their

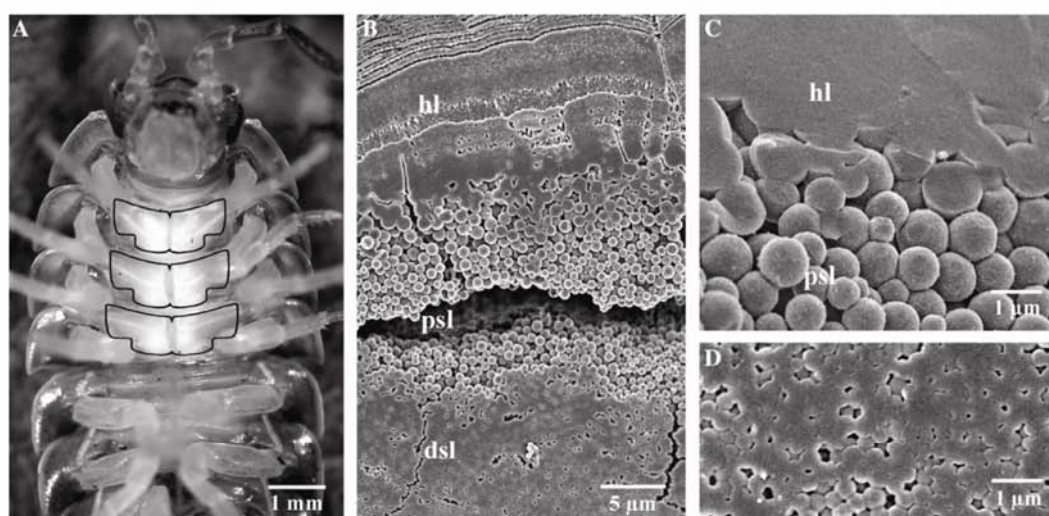


Fig. 1. The sternal CaCO_3 deposits of *P. scaber* in the late premolt stage. (A) Light micrograph outlining the deposits of the sternites 2–4. The smaller first sternite is hidden by the head. (B) Knife polished sagittal face of a fully developed deposit treated with Ches buffer pH 10 for 5 min. (dsl) distal spherular layer, (psl) proximal spherular layer, (hl) homogeneous layer. (C and D) Cleaved surfaces of untreated deposits showing that the material within hl and the spherules within psl (C) and dsl (D) appear solid.

prominent role in morphogenesis and stability of the ACC deposits we investigated the structural organization of the organic matrix within the three different layers of the deposits using HR-FESEM.

2. Materials and methods

2.1. Animals

Porcellio scaber were collected from local populations and reared in plastic containers filled with moist soil and bark. Potatoes, carrots, and dry oak leaves were offered for food. Animals in the late premolt stage were determined by the optical appearance of the sternal CaCO_3 deposits according to Messner (1965). Only specimens with fully developed deposits were used for the experiments.

2.2. Sample preparation for matrix studies

We used two different approaches to study the matrix in decalcified deposits: whole mounts for studying the proximal surface of the deposits and knife polished sagittal faces which allow the examination of all three layers within the deposits. To obtain whole mounts animals were killed by injection of a small amount of 12.5% glutaraldehyde for prefixation. The tissue around the anterior sternites was dissected off leaving the head, and the sternal integument including the CaCO_3 deposits surrounded by fatty-tissue and the ventral nerve chord. Preliminary studies have shown that preservation of various aspects of the matrix structure depends on the degree of decalcification, fixation, and the type of solvent used. We therefore tested a variety of decalcification protocols (Table 1) using different concentrations of EDTA in H_2O or triethylammonium-EDTA (TEA-EDTA) in 90% ethanol (Scott and Kyffin, 1978) at various incubation times. In most of the protocols we used glutaraldehyde (GA) to fix soluble matrix components. Decalcification was performed at RT for all protocols.

Samples decalcified in aqueous EDTA solutions were dehydrated in a series of isopropanols (30–50–70–90–100%, 10 min each), the samples in the non-aqueous triethylammonium-EDTA solution were rinsed in 90 and

100% isopropanol for 10 min each. All samples were critical-point dried in a Bal-Tec CPD 030, using carbon dioxide as transition medium. The dried specimens were further dissected by removing the head and all remaining tissue covering the CaCO_3 deposits. Then the sternites were separated from one another and mounted on sample holders using self-adhesive carbon pads. To obtain sagittally cleaved specimens CaCO_3 deposits were dissected from prefixed animals (see above) and mounted vertically on sample holders using two-component resin glue (5 min Epoxy, R&G GmbH, D-71107 Waldenbuch). After the resin cured, the samples were mounted on an ultra microtome (Leica Ultracut UCT) and a block face was trimmed by taking off 0.5 μm thick sagittal sections using dry glass knives. Diamond knives were used to polish the surface of the block face by advancing the knife successively 15 times each by 70, 30, 20, 10, and 5 nm. That way we obtained flat and smooth block faces with a minimum of knife marks. Thereafter the specimens were transferred to the decalcification media E and G and incubated for either 5, 10 or 15 min. Dehydration and critical-point drying were performed as described above. For electron microscopical examination, samples were rotary shadowed with platinum (2 nm) by electron beam evaporation in a Balzers BAF 300 freeze-etching device and viewed with a Hitachi S-5200 in-lens field-emission SEM at acceleration voltages between 1.5 and 4 kV using a secondary electron detector. To avoid contamination and drift effects during the examination, some samples were analysed in the SEM using a Gatan cryo-holder 626 at temperatures between -90 and -130°C . Brightness and contrast of the obtained digital images were adjusted with Photoshop 5.0 when necessary.

2.3. Statistical analysis

Distances between adjacent concentric matrix layers were measured within the medial plane of decalcified spherules of dsl and psl. One-way analysis of variance was used to test for differences between corresponding distances. Dunnett's multiple comparisons test was used to detect specific differences between the distance from the central sphere to the first concentric matrix layer and the following distances.

Table 1
Composition of the decalcification/fixation solutions and time of incubation

	Decalcification medium	Concentration (mol L^{-1})	Fixative	Time of incubation (min)
A	Ches buffer pH 10.0	—	—	5
B	EDTA in H_2O , pH 8.0	0.04	2.5% GA	240
C	EDTA in H_2O , pH 8.0	0.1	2.5% GA	120
D	EDTA in H_2O , pH 8.0	0.1	—	120
E	EDTA in H_2O , pH 8.0	0.1	2.5% GA	5, 15
F	EDTA in H_2O , pH 8.0	0.2	2.5% GA	60
G	EDTA in H_2O , pH 8.0	0.1	—	10
H	TEA-EDTA in 90% ethanol, pH 8.0	0.2	2.5% GA	60

Ches, 2-(N-cyclohexylamino)ethane-sulphonic acid; EDTA, ethylenediaminetetraacetic acid; GA, glutaraldehyde; TEA, triethylammonium.

3. Results

Analysis of the matrix architecture in mineralized tissues bears the problem that during demineralization parts of the organic matrix dissolve in addition to the mineral compound. Therefore, such a study requires careful experiments employing a wide variety of decalcification and fixation protocols. With increasing degree of decalcification with aqueous EDTA solutions the overall organization of the matrix gradually changes its appearance. This is demonstrated for dsl (Figs. 2A–E). Fig. 2A shows partly decalcified spherules with an increased surface roughness and irregularly shaped holes of about 30 nm in size in their surface. Filamentous strands with diameters down to about 5 nm connect the spherules (Fig. 2A). With longer exposure times or higher EDTA concentrations the spherular core structures become successively smaller while the strands radiating from the centre become more and more apparent (Fig. 2B) until large, three-dimensional networks appear (Fig. 2C). The network contains mostly bifurcate ramifications and the thickness of the filaments gradually increases to up to 40 nm. Prolonged exposure to decalcification medium results in complete disorganization of matrix structures leaving residues of fractal appearance composed of about 20 nm thick particles (Fig. 2D). Apparently these residues originate from the walls of the spherules (Fig. 2E).

In native deposits the material within the homogeneous areas and in the spherules of both dsl and psl appears solid (Figs. 1C and D). Exposure of knife polished sagittal faces of the CaCO_3 deposits to mild aqueous decalcification solutions such as 10 mM Ches buffer (pH 10) for 5 min leads to dissolution of rather unstable material within the deposits, revealing new aspects of CaCO_3 deposit organization. In dsl, this exposes a polyhedral structure of fused spherules (Fig. 2F). Half-spherules within dsl dissolve first within a region about 300 nm around their centre leaving a core structure connected to the surrounding wall by radial strands (Fig. 2F). Decalcification of knife polished dsl with aqueous EDTA reveals the substructure of the organic matrix, which is composed of up to four stacked concentric layers and radial filaments connecting the concentric spheres (Figs. 2G and H). The concentric layers are between 20 and 50 nm thick and contain particles with diameters between 10 and 40 nm (Fig. 2G). The filaments have diameters of about 20 nm. Similar filaments also connect adjacent spherules (Fig. 2G). Interestingly, the outermost concentric layers of fused spherules leave an opening at the fusion site. Here, the radial strands of the neighbouring spherules connect to each other (Fig. 2H).

The spherules of psl in knife polished sagittal faces of the CaCO_3 deposits treated with Ches buffer (pH 10) show a similar dissolution pattern as the spherules of dsl. The material begins to dissolve in a region about 300 nm from the centre, leaving a solid core and an outer wall

structure connected by radial strands (Fig. 3A). In whole mounts treated with aqueous EDTA solutions the core material is dissolved first, often leaving residual structures consisting of radial strands extending from the centre to the outer wall of the spherule, which is about 50 nm thick (Fig. 3B). Short decalcification times in knife polished specimens reveal up to eight concentric layers around a central sphere, connected by radial strands (Fig. 3C). As in spherules of the dsl the concentric layers are 20–50 nm thick and contain spherical particles 10–40 nm in diameter (Figs. 3C and D). Statistical analysis of the distances between the individual concentric spheres resulted in no significant difference between the spherules of dsl and psl. The distance between concentric spherules is about 100 nm with the distance between the innermost spherular structure to the first concentric layer being somewhat smaller (Table 2). The radial strands have diameters from 5 to 20 nm. Spherules some distance below the cutting plane, which were less exposed to decalcification medium, reveal further structural details of the concentric layers. The first sign of dissolution is the decrease in the density of the particles within the outermost layer, giving the surface a rough appearance (Fig. 3E). With further removal of material from the surface, reticular filaments appear with diameters between 10 and 20 nm underlying the solid outer wall (Figs. 3E–G). Such reticules also become visible in deposits treated with triethylammonium-EDTA in 90% ethanol (Fig. 3H). The branchings between these fibres are in almost all cases bifurcate. Right on these furcations we often observed small spherical particles that remained solid after dissolution (Fig. 3F). In inner concentric layers, where most of the spherular particles are dissolved, transversally oriented filaments connect the radial strands indicating that filamentous reticules are present in all concentric layers (Fig. 3I). At the circular contact areas with neighbouring spherules the outermost concentric layer is lacking. Residues of the reticules can be observed around these areas (Fig. 3J). Sometimes, the reticular filaments grade into sheet-like structures (Fig. 3F). However, these sheets were never observed in spherules decalcified in ethanol solutions, raising the possibility that these sheet-like structures form during the decalcification/fixation process in aqueous solutions.

Knife polished sagittal faces of the homogeneous layer treated with either Ches buffer (pH 10) (Fig. 4A) or mild aqueous EDTA solutions (Fig. 4B) reveal that it is built of stacked concentric lamellae that originate from spherules in the transition zone between psl and hl (Figs. 4B and C). In the transition zone between psl and hl, the spaces between the most proximal spherules are filled by concentric and radial matrix elements similar to those in more central regions of the spherules. This results in polyhedral structures similar to those found in fused dsl spherules (Fig. 4C). Additional matrix layers form at the proximal side of the fused spherules. Thickness and

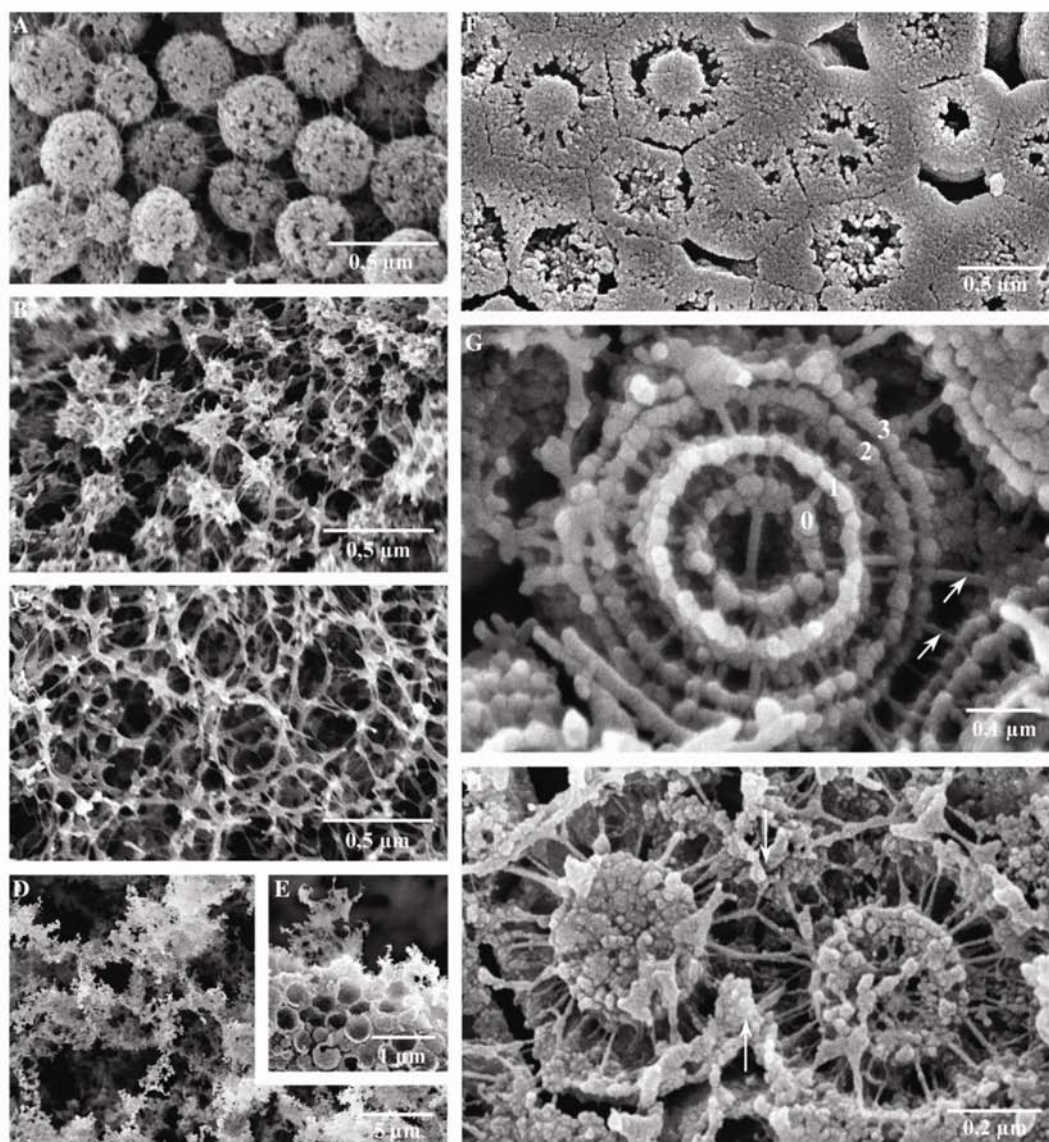


Fig. 2. Ultrastructure of the organic matrix within the distal spherular layer. (A–C) Whole mounts of increasing degree of decalcification by aqueous EDTA solutions containing 2.5% glutaraldehyde (GA) for fixation. (A) 0.04 M EDTA/240 min: spherules have a high-surface roughness and small holes appearing at the surface, filaments are visible between spherules. (B) 0.1 M EDTA/120 min: the organic matrix appears as a network with strands radiating from the core structures of dissolved spherules. (C) 0.1 M EDTA/120 min: residual three dimensional networks of interconnected matrix strands. (D) 0.1 M EDTA/120 min without GA: large, diffuse clusters of 20 nm thick particles of fractal appearance. (E) Similar structures at disintegrating spherule walls in dsl. (F) Knife polished sagittal face of dsl treated with Ches buffer pH 10/5 min. The spherules show dissolved areas around their centres and characteristic polygonal patterns. (G and H) Matrix in knife polished sagittal faces of spherules in dsl. (G) Typical spherule with four concentric layers (0–3) connected by radial strands. Similar strands (arrows) connect adjacent spherules. (H) Fused spherules, the outermost concentric layer is discontinuous in the contact area (arrows), radial strands connect the two spherules.

structure of the concentric layers equal those of the spherules in dsl and psl. With increasing distance from psl some of the stacks of matrix layers become broader from distal to proximal, while others are narrowing constantly until they discontinue (Fig. 4D). In whole mounts of deposits, which have grown just to the hl–psl transition, decalcification with triethylammonium-EDTA in 90% ethanol exposes a reticular matrix structure similar to that found in spherules. The reticules consist of filaments with a diameter of about 10 nm, with mostly bifurcate branchings (Fig. 4E).

4. Discussion

This paper presents a detailed ultrastructural investigation of the organic matrix of the sternal CaCO_3 deposits of *P. scaber*. It reveals that the ultrastructure of the organic matrix is similar within each of the three layers of the CaCO_3 deposits. Together with previous investigations on deposit composition (Becker et al., 2003; Ziegler, 1994) and structural changes during the molt cycle (Fabritius and Ziegler, 2003), the results lead to a better understanding of matrix function. They suggest

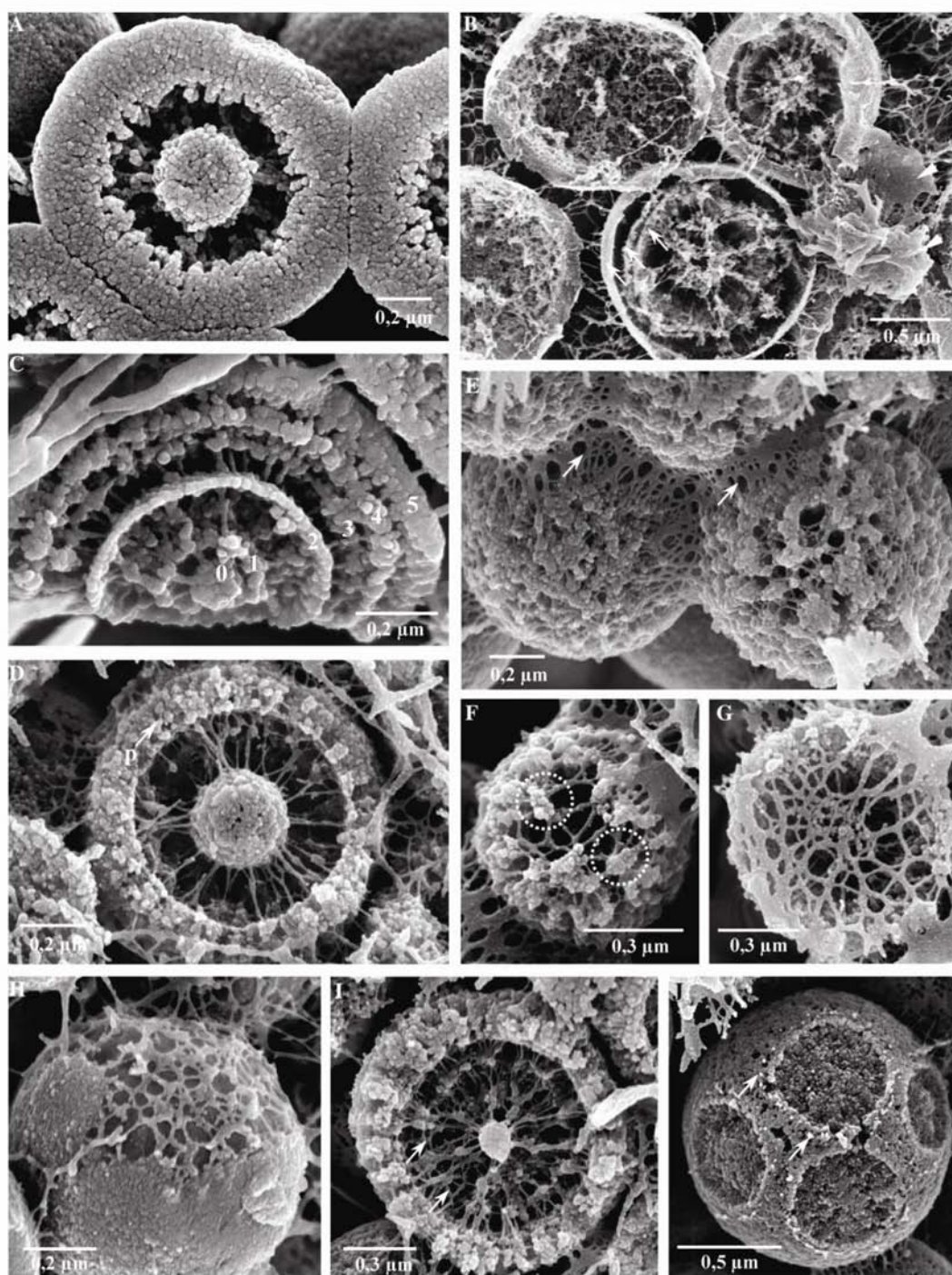


Fig. 3. Ultrastructure of the organic matrix within the proximal spherular layer (psl). (A) Knife polished sagittal face of spherules treated with Ches buffer pH 10/5 min. Areas around the centre are dissolved leaving radial strands. (B) Whole mount decalcified using 0.2 M EDTA/60 min. The core material is dissolved leaving hollow spheres and radial strands within the lumen. Sometimes more than one concentric layer is visible (arrows). Arrowheads: matrix fragments of concentric layers. (C–G) Matrix in knife polished sagittal faces of psl spherules. (C) 0.1 M EDTA/10 min: typical spherule with six concentric layers (0–5) connected by radial strands. Sample was viewed in a cryo-holder at -130°C . (D) Example of a decalcified spherule with an inner spherical structure connected to the outer wall by radial strands. The outer wall contains 10–40 nm thick particles (p). (E–G) Spherules below the cutting plane, 0.1 M EDTA + 2.5% GA/5 min. (E) Concentric reticules of filaments within the outer wall of the spherules and between adjacent spherules (arrows) appear when the nano-particles at the spherule surface dissolve. (F) The nano-particles prevail longest at the branchings of the filaments (areas in circles). (G) Residual consisting of reticular concentric matrix. The micrograph shows the inner side of the reticule. (H) Whole mount treated with 0.2 M triethylammonium EDTA + 2.5% GA/60 min: reticular matrix is exposed on the surface of a spherule. (I and J) Knife polished samples treated with 0.1 M EDTA + 2.5% GA/5 min. (I) Spherule with most of the inner concentric layers dissolved: filaments connect radial matrix elements transversally (arrows). (J) Spherule below the cutting plane: circular rows of filaments (arrows) at the edges of circular contact areas with neighbouring spherules.

Table 2

Distances between adjacent concentric matrix layers (Mean \pm standard error of the mean, N)

Sphere from centre to periphery	1	2	3	4
Distance (nm)	86 \pm 8.2, 14 ^a	101 \pm 10.3, 15	102 \pm 18.0, 9	105 \pm 25.7, 4

Since we found no significant difference the data for psl and dsl were pooled. The value for the fourth concentric sphere was recorded in spherules of psl only.

^a Indicates significant ($p < 0.05$) difference to concentric sphere number 3.

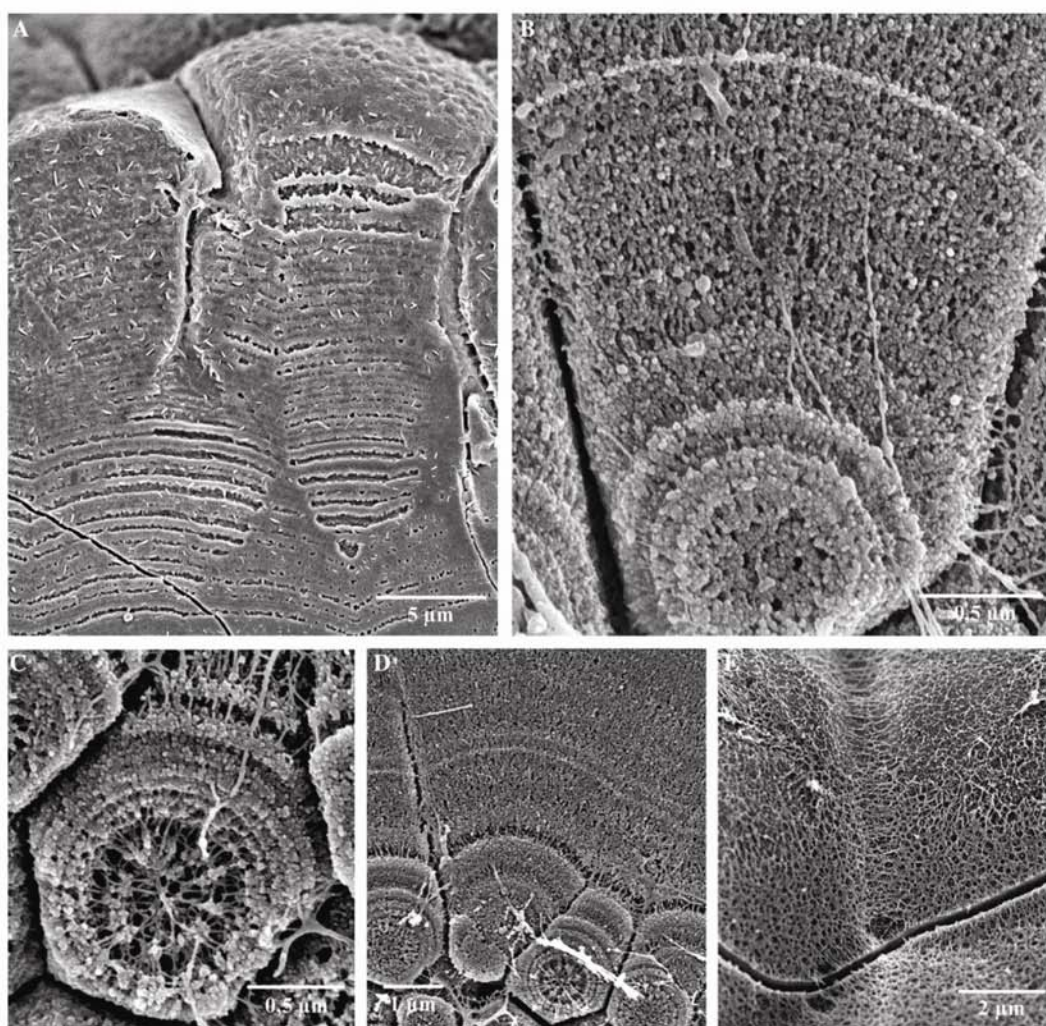


Fig. 4. Ultrastructure of the organic matrix within the homogeneous layer (hl). (A) Knife polished sagittal face treated with Ches buffer pH 10/5 min reveals that hl is formed by numerous stacked concentric lamellae. (B–D) 0.1 M EDTA + 2.5% GA/5 min. (B) Matrix in knife polished sagittal faces. The concentric lamellae are connected by radial strands extending from spherules in the transition between hl and the proximal spherular layer. (C) Spherule from the transition between hl and psl with characteristic polygonal outline. (D) Competitive growth pattern of hl segments originating from psl spherules. (E) 0.2 M triethylammonium EDTA + 2.5% GA/60 min: layer of reticular matrix exposed on the surface of hl.

that differences in the solubility of amorphous calcium carbonate within individual spherules are caused by variations in the stabilizing properties of the organic matrix. The structural organization in radial strands and concentric reticules is similar within each layer of the deposits suggesting that the transition between the three layers is caused by changes in the number of spherule nucleation sites. We propose that such a change in spherule nucleation sites has also led to the development of

two- and three-layered deposits from primordial single-layered deposits during the evolution of terrestrial isopods.

4.1. Matrix structure

One of the most interesting results of the present study is that despite their structural differences the three layers of the sternal deposits contain virtually

similar matrix components. Matrix filaments in the spherules of the distal and the proximal spherular layer (dsl and psl) and in the homogeneous layer (hl) are of the same diameter down to 5 nm. Larger strands of up to 30 nm were also similar in all three layers and are likely to be due to the assembly of additional filaments. These filaments may either be of the same type as the 5 nm filaments or of different types with larger diameters. Since we have observed an increase in the thickness of filaments or strands during decalcification (Figs. 2A–C) it may be possible that the decalcification process contributes to the variation of their thickness. At the nano-scale the filaments constitute two types of matrix structures: reticules that form concentric layers in spherules or spherical calottes in hl, and radial strands, which connect the reticular structures. The arrangement of the reticular and radial structures within the three layers is also very similar. Statistical analysis indicates that the distance between adjacent layers is similar within spherules of dsl and psl. As a consequence, the differences in the size between the spherules result from differences in the number of concentric layers rather than differences in the distance between adjacent concentric layers. Even the spherical calottes in hl, which arise from spherical structures, have distances between one another similar to the distances between the concentric layers in spherules. Together, these results make it evident that all three layers of the sternal ACC-deposits arise from the concentric growth of ACC-spherules with striking similarities in the nano-architecture of their organic matrix. These similarities raise the question of how the structural differences between the three layers, which are apparent at the micro-scale, are brought about during the formation of the CaCO_3 deposits.

4.2. Transition between layers

The similarities in the matrix architecture found in the three layers of *P. scaber* suggest that the structural differences between dsl, psl, and hl are a result of changes in the process of ACC/matrix deposition rather than the result of different matrix components within the spherules. Previous investigations of the natural development of spherules in dsl show that the spherules grow in a concentric manner from initial agglomerations of ACC granules (Fabritius and Ziegler, 2003) and begin to fuse with one another after they contact neighbouring spherules. In the present study knife polished faces of dsl treated with Ches buffered aqueous solutions indicate that the spherules continue to grow at surfaces not covered by their neighbours until the spaces between spherules are completely or partially filled. This finally leads to polyhedral structures in which the organization of the organic matrix is maintained from the centre to the corners.

For the transition from the dsl to free spherules in psl concentric growth should cease before neighbouring spherules fuse with one another. Since spherules of the psl near the transition zone have the same diameter (500 nm) than the spherules in dsl (Fabritius and Ziegler, 2003) the transition must be caused by a decrease in the number of spherule nucleation sites. Similarly, the density of nucleation sites must further decrease when the free spherules gradually increase to about 2 μm in the transition zone to hl.

The analysis of the transition between psl and hl during natural formation of the deposits has shown that proximal spherules of psl grow continuously until they contact each other (Fabritius and Ziegler, 2003). Further deposition of material in the gaps between adjacent spherules then leads to the formation of polyhedral structures. These polyhedral structures form a continuous seal, which prevents diffusion of material to the underlying spherules and restricts ACC/matrix deposition to the proximal side, where hl begins to form (Fabritius and Ziegler, 2003). Our observation of polyhedral structures within knife polished and decalcified areas of the transition zone (Figs. 4C and D) is in accordance with these results. Furthermore, the maintenance of matrix organization in the spaces between adjacent spherules indicates that the gaps between the spherules are filled by the same mechanism described for dsl.

The organization of the organic matrix also provides some evidence for the mechanism of hl formation. In hl circular concentric layers as in complete spherules are very rare indicating that the rate of nucleation site formation ceases almost completely. This results in deposition of ACC/matrix material to the proximal spherical surfaces of the last row of polyhedral shaped structures of the transition zone only. The broadening and narrowing of spherical sectors apparent in knife polished and decalcified sagittal faces of hl (Fig. 4D) indicates a competitive growth pattern of ACC/matrix material.

Taken together it appears that on the nanometer scale all three layers grow by the same principle and that the differences in appearance between the layers at the micrometer scale are brought about by differences in the number of spherule nucleation sites formed within a given volume of the developing deposit. At the present stage of investigation we do not know the nature of spherule nucleation sites. At this point it is important to note that spherule nucleation sites may be distinct from CaCO_3 nucleation sites. Proteinaceous nucleation sites for calcite formation were proposed for the postecdysial cuticle of the blue crab *Callinectes sapidus* (Coblentz et al., 1998; Shafer et al., 1995).

4.3. Interaction between matrix and mineral

High-resolution scanning electron microscopy (Fabritius and Ziegler, 2003) has shown that spherule growth

is initiated in a specialized aggregation zone, where 10–30 nm thick particles aggregate to spherical agglomerations. These agglomerations grow further by addition of more particles, which probably form at the surface of the growing spherules. This has led to the conclusion that mineral and matrix must already be incorporated in the initial granular nano-particles that are likely to be of colloidal nature. Several studies indicate that the anterior sternal epithelial cells control the ionic composition and the pH around the developing deposits (Ziegler, 2002; Ziegler et al., 2002, 2004) and it is likely that the cells of the epithelium also provide the matrix components. The constant sequence of concentric layers connected by radial structures found throughout the CaCO_3 deposits of *P. scaber* is most probably the result of a self-assembly mechanism of the proteins composing the matrix. This may possibly be supported by secretion of different matrix components at regular intervals by the cells of the anterior sternal epithelium and/or regular changes in the ionic content and pH of the medium within the ecdysial gap.

Multilayered spherules such as the both intra- and extracellularly occurring type B granules are found in a variety of invertebrates (Simkiss, 1976). These granules contain organic components and calcium carbonate, mostly in the form of calcite. The most remarkable characteristic of the spherules described here is the amorphous state of their mineral compound. ACC is 10 times more soluble than that of crystalline CaCO_3 phases and instable in vitro (Brecevic and Nielson, 1989). In contrast, the amorphous state of biogenic ACC is stable over long periods of time probably by the effect of components of the organic matrix. Stabilization of ACC, however, implies that the solubility of biogenic ACC deviates from that of synthetic ACC and may even vary within mineralized tissues. In *P. scaber* 10–30 nm thick ACC nano-particles occur in mature spherules (Becker et al., 2003) and on the surface of forming and degrading spherules (Fabritius and Ziegler, 2003). The present study shows that these 10–30 nm large particles, which probably still contain mineral, are often preserved in some of the concentric layers and at the surface of radial strands of the organic matrix (Fig. 2G). These particles must be stabilized to a higher degree than the dissolved material between radial strands and some concentric layers. As mentioned in Section 1, variations in ACC stability within individual spherules lead to a high-surface area during natural degradation facilitating a quick mobilization of calcium and carbonate. Our observations on EDTA treated spherules are in agreement with these results. It is of interest that similar particles have been described along rod-like chitin–protein fibres in the exo- and endocuticle of *Carcinus maenas* (Roer and Dillaman, 1984). Although the main mineral phase in the mature cuticle of decapods is calcite, ACC occurs in premolt

cuticles suggesting that the calcitic nano-particles in the cuticle originate from amorphous precursors.

4.4. Evolution of sternal deposits

In conjunction with a comparative analysis of deposit structure (Ziegler, 2003; Ziegler and Miller, 1997) and a previous study on deposit formation (Fabritius and Ziegler, 2003) our results raise the question of how three-layered sternal deposits of *P. scaber* evolved from primordial less complex deposits. The results of the present paper contribute to a better understanding of this issue. An important step in the evolution of isopods was the shift from marine to terrestrial life, with the development of CaCO_3 storage as an adaptation to the loss of seawater as a source to mineralize the new cuticle after molt. In terrestrial isopods three different types of sternal CaCO_3 deposits have been found, whose relative storage capacity is correlated with the degree of adaptation to terrestrial life (Ziegler and Miller, 1997). Type III deposits have just one layer consisting of free spherules only. These deposits occur in semi-terrestrial isopods of the genus *Ligia* living on rocky sea shores and cliffs. *Ligidium hypnorum*, a species living in moist woodlands, forms type II deposits with two layers, a distal layer of fused spherules and a proximal layer of free spherules. Crinochaeta, whose different members inhabit a variety of biotopes including arid, desert-like habitats, have evolved the three-layered type I deposits as found in *P. scaber*. These observations have led to the hypothesis that during the evolution of terrestrial isopods type III deposits developed first followed by the addition of a layer containing fused spherules at the distal side and finally addition of a homogeneous layer at the proximal side. However, this hypothesis is hampered by the observation that the sequence in which the three layers develop in individual *P. scaber* deviates from the proposed evolutionary sequence. This inconsistency can now be easily resolved, when we propose that an initial increase in the number of spherule nucleation sites converted the layer of free spherules to one with fused spherules. A reduction of nucleation sites per volume would then lead to the formation of a layer with free spherules at the proximal side as in type II deposits and finally to the formation of a homogeneous layer just as observed during the development of the type I deposits described for *P. scaber*. According to this sequence we propose a yet unknown intermediate stage between type III and type II deposits, which consists of one layer resembling dsl of *P. scaber*.

Acknowledgment

This work was supported by the Deutsche Forschungsgemeinschaft within the research program “Principles of Biomineralization” (SPP1117).

References

- Aizenberg, J., Lambert, G., Addadi, L., Weiner, S., 1996. Stabilization of amorphous calcium carbonate by specialized macromolecules in biological and synthetic precipitates. *Adv. Mater.* 8, 222–226.
- Aizenberg, J., Lambert, G., Weiner, S., Addadi, L., 2002. Factors involved in the formation of amorphous and crystalline calcium carbonate: a study of an ascidian skeleton. *J. Am. Chem. Soc.* 124, 32–39.
- Becker, A., Bismayer, U., Epple, M., Fabritius, H., Hasse, B., Shi, J., Ziegler, A., 2003. Structural characterisation of X-ray amorphous calcium carbonate (ACC) in sternal deposits of the Crustacea *Porcellio scaber*. *Dalton Trans.* 2003, 551–555.
- Beniash, E., Aizenberg, J., Addadi, L., Weiner, S., 1997. Amorphous calcium carbonate transforms into calcite during sea urchin larval spicule growth. *R. Soc.* 264, 461–465.
- Brecec, L., Nielson, A.E., 1989. Solubility of amorphous calcium carbonate. *J. Crystal Growth* 98, 504–510.
- Coblentz, F.E., Shafer, T.H., Roer, R.D., 1998. Cuticular proteins from the blue crab alter in vitro calcium carbonate mineralization. *Comp. Biochem. Physiol. Part B* 121, 349–360.
- Fabritius, H., Ziegler, A., 2003. Analysis of CaCO_3 deposit formation and degradation during the molt cycle of the terrestrial isopod *Porcellio scaber* (Crustacea, Isopoda). *J. Struct. Biol.* 142, 281–291.
- Graf, F., Meyran, J.-C., 1985. Calcium reabsorption in the posterior caeca of the midgut in a terrestrial crustacean, *Orchestia cavimana*. *Cell Tissue Res.* 242, 83–95.
- Greenaway, P., 1985. Calcium balance and moulting in the crustacea. *Biol. Rev.* 60, 425–454.
- Greenaway, P., Farrelly, C.A., 1991. Trans-epidermal transport and storage of calcium in *Holthuisana transversa* (Brachyura: Sundathelphusidae) during premolt. *Acta Zool. Fennica* 72, 29–40.
- Mann, S., 1997. Biomineralization: the form(id)able part of bioinorganic chemistry. *Dalton Trans.* 2003, 3953–3961.
- Messner, B., 1965. Ein morphologisch-histologischer Beitrag zur Häutung von *Porcellio scaber* Latr. und *Oniscus asellus* L. (Isopoda terrestria). *Crustaceana* 9, 285–301.
- Raz, S., Testeniere, O., Hecker, A., Weiner, S., Luquet, G., 2002. Stable amorphous calcium carbonate is the main component of the calcium storage structures of the crustacean *Orchestia cavimana*. *Biol. Bull.* 203, 269–274.
- Roer, R., Dillman, R., 1984. The structure and calcification of the crustacean cuticle. *Am. Zool.* 24, 893–909.
- Scott, J.E., Kyffin, T.W., 1978. Demineralization in organic solvents by alkylammonium salts of ethylenediaminetetra-acetic acid. *Biochem. J.* 169, 697–701.
- Shafer, T.H., Roer, R.D., Midgette-Luther, C., Brookins, T.A., 1995. Postecdysial cuticle alteration in the blue crab, *Callinectes sapidus*: synchronous changes in glycoproteins and mineral nucleation. *J. Exp. Zool.* 271, 171–182.
- Simkiss, K., 1976. Biomineralization, intracellular and extracellular routes. In: C.J. Duncan (Ed.), *Calcium in biological systems*, Symposium of the Society for Experimental Biology, vol. 30. pp. 423–444.
- Sparkes, S., Greenaway, P., 1984. The haemolymph as a storage site for cuticular ions during premolt in the freshwater/land crab *Holthuisana transversa*. *J. Exp. Biol.* 113, 43–54.
- Steel, C.G.H., 1993. Storage and translocation of integumentary calcium during the moult cycle of the terrestrial isopod *Oniscus asellus* (L.). *Can. J. Zool.* 71, 4–10.
- Taylor, M.G., Simkiss, K., Greaves, G.N.O., Mann, S., 1993. An X-ray absorption spectroscopy study of the structure and transformation of amorphous calcium carbonate from plant cystoliths. *R. Soc.* 252, 75–80.
- Ziegler, A., 1994. Ultrastructure and electron spectroscopic diffraction analysis of the sternal calcium deposits of *Porcellio scaber* Latr. (Isopoda, Crustacea). *J. Struct. Biol.* 112, 110–116.
- Ziegler, A., 2002. X-ray microprobe analysis of epithelial calcium transport. *Cell Calcium* 31, 307–321.
- Ziegler, A., 2003. Variations of calcium deposition in terrestrial isopods. In: Sfenthourakis, S., De Araujo, P.B., Hornung, E., et al. (Eds.), *The Biology of Terrestrial Isopods, Crustaceana Monographs*, vol. 2, Koninklijke Brill NV, Leiden, pp. 299–309.
- Ziegler, A., Miller, B., 1997. Ultrastructure of CaCO_3 deposits of terrestrial isopods (Crustacea, Oniscidea). *Zoomorphology* 117, 181–187.
- Ziegler, A., Scholz, F.H.E., 1997. The ionic hemolymph composition of the terrestrial isopod *Porcellio scaber* Latr. during molt. *J. Comp. Physiol. B* 167, 536–542.
- Ziegler, A., Weihrauch, D., Hagedorn, M., Towle, D.W., Bleher, R., 2004. Expression and polarity reversal of V-type H^+ -ATPase during the mineralization–demineralization cycle in *Porcellio scaber* sternal epithelial cells. *J. Exp. Biol.* 207, 1749–1756.
- Ziegler, A., Weihrauch, D., Towle, D.W., Hagedorn, M., 2002. Expression of Ca^{2+} -ATPase and $\text{Na}^+/\text{Ca}^{2+}$ -exchanger is upregulated during epithelial Ca^{2+} transport in hypodermal cells of the isopod *Porcellio scaber*. *Cell Calcium* 32, 131–141.

5.3 Structural characterisation of X-ray amorphous calcium carbonate (ACC) in sternal deposits of the Crustacea *Porcellio scaber*.

Structural characterisation of X-ray amorphous calcium carbonate (ACC) in sternal deposits of the crustacea *Porcellio scaber*

Alexander Becker,^a Ulrich Bismayer,^b Matthias Epple,^{*a} Helge Fabritius,^c Bernd Hasse,^a Jianmin Shi^b and Andreas Ziegler^{*c}

^a Solid State Chemistry, Faculty of Chemistry, University of Bochum, D-44780 Bochum, Germany. E-mail: matthias.epple@ruhr-uni-bochum.de

^b Institute for Mineralogy and Petrography, University of Hamburg, Grindelallee 48, D-20146 Hamburg, Germany

^c Central Facility for Electron Microscopy, University of Ulm, Albert-Einstein-Allee 11, D-89069 Ulm, Germany. E-mail: andreas.ziegler@medizin.uni-ulm.de

Received 25th October 2002, Accepted 2nd January 2003

First published as an Advance Article on the web 23rd January 2003

Mineral deposits in land-based woodlice (crustacea, *Porcellio scaber*) were analysed by high-resolution X-ray diffraction, X-ray absorption spectroscopy (EXAFS) and infrared microscopy. Calcium carbonate is stored within the first four anterior sternites before changing the cuticle (shell). These deposits consist of fully X-ray amorphous calcium carbonate (primary particle size less than 100 Å). The short-range order is comparable to crystalline calcium carbonate phases (first coordination shell), but there is increasing structural disorder beyond about 3 Å. This high degree of structural disorder gives a high solubility, *i.e.* an easy mobilisation within the biological system. The results are compared with EXAFS data from the literature on other biogenic amorphous calcium carbonates.

Introduction

Inorganic minerals are used in many biological systems for different purposes, with teeth, bones and shells being only the most prominent examples.^{1–6} While many biominerals occur in a crystalline form (like molluscan shells consisting of CaCO₃ in its calcitic or aragonite modification) there are a number of cases where the biomineral is X-ray amorphous (like in all structures consisting of silica: SiO₂·*n*H₂O). In the last decade the attention has increasingly turned to amorphous phases that earlier remained mostly undetected due to a lack of suitable analytical techniques.

In particular, recent investigations suggest that amorphous CaCO₃ plays an important role in the initiation of the biomineralisation process. Because the solubility of amorphous CaCO₃ is about ten times higher than that of crystalline CaCO₃,⁷ it can be used as temporary storage for calcium. Although amorphous CaCO₃ is unstable *in vitro*, it is quite stable in some biominerals, and an increasing number of reports indicate that amorphous CaCO₃ occurs in a variety of biological systems, be it as precursor phase on the way to crystalline calcium carbonate,^{8–12} as final biomineralised product,^{13–17} or for intermediate storage of calcium.^{18–20} It has been detected *inter alia* in woodlice of the type *Oniscus asellus*,¹⁸ in plant cystoliths in the leaf of *Ficus retusa*¹³ and *Ficus microcarpa*,¹⁷ in larval shells of the freshwater snail *Biomphalaria glabrata*^{9,11} and of the marine bivalves *Mercenaria mercenaria*¹² and *Crassostrea gigas*,¹² in body spicules of the ascidian *Pyura pachydermatina*,^{15,17} and in the carapace of the american lobster *Homarus americanus*.¹⁷ Weiss *et al.* have recently demonstrated by vibrational spectroscopy that ACC acts as a precursor phase for aragonite in mollusc larval shells.¹²

Crustaceans are excellent models to investigate biomineralisation. Many crustaceans have a rigid cuticle which contains an organic matrix and large amounts of CaCO₃ as the main mineral component. This cuticle cannot expand during growth of the animal. Hence, it is shed regularly during growth and replaced by a larger cuticle. During this moulting process calcium which is left within the old cuticle is lost and must be replaced to mineralise the new cuticle. In a marine environment calcium is readily available from seawater and most crustaceans can quickly replace lost calcium by taking up Ca²⁺ from the

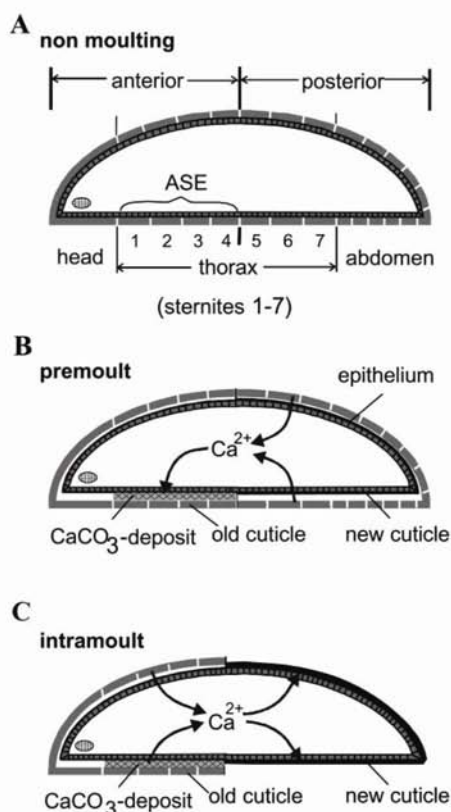
seawater across the gills.²¹ Therefore, storage or recycling of calcium is of rather low significance for marine crustaceans. Terrestrial crustaceans, however, are under high environmental pressure to store and recycle calcium since they can replace lost calcium with food or freshwater only.²²

About half of the 9000 known isopod species belong to the terrestrial isopods (*Oniscidea*), which among crustaceans developed the most elaborate adaptations to the terrestrial environment and became fully independent from aquatic habitats. Therefore, terrestrial isopods are regarded as the only “true-terrestrial” group of the crustacea. Most terrestrial isopods store CaCO₃ in large deposits within the ecdysial space between the cuticle secreting epithelium and the old cuticle of the first four sternites (Figs. 1A, 2A). The formation of these CaCO₃ reservoirs is accompanied by an interesting sequence of resorption and deposition of cuticular calcium (Figs. 1B, 1C), linked to the unique biphasic moult of isopods²³ which moult first the posterior (tailside) and then the anterior (frontside) half of the body. Before the moult of the posterior cuticle (pre-moult, Fig. 1B), calcium ions and probably also carbonate ions are resorbed from the posterior cuticle and stored within the first four sternites.²⁴ During the short period of less than one day between the moult of the posterior and anterior half of the body (intramoult, Fig. 1C) the sternal deposits are fully dissolved and the calcium of the deposits and part of the calcium within the anterior cuticle is used to mineralise the new posterior cuticle.

For *P. scaber* the structure and composition of the deposits were investigated previously by light microscopy, electron microscopy and X-ray microprobe analysis.^{19,20,25} The sternal deposits consist of a homogeneous layer of glassy appearance facing the epithelium and an opaque layer adjacent to the old cuticle (Fig. 2B). Electron microscopy has shown that the opaque layer is composed of numerous spherules with diameters of up to 1.7 µm. This spherular layer can be subdivided into a proximal (towards the body center) spherular layer consisting of free spherules (Fig. 2C) and a distal (towards the body surface) spherular layer composed of smaller spherules, which often appear fused together (Fig. 2D). Both the homogeneous layer and the spherules consist of an X-ray amorphous (probably hydrated) CaCO₃ compound and contain an organic matrix.¹⁹

Table 1 Ca K-edge EXAFS data of ACC deposits in *Porcellio scaber*, together with EXAFS data for the three water-free crystalline calcium carbonate polymorphs and for monohydrocalcite

Sample	E_0/eV	First shell: oxygen			Second shell			Third shell			Fourth shell: six Ca	
		N	$R/\text{\AA}$	$10^3\sigma^2/\text{\AA}^2$	N	$R/\text{\AA}$	$10^3\sigma^2/\text{\AA}^2$	N	$R/\text{\AA}$	$10^3\sigma^2/\text{\AA}^2$	$R/\text{\AA}$	$10^3\sigma^2/\text{\AA}^2$
<i>Porcellio scaber</i> , sternal deposit of ACC	+0.33	3.8 ^a	2.38 ^a	14	1.4 C ^a	3.00	7	0.4 C ^a	3.72	1	3.89	109
Aragonite reference	-1.04	9 ^b	2.47	33	3 C ^b	2.98	3	3 C ^b	3.26	10	3.94	28
Calcite reference	-0.29	6 ^b	2.33	9	6 C ^b	3.27	35	6 O ^b	3.65	16	4.05	9
Vaterite reference	+1.62	6 ^b	2.37	7	2 O, 2 C ^b	3.09	21	—	—	—	4.24	15
Monohydrocalcite reference ¹⁵	+1.3...1.5	7.4 ^a	2.37	9	1.5 C ^a	3.03	7	3 C ^a	3.36	0	—	—

^a Fit result. ^b Number fixed to crystallographic value.**Fig. 1** Schematic presentation of calcium fluxes in *Porcellio scaber*. (A) General morphology of *P. scaber*. (B) During premoult calcium from the posterior cuticle is resorbed into the hemolymph and transported across the anterior sternal epithelium (ASE) to sternal CaCO_3 deposits. (C) After moulting of the posterior half of the body, calcium from the deposits and the anterior cuticle is resorbed and used to mineralise the new posterior cuticle. Arrows: direction of Ca^{2+} fluxes. Modified from ref. 35.

In order to further characterise the structure of the sternal CaCO_3 deposits we applied high resolution X-ray diffractometry (XRD), X-ray absorption spectroscopy (Extended X-ray absorption fine structure; EXAFS) and reflection infrared microscopy (IR). The results are compared with literature EXAFS data obtained on X-ray amorphous calcium carbonate (ACC) by other authors. For comparison, the three crystalline anhydrous polymorphs of CaCO_3 (calcite, aragonite and vaterite) were also studied by EXAFS.

Results and discussion

Field-emission scanning electron micrographs of cleaved surfaces of the homogeneous layer and of spherules show that the spherical deposits consist of particles between 10 and 30 nm in

size (Figs. 2E, 2F). High-resolution high-intensity X-ray diffraction was performed on isolated sternal deposits (mineral phase only). Fig. 3 shows that there are no visible diffraction peaks at all, *i.e.* there are not even traces of crystalline phases present (detection limit about 0.5 to 1 wt%). If we assume Scherrer broadening of the diffraction peaks, we can estimate that the size of the coherently scattering domains must be smaller than ~ 100 Å.

For further structural elucidation, X-ray absorption spectroscopy (EXAFS) at the calcium K-edge was employed. Fig. 4 shows the primary EXAFS oscillations, Fig. 5 shows the Fourier transform magnitude of this spectrum together with a fit to a suitable model. For comparison, the results for the crystalline phase vaterite are also shown. As the structure of this ACC phase is unknown, a suitable model derived from crystalline calcium carbonate was used. Table 1 contains the fit results, together with reference data. A comparison to the crystalline calcium carbonate phases is possible by analysing the first coordination sphere that always consists of oxygen. As EXAFS is very sensitive for coordination distances of the first shell (about ± 0.02 Å), these values are characteristic for the short-range order. For the three crystalline phases calcite, aragonite and vaterite, the Ca-6 Ca shell at about 4 Å is also important as the coordination number is always the same. The two other shells between 3 and 3.8 Å are less characteristic to distinguish between the different polymorphs as they differ considerably in the different calcium carbonate phases in distance and nature of neighbouring atom (C, O) (see Table 1). Another pseudopolymorph is monohydrocalcite $\text{CaCO}_3 \cdot \text{H}_2\text{O}$ for which EXAFS fit data for the first shells are available.¹⁵

We can conclude from the fit results for the first shell that the calcium-oxygen distance in this ACC phase resembles either vaterite or monohydrocalcite. The coordination number N for Ca-O of 3.8 is associated with an estimated error of about 30%, but is closer to 6 (calcite, vaterite) or 7.4 (monohydrocalcite) than to 9 (aragonite). We do not to make definite statements for the higher shells as they are all rather weak. The characteristic fourth shell (Ca-6 Ca) is especially weak in the sternal deposits as indicated by the high Debye-Waller factor (see also the Fourier transform magnitude in Fig. 5). These observations indicate a high degree of disorder in this ACC phase beyond the first coordination shell. We can conclude that the mineral has a well-defined short-range order in the first coordination shell with calcium coordinated by carbonate groups *via* the oxygen atoms. The coordination number is closer to 6 than to 9.

Table 2 shows the EXAFS data from the literature for all ACC phases investigated with this technique so far. It is evident that not all ACC phases are identical in structure. To cite from Sagi *et al.*:¹⁷

...the general term 'amorphous calcium carbonate' includes materials that are structurally different. These differences may account for the various mechanisms of their formation and stabilisation...

Table 2 Results reported in the literature for EXAFS spectra of X-ray amorphous calcium carbonates found in biology, together with crystalline phases. The entries are sorted with ascending distance of the first coordination shell of oxygen. The second, third and fourth shells in the sternal deposits of *Porcellio scaber* are weak and of poor significance

Sample	Shell distance by EXAFS (Å)			
	First shell: Ca–O	Second shell: Ca–C or Ca–O	Third shell: Ca–C or Ca–O	Fourth shell: Ca–6 Ca
ACC in carapaces of <i>Homarus american</i> ¹⁷	2.27	— ^a	3.47	3.79
ACC in plant cystoliths of <i>Ficus microcarpa</i> ¹⁷	2.31	— ^a	3.48	3.79
Calcite (this work)	2.34	3.30	3.64	4.05
Calcite ¹³	2.35	3.23	3.48	3.98
ACC in plant cystoliths of <i>Ficus retusa</i> ¹³	2.36	3.22	3.39	4.06
Calcite ¹⁵	2.37	3.21	3.52	4.11
Monohydrocalcite ¹⁵	2.37	3.03	3.36	— ^a
Vaterite (this work)	2.37	3.09	— ^a	4.24
ACC in spicules of <i>Pyura Pachydermatina</i> ¹⁵	2.37	3.03	3.36	— ^a
ACC in sternal deposits of <i>Porcellio scaber</i> (this work)	2.38	3.00	3.72	(3.89)
ACC in larval shells of <i>Biomphalaria glabrata</i> ^{9,11}	2.44	— ^a	— ^a	3.92
Aragonite (this work)	2.47	2.98	3.26	3.94

^a Shell not included in fit.

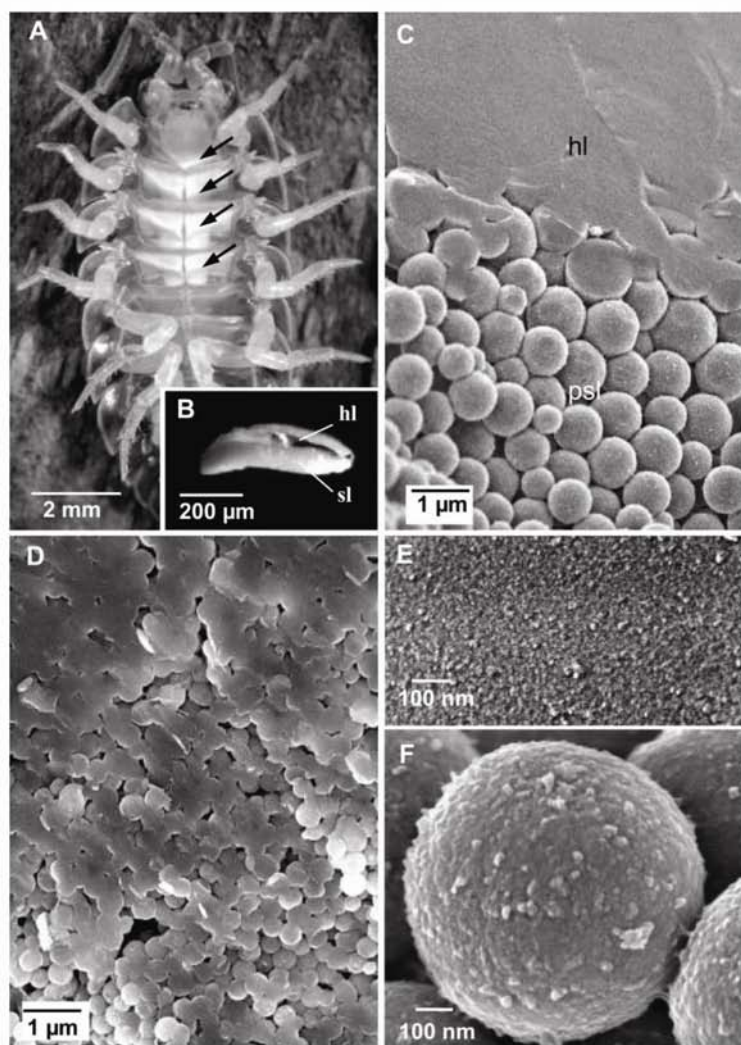


Fig. 2 Structure of the sternal CaCO_3 deposits of *Porcellio scaber* in late premoult. (A) Light micrograph of the ventral body surface showing the four sternal CaCO_3 deposits (arrows). (B) Light micrograph of a CaCO_3 deposit fractured in its central region showing the proximal homogeneous layer (hl) of glassy appearance and the distal spherular layer (sl). (C) Overview of the homogeneous layer and the proximal part of the spherular layer of CaCO_3 (psl). (D) Overview of the distal spherular layer. (E) Surface structure of the homogeneous layer in high magnification. (F) Surface structure of a spherule.

In this particular case of the sternal deposits, the long-range order is particularly poor, *i.e.* we can assume that the thermodynamic stability is low, leading to a high solubility. As the

material is temporarily deposited for later remobilisation, this makes sense from the viewpoint of the organism.

Further information was derived from microscopic IR

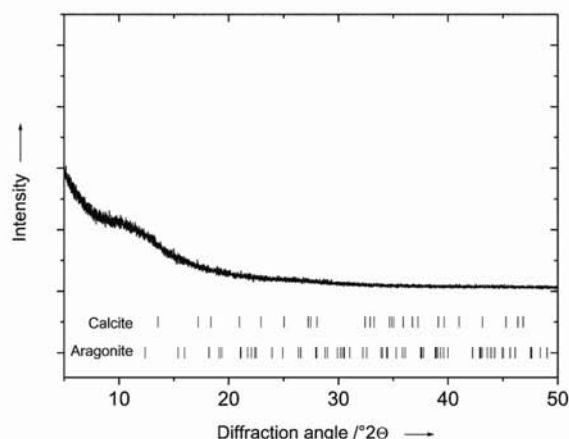


Fig. 3 High-resolution X-ray powder diffractogram of sternal deposits of *Porcellio scaber* ($\lambda = 0.90826$ Å). The diffraction peak positions that would be expected for calcite or aragonite are indicated for comparison. The material is fully X-ray amorphous.

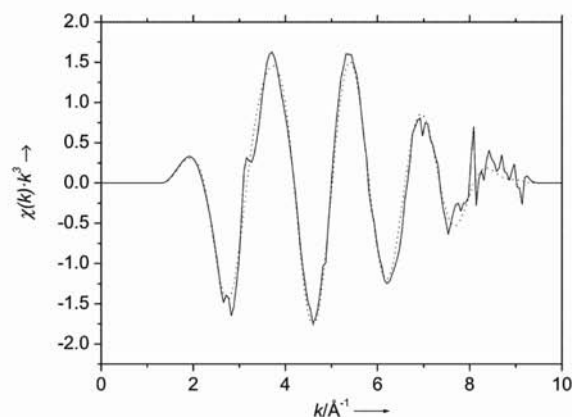


Fig. 4 Primary Ca K-edge EXAFS data $\chi(k)$ of sternal deposits of *Porcellio scaber*. Solid line: Experimental data. Dotted line: Fit data.

reflection spectra of the glassy natural surface (hl) and of the proximal spherular layer (psl) (see Fig. 2B). The data are shown in Fig. 6. These spectra reveal the presence of nanocrystalline calcium carbonate material with some degree of short-range order. In the range $600\text{--}1500\text{ cm}^{-1}$ calcium carbonate signals can be clearly distinguished from the excitations of organic components. The IR bands due to CO_3^{2-} vibrations in CaCO_3 display excitations near 1400 and 1480 cm^{-1} (E_u) and 860 cm^{-1} (A_{2u}). The band near 1400 cm^{-1} shows strong intensity and might be induced by the small particle size of the crystallites. The bands at $1400/1480\text{ cm}^{-1}$ are due to the transverse optic (TO) component of the antisymmetrical stretching mode (for calcite: in the crystallographic ab -plane) whereas the band at 860 cm^{-1} corresponds to the longitudinal optic (LO) component of the out-of-plane mode (for E II c). Near 710 cm^{-1} the antisymmetrical bending mode E_u occurs in the ab -plane of the carbonate group. The excitations were assigned according to literature data.^{26–28} Both spectra show similar bands, except one additional excitation which occurs in the homogeneous glassy surface (hl) near 1630 cm^{-1} (not related to calcium carbonate but probably to organic material).²⁹ Bands in the range of 2000 to 3500 cm^{-1} are likely to be caused by OH and water vibrations whereas the modes at higher energies are assumed to result from organic material. A comparison of the A_{2u} mode at 860 cm^{-1} with standard IR spectra of calcium carbonate²⁹ suggests that the structure resembles aragonite (860 cm^{-1}), but within the error limit calcitic (876 cm^{-1}) or vateritic (877 cm^{-1}) structures cannot be completely ruled out.

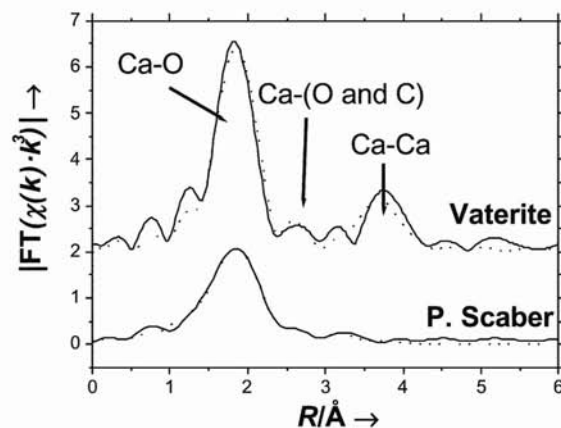


Fig. 5 Ca K-edge EXAFS Fourier transform magnitude of well-crystalline vaterite (top) and of the X-ray amorphous sternal deposits of *Porcellio scaber* (bottom). The higher shells (especially Ca–Ca) show up to a much lesser extent in the ACC deposits compared to vaterite, indicating a high degree of disorder. Solid lines: Experimental data. Dotted lines: Fit data.

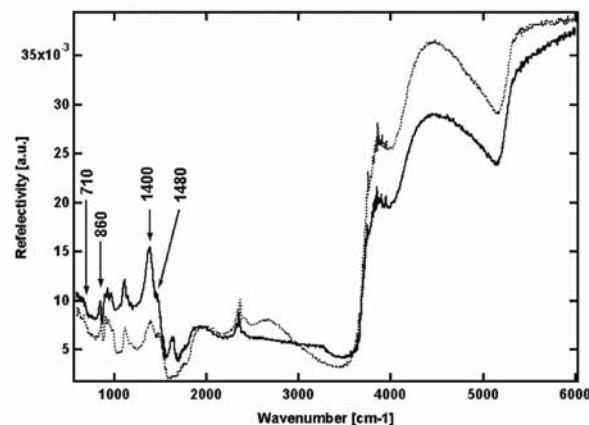


Fig. 6 IR-reflection spectra of calcium carbonate surfaces displayed in Fig. 2B of *Porcellio scaber*. The solid line represents the spectrum of the homogeneous glassy layer (hl) and the dotted line that of the proximal spherular layer (psl). The indicated IR bands correspond to calcium carbonate (see text).

As the material leads only to diffuse X-ray diffraction but to excellent infrared light scattering signals we conclude that the particle size of the corresponding coherent lattice must be smaller than about 100 Å (as estimated from Scherrer broadening of diffraction peaks) but larger than a few interatomic distances. Corresponding signals have been observed in the case of small clusters of ferroic materials³⁰ which were of the order of 30 Å .

In conclusion, it could be shown that the sternal deposits are fully X-ray amorphous, but that they are not without structure. This corresponds well to results obtained for other biogenic ACC phases (Table 2). There is a defined first-shell coordination of oxygen around calcium, and the primary particle size is of the order of a few nanometers. The question how the material is prevented from crystallisation under ambient conditions and how it is precipitated must await further studies on the biological side of this system. However, it has been shown that specialised proteins are able to nucleate and stabilise amorphous calcium carbonate (which is almost impossible to prepare in the laboratory).^{8,14} After all, a delicate interaction between biological compounds and the inorganic material is present in this kind of material.

Experimental

Woodlice (*Porcellio scaber* Latr., 1804) were bred in plastic containers filled with soil and bark and fed on oak leaf litter and fresh potatoes. We identified animals in the premoult stage by their sternal deposits that can be seen as white spots at the ventral side (belly) of the living individuals. About 20 animals with well-developed sternal deposits were sacrificed and the cuticle and CaCO_3 deposits of the sternites 1–4 were gently removed, washed in bi-distilled water for about one second to remove any remaining body fluids (which have a high concentration of Na, Mg, K, Ca, and Cl).³¹ In order to prevent (re-)crystallisation of ACC, the washing water was quickly removed by dipping the specimens in 100% methanol for about another second. Preliminary experiments showed that treatment with 100% methanol for one month had no apparent effect on the high-resolution X-ray diffraction patterns of the CaCO_3 deposits, i.e. no crystallisation occurred (data not shown). Then the specimens were air-dried and the CaCO_3 deposits were carefully removed from the cuticle using fine tweezers and collected to yield about 10 mg of material.

For field-emission scanning electron microscopy, sternites of animals in the late premoult stage were prepared as described above. CaCO_3 deposits were cleaved, mounted and rotary shadowed with platinum (2 nm) in a Balzers BAF 300 freeze-fracturing device and viewed with a Hitachi S-5200 field emission scanning electron microscope at acceleration voltages of 4 and 10 kV using a secondary electron detector.

EXAFS experiments were carried out at the Hamburger Synchrotronstrahlungslabor (HASYLAB) at Deutsches Elektronen-Synchrotron (DESY), Hamburg, at beamline E4. The DORIS III storage ring was operated at 4.5 GeV positron energy and currents of 70–150 mA. The incoming synchrotron beam was monochromated by a Si double-crystal. Experiments were performed at the Ca K-edge (ca. 4038 eV) in transmission mode at liquid nitrogen temperature. The slightly ground samples were fixed in a thin layer on adhesive tape. For quantitative data evaluation we used the programs SPLINE and XFIT.³² Theoretical standards were computed with the program FEFF 6.01a.³³ All fits were carried out with k^3 -weighted data in R -space. The amplitude reduction factor S_0^2 was fixed to 0.60. For the reference compounds calcite, aragonite and vaterite, the coordination numbers were kept to the values derived from the crystal structure. For the ACC sample, the coordination numbers were allowed to vary. The error in this variable coordination number is about $\pm 30\%$ as there is a strong mathematical correlation with the Debye–Waller factor σ^2 . The typical error margin of EXAFS experiments for the first shell distance is about $\pm 0.02 \text{ \AA}$.³⁴ These estimated errors are significantly higher for the second, third and fourth shells which are less well defined. The experimental data shown in Fig. 4 were treated with a window function but not Fourier-filtered.

High-resolution X-ray powder diffractometry was carried out in transmission geometry at room temperature (ground samples on Kapton foil) at beamline B2 at HASYLAB/DESY, Hamburg, Germany, at a wavelength of $\lambda = 0.90826 \text{ \AA}$.

Unpolarised IR spectra between 600 and 6000 wavenumbers were recorded using a Bruker IFS 55 spectrometer equipped with a microscope, the beam diameter was about 100 μm with 512 spectral scans per sample.

Acknowledgements

The authors thank the Deutsche Forschungsgemeinschaft for support within the research program "Principles of Biomineralisation". M. E. also thanks the Fonds der Chemischen Industrie for financial support. We thank C. Günther and G. Wolf, Freiberg/Sachsen, for providing the sample of phase-pure vaterite. Beamtime at the Hamburger Synchrotronstrahlungslaboratorium (HASYLAB at DESY) was generously provided.

References

- 1 H. A. Lowenstam and S. Weiner, *On biomineralisation*, Oxford University Press, Oxford, 1989.
- 2 S. Mann, ed., *Biomimetic materials chemistry*, VCH, Weinheim, 1996.
- 3 S. Weiner and H. D. Wagner, *Annu. Rev. Mater. Sci.*, 1998, **28**, 271.
- 4 E. Baeuerlein, ed., *Biomineralisation*, VCH, Weinheim, 2000.
- 5 S. Mann, *Biomineralisation*, Oxford University Press, Oxford, 2001.
- 6 S. V. Dorozhkin and M. Eppe, *Angew. Chem., Int. Ed.*, 2002, **41**, 3130.
- 7 L. Brecevic and A. E. Nielson, *J. Cryst. Growth*, 1989, **98**, 504.
- 8 E. Beniash, J. Aizenberg, L. Addadi and S. Weiner, *Proc. R. Soc. London B*, 1997, **264**, 461.
- 9 B. Hasse, H. Ehrenberg, J. C. Marxen, W. Becker and M. Eppe, *Chem. Eur. J.*, 2000, **6**, 3679.
- 10 S. Raz, S. Weiner and L. Addadi, *Adv. Mater.*, 2000, **12**, 38.
- 11 J. C. Marxen, W. Becker, D. Finke, B. Hasse and M. Eppe, *J. Mollusc. Stud.*, 2003, **69**, in press.
- 12 I. M. Weiss, N. Tuross, L. Addadi and S. Weiner, *J. Exp. Zool.*, 2002, **293**, 478.
- 13 M. G. Taylor, K. Simkiss, G. N. Greaves, M. Okazaki and S. Mann, *Proc. R. Soc. Lond. B*, 1993, **252**, 75.
- 14 J. Aizenberg, G. Lambert, L. Addadi and S. Weiner, *Adv. Mater.*, 1996, **8**, 222.
- 15 Y. Levi-Kalishman, S. Raz, S. Weiner, L. Addadi and I. Sagi, *J. Chem. Soc., Dalton Trans.*, 2000, 3977–3982.
- 16 J. Aizenberg, G. Lambert, S. Weiner and L. Addadi, *J. Am. Chem. Soc.*, 2002, **124**, 32.
- 17 Y. Levi-Kalishman, S. Raz, S. Weiner, L. Addadi and I. Sagi, *Adv. Funct. Mater.*, 2002, **12**, 43.
- 18 S. R. Wood and J. D. Russel, *Crustaceana*, 1987, **53**, 49.
- 19 A. Ziegler, *J. Struct. Biol.*, 1994, **112**, 110.
- 20 A. Ziegler and B. Miller, *Zoomorphology*, 1997, **117**, 181.
- 21 D. S. Neufeld and J. N. Cameron, *J. Exp. Biol.*, 1993, **184**, 1.
- 22 P. Greenaway, *Biol. Rev.*, 1985, **60**, 425.
- 23 B. Messner, *Crustaceana*, 1965, **9**, 285.
- 24 C. G. H. Steel, *Can. J. Zool.*, 1993, **71**, 4.
- 25 A. Ziegler, *Cell Calcium*, 2002, **31**, 307.
- 26 V. C. Farmer, *The Infrared Spectra of Minerals*, Mineralogical Society, London, 1974.
- 27 K. Nakamoto, *Infrared spectra of inorganic and coordination compounds*, Wiley, Weinheim, 1978.
- 28 J. C. Decius and R. M. Hexter, *Molecular Vibrations in Crystals*, McGraw-Hill, New York, 1987.
- 29 G. Falini, S. Albeck, S. Weiner and L. Addadi, *Science*, 1996, **271**, 67.
- 30 U. Bismayer, *Rev. Mineral. Geochem.*, 2000, **39**, 265.
- 31 A. Ziegler and F. H. E. Scholz, *J. Comp. Physiol., B*, 1997, **167**, 536.
- 32 P. J. Ellis and H. C. Freeman, *J. Synchrotron Rad.*, 1995, **2**, 190.
- 33 S. I. Zabinsky, J. J. Rehr, A. Ankudinov, R. C. Albers and M. J. Eller, *Phys. Rev. B*, 1995, **52**, 2995.
- 34 H. Bertagnolli and T. S. Ertel, *Angew. Chem., Int. Ed. Engl.*, 1994, **33**, 45.
- 35 A. Ziegler, D. Weihrauch, D. W. Towle and M. Hagedorn, *Cell Calcium*, 2002, **32**, 131.

6. Appendix

6.1 Material and Methods

All chemicals used for this study were obtained from Sigma-Aldrich Co. or Carl Roth GmbH + Co. KG unless stated otherwise.

6.1.1 Culture of *Porcellio scaber*

Porcellio scaber Latreille, 1804 were collected in the field at various locations around the city of Ulm. The species was determined using the determination key for terrestrial isopods in Germany published by Gruner (1966). In the laboratory the animals were reared in plastic containers filled with natural soil as substrate and pieces of wood and bark for hiding places. The substrate was watered every two to three days and the containers were covered with lids in order to maintain sufficient air humidity. Additionally, Petri-dishes containing pieces of paper towels soaked in water were provided to create different micro climates, which allowed the animals to choose their preferred conditions. Potatoes, carrots and dry oak leaves were offered for food. The animals were kept at room temperature and exposed to the natural light cycle. The containers were regularly inspected for molting animals which were then isolated to monitor their molting stage. For this, they were transferred to Petri-dishes containing filter paper, a piece of bark, a moisture source consisting of an Eppendorff-cup filled with humid paper tissue and small pieces of potato for food. Females preparing for the parturial molt were not used, since their deposits differ from those produced during regular molts. The offspring of these females developed well in the culture and served for replenishing the stock of isopods. The molting stage of individual *P. scaber* was determined by the shape of the deposits according to a staging adopted from Wieser (1964) and Messner (1965) (Table 1). Under the employed culture conditions it takes about 7 days from the first sign of CaCO_3 deposition to the posterior molt. In our case, stages I and II in which the deposits just started to appear occur more than 7 days, stages III and IV with half way developed deposits 3-7 days, stage V 2-3 days and stage VI with fully developed deposits 1 day before posterior molt. The observed times differ slightly from those given by other sources, but it has been shown that in nature these time intervals vary with different environmental conditions like the season, climate, and food supply (Drobne and Štrus, 1996; Messner, 1965).

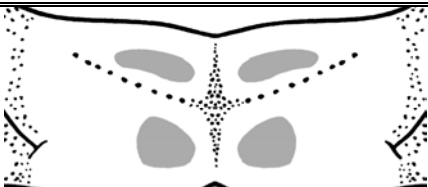
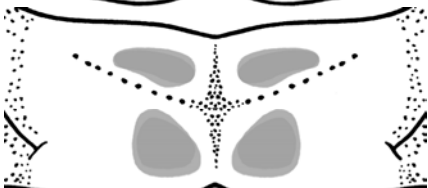
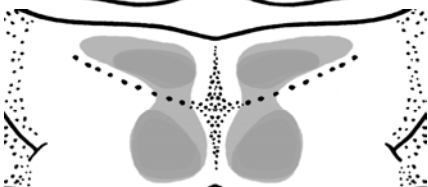
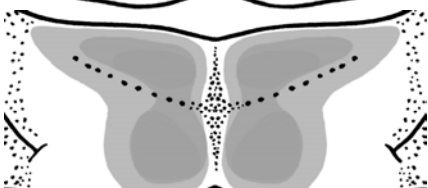
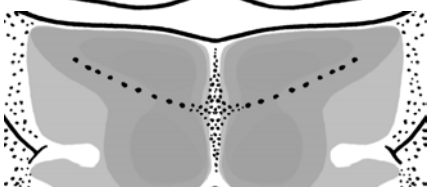
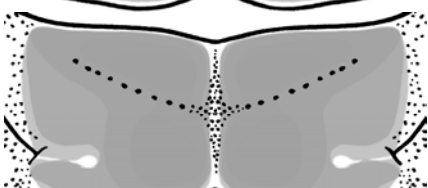
premolt stage	appearance of deposits	time of occurrence
I		> 7 days before posterior molt
II		> 7 days before posterior molt
III		~ 7 days before posterior molt
IV		3-7 days before posterior molt
V		2-3 days before posterior molt
VI		1 day before posterior molt

Table 1. The development of the sternal CaCO_3 deposits of *P. scaber* during the premolt phase shown exemplary for the third sternite. The molting stages are determined by the shape of the deposits according to Wieser (1964). The different shades of gray in the schematics correspond to the thickness of the deposits, darker shades of gray indicate a higher thickness than lighter areas. The period of time before posterior molt in which the deposits showed a specific appearance varied considerably in individual animals.

6.1.2 Transmission electron microscopy of the aggregation zone in early premolt

Preparation of high pressure frozen and freeze substituted thin sections

Two medium sized animals in early premolt stage (Table 1, stage I) were decapitated and small pieces of the ventral cuticle from the first four anterior sternites were carefully dissected together with the developing deposits and the anterior sternal epithelium. The pieces were then immersed in hexadecene for an optimal pressure and cooling transfer and placed between two

small aluminum dishes. Subsequently, every sample was mounted in the holder, high pressure frozen (HPF 01, Engineering Office M. Wohlwend GmbH, Switzerland) and immediately transferred to liquid nitrogen. From there the sample were transferred into a custom made computer-controlled substitution device (A. Ziegler and W. Fritz, University of Ulm) and freeze substituted over night in acetone with 1.6 % osmium tetroxide, 0.1 % uranyl acetate and 5 % water by slowly raising the temperature from -90 to 0°C. After bringing the samples to room temperature they were washed in acetone and transferred to 50% Epon resin (Fluka, Germany) in acetone for 1 h and 100 % Epon for 6 h. The Epon was then polymerized at 60°C. Thin sections (60nm) were cut with a Leica Ultracut UCT ultramicrotome using a diamond knife (Diatome, Switzerland) and transferred to copper grids. The samples were imaged with a Philips 400 transmission electron microscope at an acceleration voltage of 80 kV (Fig. 9).

Preparation of chemically fixed thick sections

The samples used for this investigation were kindly provided by PD Dr. A. Ziegler, who prepared them in the course of a previous study on the ultrastructure of the sternal CaCO_3 deposits of *P. scaber* (Ziegler, 1994) using the following procedure: Animals in early premolt stage were killed by injection of 10-15 μl of 12.5% glutaraldehyde and their sternal plates with the CaCO_3 deposits then dissected and fixed in 2.5% glutaraldehyde and 2% paraformaldehyde in 0.1 M sodium cacodylate buffer for 1 h. Subsequently, the specimens were washed three times, postfixed in 2% osmium tetroxide in the same buffer and decalcified using 0.1 M EGTA for 2 h. After dehydration in a series of ethanols, the specimens were block stained in 2% uranyl acetate in ethanol and embedded in Epon resin. From these blocks, 500 nm thick sections were cut on a Reichert Ultracut microtome using a diamond knife. The sections were transferred to a hot water surface for stretching. They were placed on coated formvar film on copper grids and viewed in an energy filtered Zeiss CM 902 transmission electron microscope at an energy loss (ΔE) of 30 eV (Fig. 10).

6.1.3 Isolation of the organic matrix from the deposits

For the isolation of organic matrix the calcium carbonate deposits of 100 adult *Porcellio scaber* with a body length of over 10 mm were collected and pooled. Special care was taken to use only individuals in late premolt stage whose epimeres and anterior tergites already showed a flat white color indicating they are just about to molt. The animals were sacrificed by decapitation and their ventral anterior cuticle with the attached deposits was dissected and washed in double distilled water (ddw) and 100% methanol for 1s each to remove residual tissue and body fluids. Subsequently, the deposit material was carefully separated from the cuticle

using ultrafine tweezers and a stereomicroscope. The obtained dry mass of 29.8 mg of pure deposits were pooled in Eppendorff cups and stored at -30°C to prevent decomposition and recrystallization effects. For decalcification, the deposits were suspended in 4ml double distilled water containing 1% protease inhibitors (Sigma) and transferred to dialysis tubing (Thomapor MWCO 7000, Reichelt Chemietechnik). Dialysis was conducted against 1liter of ddw followed by Na-acetate buffer pH 6 under continuous stirring at 5°C for one week each. Then the sample was dialyzed against Na-acetate buffer pH 6.5 (1 d) and washed against ddw (1 d). Subsequently the sample solution was removed from the tubing and centrifuged for 30 min at 13000/min, 4°C. The supernatant containing the water soluble matrix components was separated from the pellet (insoluble fraction) and stored frozen at -30°C. The insoluble fraction was transferred to 8M urea in H₂O with 1% protease inhibitors and subsequently dialyzed against water to remove the urea. The centrifuged solution containing the insoluble matrix components and the insoluble white residue were stored frozen at -30°C. A Bradford-test using a spectral photometer (Biorad) was performed on the fraction of water soluble matrix components and revealed a protein concentration of 0.1250 mg/ml. This fraction was further used for SDS poly-acrylamide gel-electrophoresis and MALDI-TOF.

6.1.4 SDS poly-acrylamide gel-electrophoresis (PAGE) of the water soluble matrix fraction

The water soluble matrix components were separated using a 12% SDS polyacrylamide gel prepared in the laboratory (14.5 cm x 16.5 cm; separating gel: 4.9 ml H₂O, 6 ml 30%mix (29.2% acrylamide + 0.8% N,N'-methylene-bis-acrylamide), 3.7 ml 1.5M Tris pH 8.8, 0.2 ml 10% SDS, 0.2 ml 10% APS (ammonium persulfate), 0.008 ml TEMED (N,N,N',N'-tetramethylethylenediamine); stacking gel: 5.5 ml H₂O, 1.3 ml 30%mix, 1.0 ml 1M Tris pH 6.8, 0.08 ml 10% SDS, 0.08 ml 10% APS, 0.008 ml TEMED). The gel was mounted in the electrophoresis chamber (custom build) and loaded with 5 µg of matrix proteins, 15 µg of BSA and Sigma SDS Molecular weight marker cocktail (carbonic anhydrase, egg albumin, bovine albumin, phosphorylase B, β-galactosidase and myosin) suspended in SDS sample buffer (2% SDS, 100 mM DTT (dithiothreitol), 60 mM Tris pH 6.8) (Laemmli, 1970). Electrophoresis was performed at 125 V for 120 min in running buffer according to Laemmli (1970) (3.03% Tris, 14.42% glycine, 1% SDS in H₂O). Subsequently, the gel was transferred without a fixation step to a plastic container and stained in undiluted Sypro Ruby (Molecular Probes) luminescent protein gel stain for 3 h under gentle agitation and protected from light. To reduce background fluorescence and increase sensitivity, the gel was washed in 10% methanol + 7% acetic acid for 30 min. Next, the gel was visualized in a transilluminator (Biorad) at an excitation wavelength of 300 nm. The protein bands (Fig. 11) were excised from the gel and stored individually in Eppendorf tubes at -20°C.

6.1.5 Preparation of the isolated proteins for MALDI-TOF mass spectrometry

The excised protein bands were incubated in a mixture of acetonitrile/water 3:2 for 10 min and subsequently dried using a SpeedVac concentrator equipped with a liquid nitrogen cooling trap. In the next step the gel slices were incubated in 10mM DTT in 50mM ammonium bicarbonate for 1h at 56°C in order to reduce disulfide bonds followed by a 10 min wash in 50mM ammonium bicarbonate. Subsequently, the gel slices were incubated in a mixture of acetonitrile/water 3:2 for 10 min, dried in the SpeedVac concentrator and rehydrated in 50mM ammonium bicarbonate for 10min. After repeating these three steps another two times the gel slices were again lyophilized. The dry gel slices were incubated on ice in cooled Trypsin (Sigma, sequencing grade, 12.5 ng/μl) in 1mM HCl for 10 min. After removing the supernatant the gel slices were moistened with 50mM ammonium bicarbonate and stored for 12 h at 37°C for protein digestion. The supernatant was removed and stored in order to preserve protein fragments that had already diffused from the gel, the remaining peptides were eluted with acetonitrile/water 3:2 for 3 h under continuous agitation. Subsequently, the extracts were combined and lyophilized using the SpeedVac concentrator. The dry peptide samples were then transferred to Dr. Markus Wunderlin, Abteilung Pharmakologie und Toxikologie, in the Sektion Massenspektrometrie of the University of Ulm for MALDI-TOF mass spectrometry.

6.2 Analytical techniques used for studying the sternal CaCO₃ deposits of *P. scaber*

High resolution field emission scanning electron microscopy (HR-FESEM)

Modern state of the art scanning electron microscopes for high resolution imaging combine the high brightness and stability of cold field emission electron sources with the low aberrations of in-lens detectors and eucentric, side-entry goniometer stages which improve mechanical stability and reduce susceptibility to stray fields. For this work, a Hitachi S-5200 in-lens FESEM was used. This microscope is capable of achieving resolutions of about 0.5 nm at 30 kV and 1.8 nm at 1 kV and an outstanding image quality. The good resolution at low voltages makes this type of SEM ideal for the observation of delicate, nanostructured biological samples like the sternal ACC deposits of *P. scaber*, which are very sensible to contamination and radiation damage. To further minimize radiation damage, some of the samples used for studying the architecture of the organic matrix were viewed using a computer controlled Gatan 626 cryo holder operated with liquid nitrogen.

High resolution X-ray diffractometry (XRD)

X-ray diffractometry is a technique in which the pattern produced by the diffraction of an X-ray beam through the lattice of a material with a defined order of atoms or ions (eg. a crystal)

is recorded. By comparing the obtained diffractograms with data of known structures, the crystal phase of the investigated mineral can be determined.

X-ray absorption spectroscopy (Extended X-ray absorption fine structure; EXAFS)

The EXAFS technique is based on the fact that an atom absorbing an X-ray photon is excited and emits an electron whose kinetic energy depends on the energy of the incoming photon. The emitted photoelectron can be backscattered by neighbouring atoms causing constructive or destructive interference depending on the wavelength of the photoelectron. This interference determines whether the X-ray photon is absorbed. If the energy of the X-ray beam is varied, the energy and thus the wavelength of the emitted electrons change and cause energy dependent variations in X-ray absorption. These oscillations of the X-ray absorption can be recorded in an extended energy domain (up to several hundred eV) above the absorption edge of a specific element like calcium in CaCO_3 . The obtained spectra provide information about the chemical nature, the number and the distance of the atoms in the neighbouring shells around the excited atom. In our case, EXAFS was employed at the calcium K-edge. The obtained primary EXAFS oscillations were Fourier transformed and fitted to a suitable model derived from crystalline CaCO_3 . The resulting Fourier transform magnitude for the deposits was compared to data for aragonite, calcite, vaterite and monohydrocalcite. The first coordination sphere giving the distance between calcium and oxygen (Ca-O shell) and the fourth shell indicating the distance between neighbouring calcium atoms (Ca-Ca) are particularly important for the comparison to the crystalline CaCO_3 phases.

Reflection infrared microscopy (IR)

With IR spectroscopy, the absorbed energy from a beam of infrared light passing through the sample across a range of interest is recorded. Because each chemical bond has a specific resonant frequency which is dependent on its length and the mass of the atoms at either end of it, each particular bond type can be identified and the chemical composition of the material can be determined.

High pressure freezing and freeze substitution

For investigation in a transmission electron microscope, biological specimens must be immobilized and fixed. Conventional chemical fixation bears the problem that it is relatively slow, which allows for changes in structure that may lead to artifacts. To avoid this, cryo-fixation can be used which is fast, but also bears the problem of structural damage through the formation of ice crystals, particularly in larger samples. In recent years, high-pressure freezing has become the state of the art method for the preparation of biological samples for TEM. This

method is based on fast freezing (< 30 msec) using liquid nitrogen combined with the simultaneous application of a pressure of about 2300 bar. The pressure reduces the formation of ice crystals to a minimum and allows freezing of native samples with a thickness of up to 200 μm and a diameter of 2mm without ice crystal damage. To prepare the high pressure frozen specimen for viewing in a TEM, they must be dehydrated and fixed, which is done by freeze-substitution. Thereby, the frozen samples are transferred to a cooled organic solvent (-90°C), which may contain fixatives like glutaraldehyde, osmiumtetroxide or uranylacetate. Over a period of hours or even days the samples are slowly warmed up allowing the organic solvent to substitute the ice and gently dehydrate the sample. Simultaneously, the fixatives can react with the structure and fix the samples. The dehydrated samples are then embedded in resin and can be sectioned using an ultra-microtome to the desired thickness for viewing in the TEM.

Electron energy loss spectroscopy (EELS)

Electron energy loss spectroscopy uses the fact that high-energy electrons passing through a sample can interact with sample electrons by inelastic scattering, resulting in a loss of energy. This energy loss is characteristic for the element in the sample that has interacted with an incoming electron. In a transmission electron microscope, this effect can be used in two different ways. By passing the emerging electron beam through a magnetic prism, the varying flight path of the electrons caused by their varying energy can be used to record spectra (electron energy loss spectroscopy or EELS). The other possibility is to pass the emerging electron beam through an adjustable slit, which allows selecting electrons with a certain range of energies to form an image on the detector. This allows to select either elastically scattered electrons that have no energy loss or to select electrons that have lost a specific energy. Using inelastically scattered electrons will result in images of very good contrast. Setting the spectrometer to a specific energy loss allows to record elementally sensitive images. In order to minimize the background effect, images have to be recorded using electrons at the energy of the maximum of the absorption peak for a particular shell of the desired element, the excitation edge, and subtracted by images recorded just before the ionisation energy. EELS is best suited for elements with relatively low atomic numbers with sharp and well defined absorption edges. In this study EELS was used for image contrast enhancement, since filtering of the inelastically scattered electrons (adjustment of slit at 30 ± 5 eV) together with signal amplification enables the examination of thick sections like the chemically fixed 500 nm sections of developing deposits used for investigation of spherule formation.

7. Deutschsprachige Zusammenfassung

Anorganische Mineralien erfüllen in einer Vielzahl von Organismen wichtige Funktionen als Material zur Bildung von Knochen, Schalen, Zähnen und einer Vielzahl weiterer Strukturen. Kalziumkarbonat ist eines der am weitesten verbreiteten Biomineralien, welches vor allem von Invertebraten wie Korallen, Mollusken und Crustaceen zur Mineralisation von Skelettstrukturen genutzt wird. Wie alle Arthropoden besitzen Crustaceen ein Exoskelett, welches um wachsen zu können regelmäßig durch ein neues, größeres ersetzt werden muss. Dabei geht jedoch in der Regel das eingelagerte CaCO_3 verloren. Für die in der überwiegenden Mehrheit marinen oder limnischen Krebsarten stellt dies jedoch kein Problem dar, da verlorenes CaCO_3 zügig durch Aufnahme über die Kiemen aus dem umgebenden Wasser ersetzt werden kann und so die Schutzfunktion der Kutikula rasch wiederhergestellt wird. Im Gegensatz dazu können landlebende Krebse wie die terrestrischen Isopoden während der Häutung verlorenes CaCO_3 nur über ihre Nahrung ersetzen, die in der Regel nur geringe Mengen an Kalzium enthält. Aus diesem Grund haben terrestrische Isopoden einen Mechanismus zur Konservierung kutikulären Kalziums entwickelt, der eng mit dem allen Isopoden gemeinsamen biphasischen Häutungszyklus zusammenhängt. Dabei häuten die Tiere zuerst die posteriore und danach erst die anteriore Körperhälfte. Vor der posterioren Häutung werden große Mengen CaCO_3 aus der posterioren Kutikula resorbiert, über die Hämolymphe und das anteriore sternale Epithelium in den Exuvialsplatt der ersten vier anterioren Sternite transportiert und dort in Form von sternalen Kalkablagerungen gespeichert. Unmittelbar nach der posterioren Häutung werden die Kalkablagerungen sehr schnell resorbiert und zusammen mit Kalzium und vermutlich auch Karbonat aus der anterioren Kutikula dazu verwendet, die neue posteriore Kutikula zu mineralisieren. Nachdem die Kalziumreservoir vollständig resorbiert sind, häuten die Tiere die vordere Körperhälfte. Neben sternalen Kalziumreservoir haben einige terrestrische Isopoden auch andere Arten der transienten Kalziumspeicherung entwickelt wie zusätzliche pleonale Reservoir oder Ablagerungen im Körper selbst in Form von Reservoir im Hämolympdraum oder kleinen Sphärolithen im lateralen Fettkörper. Bei den Arten mit sternalen Kalziumreservoir lässt sich eine Korrelation zwischen deren Ultrastruktur und dem Grad der Anpassung ans Landleben feststellen. So bestehen die Reservoir von semi-aquatischen Klippenasseln der Gattung *Ligia* aus einer Schicht von kleinen Sphärolithen, während die Reservoir der in Feuchtgebieten lebenden Art *Ligidium hypnorum* zusätzlich eine distale Schicht von miteinander verbackenen Sphärolithen aufweisen. Rein terrestrische Arten bilden dreischichtige Kalziumreservoir. Bei unserem Modellorganismus, der Kellerassel *Porcellio scaber*, bestehen diese aus einer distalen Schicht von 500 nm großen, verbackenen Sphärolithen,

einer proximalen Schicht von freien, bis zu 3 µm großen Sphärolithen und einer dem Epithel anliegenden homogenen Schicht. Vorangegangene Untersuchungen haben gezeigt, dass sowohl die Sphärolithe als auch das homogene Material aus amorphem Kalziumkarbonat (ACC) bestehen das von einer organischen Matrix stabilisiert wird und dessen hohe Löslichkeit zusammen mit der großen Oberfläche der Sphärolithen die schnelle Resorption der Kalziumreservoir nach der posterioren Häutung begünstigt. In jüngster Zeit wurde die große Bedeutung von ACC bei der Bildung von CaCO₃-basierten Biomineralen erkannt. Da sie vollständig aus ACC bestehen, stellen die Kalkreservoir von *P. scaber* ein lohnendes Untersuchungsobjekt dar. Jedoch sind die Prozesse der Bildung, Resorption und Ablagerung von ACC im Exuvialsalt während der Häutung von *P. scaber* bisher nur unzureichend verstanden. Ferner gibt es weder zur strukturellen Organisation noch zur molekularen Zusammensetzung der organischen Matrix in den Reservoiren Informationen und auch evolutionäre Aspekte der Reservoirmorphologie bedürfen noch der Klärung.

Ziel dieser Arbeit war es deshalb, den Prozess der Bildung von Sphärolithen zu untersuchen und dabei zu klären, wie und wo die Sphärolithen angelegt werden, wie Mineral und organische Matrix während dieses Prozesses interagieren, wie Sphärolithen wachsen und welche Faktoren ihre endgültige Größe festlegen. Des Weiteren sollte geklärt werden wie die drei strukturell unterschiedlichen Schichten der Reservoire entstehen und warum die Sphärolithen der distalen Schicht miteinander verbacken, die der proximalen sphärolithen Schicht aber nicht. Außerdem soll verstanden werden warum zum Ende der Häutungs Vorbereitung statt Sphärolithen homogenes Material gebildet wird, das die schnelle Auflösung der Reservoire scheinbar behindert. Schließlich sollte die Struktur und die molekularen Bestandteile der organischen Matrix näher charakterisiert werden.

Zur Klärung dieser Fragen wurde der Auf- und Abbau der sternalen Kalziumreservoir von *P. scaber*, die Ultrastruktur der organischen Matrix in den drei strukturell verschiedenen Schichten sowie die Prozesse der Sphärolithenbildung und -Auflösung mittels hochauflösender Raster-Elektronenmikroskopie untersucht. Basierend auf den Ergebnissen, wurde die Initialphase des Sphärolithenwachstums während der frühen Häutungs Vorbereitung Hilfe der Transmissionselektronenmikroskopie analysiert. In Kollaboration mit Prof. Eppe (Univ. Essen) und Prof. Bismayer (Univ. Hamburg) wurde die mineralische Phase der Reservoire mittels hochauflösender Röntgenbeugung, Röntgen-Absorptions-Spektroskopie und Infrarot-Reflektionsmikroskopie untersucht. Aus den Reservoiren isolierte Matrixproteine wurden gelelektrophoretisch getrennt und es wurden erste Versuche durchgeführt um ausgewählte Proteine mittels MALDI-TOF Massenspektrometrie zu charakterisieren.

Die Ergebnisse zeigen, dass die Sphärolithe in einer spezialisierten Aggregationszone angelegt werden. Dies geschieht durch Bildung von granulären Nanopartikeln aus CaCO_3 und organischen Matrixkomponenten die vom anterioren sternalen Epithel sezerniert werden. Das CaCO_3 wird dabei von den Matrixproteinen als ACC stabilisiert das zwar röntgenamorph ist, jedoch eine nanokristalline Struktur mit einer Partikelgröße im Bereich weniger Kristallgitterebenen, aber nicht größer als 10 nm, aufweist. In einer sich einige μm weit von der Aggregationsszone erstreckenden Wachstumszone nehmen die initialen Sphärolithe konzentrisch an Größe zu, möglicherweise durch kontinuierliche Bildung weiterer Nanopartikel an ihrer Oberfläche. In allen drei Schichten der Kalziumreservoirie formt die organische Matrix konzentrische Netze aus Filamenten die durch radiale Filamentstränge verbunden sind, wahrscheinlich durch Selbstorganisierungsprozesse. Die Entstehungsabfolge der drei strukturell unterschiedlichen Reservoirschichten kann durch eine Abnahme der Nukleation neuer Sphärolithe während der Bildung der Kalziumreservoirie erklärt werden. Zusammen mit dem konzentrischen Wachstum der Sphärolithe führt dies von den anfänglich vielen und gleich großen, verbackenen Sphärolithen der distalen Schicht zur Bildung der freien, größer werdenden Sphärolithe der proximalen Schicht. Gegen Ende der Häutungsvorbereitung werden keine neuen Sphärolithe mehr nukleiert, so daß die zuletzt gebildeten weiter wachsen bis sie aneinander stoßen, verschmelzen und schließlich homogenes Material abgelagert wird. Eine solche Abnahme der Anzahl neu gebildeter Sphärolithe während des Aufbauprozesses hat wahrscheinlich auch während der Evolution der terrestrischen Isopoden zur Entwicklung von zwei- und dreischichtigen sternalen Kalziumreservoirien aus ursprünglich einer Schicht von freien Sphärolithen geführt.

8. Curriculum vitae

Personal Details

Name: Helge-Otto Fabritius

Date of Birth: 20th September 1970

Place of Birth: Agnetheln, Romania

Nationality: German

Education

1983 – 1990 Elly-Heuss-Knapp-Gymnasium, Heilbronn, achieving Abitur

1990 – 1991 Military service

1991 – 1999 Studies at the University of Ulm achieving the Diploma Degree in Biology (sehr gut)

1998 – 1999 Diploma-thesis „Morphologie, Phylogenie und Evolution der Flosculariidae (Rotifera)“ at the Sektion für biosystematische Dokumentation, University of Ulm

2000 – 2001 Postgraduate-studies on sessile rotifers at the Sektion für biosystematische Dokumentation, University of Ulm

2001 – 2005 PhD-studies at the Zentrale Einrichtung Elektronenmikroskopie, University of Ulm on the project “Nano-architecture and mineralisation of the amorphous CaCO₃ deposits during the molt cycle of the terrestrial isopod *Porcellio scaber* (Crustacea)”; funded by the Deutsche Forschungsgemeinschaft DFG (Biom mineralization SPP 1117)

Since 2005 Scientific assistant at the Max-Planck-Institut für Eisenforschung GmbH, Düsseldorf on the project “Microstructure and mechanical properties of biological materials” funded by the DFG under the framework of the Gottfried Wilhelm Leibniz award and by the Max Planck Society

Additional activities

September 1994 Participation at the course “Marine Biology” at the IfMB, Giglio, Italy

October 2001 Participation at the 2nd Summer school of the European Chitin Society “EUCHIS” at the University of Ulm, Germany

September 2004 Participation at the course „Immunmarkierung von Dünnschnitten für die Licht- und Elektronenmikroskopie“ at the Max-Planck-Institute for Developmental Biology, Tübingen, Germany

9. List of Publications

9.1 Scientific Journals

Publications related to this thesis

Fabritius, H., Walther, P. and Ziegler, A., 2005. Architecture of the organic matrix in the sternal CaCO_3 deposits of *Porcellio scaber* (Crustacea, Isopoda). *Journal of Structural Biology* **150**, 190-199.

Ziegler, A., **Fabritius, H.** and Hagedorn, M., 2005. Microscopical and functional aspects of calcium-transport and deposition in terrestrial isopods. *Micron* **36**, 137-152.

Fabritius, H. and Ziegler, A., 2003. Analysis of CaCO_3 deposit formation and degradation during the molt cycle of the terrestrial isopod *Porcellio scaber* (Crustacea, Isopoda). *Journal of Structural Biology* **142**, 281-291.

Becker, A., Bismayer, U., Eppler, M., **Fabritius, H.**, Hasse, B., Shi, J. and Ziegler, A., 2003. Structural characterisation of X-ray amorphous calcium carbonate (ACC) in sternal deposits of the Crustacea *Porcellio scaber*. *Dalton Transactions* 2003, 551-555.

Further publications

Sachs, C., **Fabritius, H.** and Raabe, D., 2008. Influence of microstructure on deformation anisotropy of mineralized cuticle from the lobster *Homarus americanus*. *Journal of Structural Biology* **161**, 120-132.

Raabe, D., Al-Sawalmih, A., Yi, S.B. and **Fabritius, H.**, 2007. Preferred crystallographic texture of α -chitin as a microscopic and macroscopic design principle of the exoskeleton of the lobster *Homarus americanus*. *Acta Biomaterialia* **3**, 882-895.

Boßelmann, F., Romano, P., **Fabritius, H.**, Raabe, D. and Eppler, M., 2007. The composition of the exoskeleton of two crustacea: The American lobster *Homarus americanus* and the edible crab *Cancer pagurus*. *Thermochimica Acta* **463**, 65-68.

Romano, P., **Fabritius, H.** and Raabe, D., 2007. The exoskeleton of the lobster *Homarus americanus* as an example of a smart anisotropic biological material. *Acta Biomaterialia* **3**, 301-309.

Sachs, C.; **Fabritius, H.**, Raabe, D., 2006. Experimental investigation of the elastic-plastic deformation behavior of mineralized cuticle by digital image correlation. *Journal of Structural Biology* **155**, 409-425

Sachs, C., **Fabritius, H.**, Raabe, D., 2006. Hardness and elastic properties of dehydrated cuticle from the lobster *Homarus americanus* obtained by nanoindentation. *Journal of Materials Research* **21**, 1987-1995.

Raabe, D., Romano, P., Sachs, C., **Fabritius, H.**, Al-Sawalmih, A., Yi, S.-B., Servos, G., Hartwig, H.G., 2006. Microstructure and crystallographic texture of the chitin-protein network in the biological composite material of the exoskeleton of the lobster *Homarus americanus*. *Materials Science and Engineering A* **421**, 143-153.

9.2 Abstracts

Abstracts related to this thesis

Fabritius, H. and Ziegler, A., 2004. The sternal CaCO_3 deposits of *Porcellio scaber* (Crustacea): an ultrastructural study of a biomineralisation process, EMC 2004: 13th European Microscopy Congress, Antwerp, Belgium.

Fabritius, H. and Ziegler, A., 2003. Nano-architecture and structural changes in the sternal CaCO_3 deposits of the terrestrial isopod *Porcellio scaber* during the molt cycle. Microscopy Conference 2003: 31 Tagung der DGE, Dresden, Germany.

Fabritius, H. and Ziegler, A., 2003. Structure and assembly of spherules within the sternal CaCO_3 deposits in *Porcellio scaber* (Crustacea, Isopoda). 96. Jahresversammlung der Deutschen Zoologischen Gesellschaft, Berlin, Germany.

Fabritius, H. and Ziegler, A., 2003. Aufbau, Abbau und Ultrastruktur der sternalen CaCO_3 -Reservoirs während des Häutungszyklus von *Porcellio scaber* (Isopoda, Oniscidea). 11. Crustaceologentagung, Ulm, Germany.

Fabritius, H. and Ziegler, A., 2002. Formation and degradation of sternal CaCO_3 deposit layers in *Porcellio scaber* (Isopoda, Crustacea) as revealed by field emission scanning electron microscopy, 95. Jahresversammlung der Deutschen Zoologischen Gesellschaft, Halle, Germany.

Further abstracts

Fabritius, H., Sachs, C. and Raabe, D., 2007. Influence of structural principles on the mechanics and efficiency of different biological materials using lobster cuticle as a model material. ICMOBT 2007: Second International Conference on Mechanics of Biomaterials & Tissues, Lihue, Kaua'i, HI, USA.

Fabritius, H., Romano, P., Sachs, C., Al-Sawalmih, A. and Raabe, D., 2005. Arthropod cuticle as an example for bio-composite materials with a strong hierarchical order from the nano- to the macro-level of organization. MRS Fall Meeting 2005, Boston, MA, USA.

Fabritius, H. and Ahlrichs W. H., 1999. Phylogenie und Evolution des Taxons *Floscularia* Cuvier, 1789 (Rotifera, Flosculariidae). 2. Jahrestagung der Gesellschaft für Biologische Systematik (GfBS), Jena, Germany.

10. Acknowledgements

In the first place I wish to express my sincere thanks to PD Dr. Andreas Ziegler, who not only gave me the opportunity to work on this interesting topic, but also shared his knowledge in many constructive discussions and supported and motivated me throughout the whole project. Andreas, thank you for your enthusiasm, your encouragement and for teaching me all the skills needed to become a scientist, but most of all thank you for your patience and understanding even though I have let you down.

I am very grateful to Prof. Dr. Paul Walther for his continuous support and help throughout the project especially in everything where microscopy was involved and of course for providing the excellent working conditions in the department.

I also wish to thank Prof. Dr. Klaus Dieter Spindler, who agreed to be coreferent of this thesis and gave me the opportunity to use his equipment for the molecular biologic part of the project.

I am very thankful to all members of the Z. E. Elektronenmikroskopie for their continuous support and help in technical questions, but most of all for the informal and friendly atmosphere which made my time in the department pass way too fast. Therefore, very special thanks go to my colleagues Monika Hagedorn, Christopher Buser, Holger Krisp and Reiner Bleher for all the helpful discussions and the fun we had after work, and to Prof. Dr. Rainer Martin, PD Dr. Sabine Hild, Wolfgang Fritz, Sabine Grözinger, Gabriele Kräutle, Carmen Litschel, Jutta Passon, Eberhard Schmid and Reinhard Weih.

Also, I am very grateful to our cooperation partners on this project Dipl. Chem. Alexander Becker and Prof. Dr. Matthias Epple from the University of Duisburg-Essen and Prof. Dr Ulrich Bismayer and co-workers from the University of Hamburg.

I would like to acknowledge gratefully the Deutsche Forschungsgemeinschaft who funded this project within the research program “Principles of Biomineralization” (SPP 1117).

Finally, I wish to thank my family, especially my parents who have always supported and encouraged me, Fizz who is always an unselfish friend, and most of all my beloved wife Kathia and our unborn daughter, to whom I wish to dedicate this work and the rest of my life.

Erklärung

Ich versichere hiermit, dass ich die vorliegende Arbeit selbständig angefertigt habe. Ich habe keine anderen als die angegebenen Hilfsmittel und Quellen benutzt, sowie wörtlich oder inhaltlich übernommene Stellen als solche kenntlich gemacht.

Ulm, den 12. 03. 2008

Helge Fabritius